

Gravimetric Study of Cyclohexane Transport in Nanoscale Bitumen Films

by

Vadim Kislitsin

A thesis submitted in partial fulfillment of the requirements for the degree of

Doctor of Philosophy

in

Chemical Engineering

Department of Chemical and Materials Engineering

University of Alberta

© Vadim Kislitsin, 2020

Abstract

In view of the increasing environmental concerns about the current water-based bitumen extraction process, there have been numerous efforts to develop a non-aqueous extraction (NAE) method for the recovery of bitumen from oil sands. The research reported in this thesis was carried out to study the fundamentals of the NAE process with the hope of obtaining a better understanding of the solvent recovery step.

Firstly, the initial estimation of the bitumen contents adsorbed on the residual solid particles made up of sand and clay was made and it was found that the bitumen film thickness appeared to be in the range of 10 to 10^2 nm (i.e., nano-scale films). Then, the decision to recreate the gangue with controlled composition was made, first with the glass particles of a single size and then by adding fine clay particles. In the first experimental study, the mass uptake of cyclohexane vapor by three different samples at two different relative saturations was evaluated. The gravimetric data from three samples (the two mentioned above and one actual residual solids sample) was collected, the shape of mass uptake curves was analysed, and the equilibrium solvent concentrations and initial stage diffusion coefficients were calculated. Comparison of the mass uptake curves to different models was made and it was found that the double-first-order kinetics model fits the experimental data best, which suggested that there are two (at least) different mechanisms with different rate constants involved in the uptake and transport of cyclohexane in bitumen. Also, it was observed a linear positive thickness dependence of diffusion coefficient on the bitumen film. The equilibrium concentration of cyclohexane was higher for the higher cyclohexane relative saturation in the carrier gas but did not significantly depend on the film thickness. Owing to the heterogeneous chemical nature of the bitumen films (each film is

composed of different types of molecules with different polarities), there existed a gradient of polar and nonpolar molecules established prior to the cyclohexane uptake.

In the substrate properties study, two types of samples were considered. Both had the same large particle size distribution as the actual residual solids after bitumen extraction, while the fraction of fine particles varied from 5 to 20 wt%. One sample was made up only of glass spherical particles, while the other was made up of glass spherical particles with a fine fraction made up of kaolin clay particles with an irregular shape. It turned out that the chemical composition of the substrate significantly affected the initial rate of relative mass uptake. The rate of initial mass uptake exhibited a negative film thickness (bitumen content) dependence. The diffusion coefficient values were lower for the particles with a higher fine particle content due to a decreased thickness. The rate of initial mass uptake was not affected by this parameter.

Lastly, the mass uptake and mass release processes were compared. The same samples as in the first two set of experiments were made. The absorption rate was observed to be up to two times faster than that of the desorption rate. The absorption rate exhibited a linear negative film thickness dependence, while for the desorption process this negative dependence was exponential. The diffusion coefficient values had a positive linear thickness dependence in all the cases and were higher in the absorption than in the desorption experiment. One interesting observation was that in the early stages of the desorption experiment, mass uptake rather than mass release was observed in the early stage of the process. The data show that this unexpected phenomenon would probably occur in the case of nanoscale bitumen films.

Preface

A version of Chapter 3 was published as: Kislitsin, V., Choi, P. “**Thickness Dependence of the Diffusivity and Solubility of Cyclohexane in Nanoscale Bitumen Films,**” *ACS omega*, (2019), 4, (25), 21578-21586. I was responsible for the experimental design, data collection and analysis, and manuscript composition.

A version of Chapter 4 was published as Kislitsin, V., Choi, P., “**Initial mass uptake dynamics and diffusivity of cyclohexane vapor in nano-scale bitumen films coated on substrates with different degrees of hydrophilicity,**” *Fuel*, (2020), 271, 117507. I was responsible for the experimental design, data collection and analysis, and the manuscript composition.

A version of Chapter 5 was published as Kislitsin, V., & Choi, P. “**Comparison between the kinetics of cyclohexane absorption and desorption for heterogeneous bitumen nanofilms**”, *Fuel*, (2020), 283, 118836. I was responsible for the experimental design, data collection and analysis, and the manuscript composition.

In all the aforementioned publications, Dr. Phillip Choi contributed to the manuscript composition and editing.

Dedication

To my beloved Aly Pascual, who always believes in me.

Acknowledgements

I want to thank my supervisor, Dr. Phillip Choi for his patience, great mentorship, and valuable advice not only related to the research. Thanks to Xiaoli Tan for understanding, permitting access to the instruments, and proper training. I also want to thank members of Institute of Oil Sands Innovation (IOSI) group, Brittany Mackinnon and Lisa Brandt, for their wise guidance and suggestions. Thanks to my colleague Reza Khalkhali for his ideas. Thanks to my closest buddies from other labs: Birendra Adhikari, Daniel Moran Nava, Anuar Caldera, Agustin Vicente, Abdulrahman Albeladi, Alireza Kheradmand, Anuja Tripathi, and Sahar Saadat for lots of fun and making this journey brighter. I also want to thank the Natural Sciences and Engineering Research Council of Canada for funding.

Table of Contents

Chapter 1	1
Problem statement	1
1.1 Broad problem statement	1
1.2 Specific problem statement	4
1.3 Scope and objectives	9
Chapter 2	11
Literature review	11
2.1 Oil sands: origin, terminology, and composition	11
2.1.1 <i>A few words about the origin of petroleum</i>	11
2.1.2 <i>Composition and properties of oil sands</i>	13
2.1.3 <i>Chemical composition of bitumen</i>	18
2.2 Solvent extraction	23
2.2.1 <i>Procedure background</i>	23
2.2.2 <i>Choice of solvent</i>	24
2.2.3 <i>Recent study and commercialization issues</i>	26
2.3 Sorption and mass uptake theory	28
2.3.1 <i>Some information about intermolecular forces</i>	29
2.3.2 <i>Solution theory</i>	33
2.3.3 <i>Diffusion and mass transfer</i>	37
2.3.4 <i>Diffusion coefficient types</i>	42

2.3.5 Diffusion coefficient estimation and measurement	45
Chapter 3	54
Thickness Dependence of the Diffusivity and Solubility	54
of Cyclohexane in Nanoscale Bitumen Films.....	54
3.1 Abstract.....	54
3.2 Introduction.....	55
3.3 Theory on the measurement of diffusion coefficient	57
3.4 Results and discussions.....	59
3.5 Conclusion	73
3.6 Experimental section.....	74
Chapter 4	80
Initial mass uptake dynamics and diffusivity of cyclohexane vapor in nano-scale bitumen films	
coated on substrates with different degrees of hydrophilicity	80
4.1 Abstract.....	80
4.2 Introduction.....	81
4.3 Theory.....	83
4.3 Materials and methods	84
4.4 Results and Dussions	87
4.5 Conclusions.....	97
Chapter 5	98
Comparison between the kinetics of cyclohexane absorption and desorption	98
for heterogeneous bitumen nanofilms	98

5.1 Abstract	98
5.2 Introduction.....	99
5.3 Theoretical background.....	101
5.4 Experimental section.....	102
5.5 Results.....	105
5.6 Discussions	111
5.7 Conclusions.....	122
Chapter 6	124
Concluding notes and future work.....	124
6.1 Novelty and contribution	125
6.2 Practical implementation.....	126
6.3 Future work.....	129
References:.....	131
APPENDIX.....	150
Appendix A.....	150
Experimental Setup	151
Appendix B.....	152
Thickness Dependence of the Diffusivity and Solubility	152
of Cyclohexane in Nanoscale Bitumen Films.....	152
Appendix C.....	166
Comparison between the kinetics of cyclohexane absorption and desorption	166
for heterogeneous bitumen nanofilms	166

List of Figures:

Figure 1-1: Production of conventional fossil hydrocarbons in Alberta since 2008 (Adopted from Canada Energy Regulator: https://www.cer-rec.gc.ca/nrg/ntgrtd/mrkt/nrgsstmprfls/ab-eng.html)	2
Figure 2-1: Schematic “tree” of petrochemicals (adopted from Strausz [43])	11
Figure 2-2: Mineral composition of Alberta oil sand (adopted from Sanford [43,59])	16
Figure 2-3: Class composition of Alberta bitumen as used by Syncrude (Adopted from Strausz [43,74])	21
Figure 2-4: Oil sand aggregate schematic (adopted from Cormack [82])	23
Figure 2-5: Simplified scheme of NAE process (adopted from Cottrell [81])	24
Figure 2-6: Unit volume element (adopted from Crank [107])	40
Figure 3-1: SEM images. Left images represent the particles before coating (scale bar = 100 μm); right images show the particles after coating (scale bar = 20 μm): (a) – Sample A; (b) – Sample B; (c) – Sample C	60
Figure 3-2: Calculated bitumen film thickness based upon the amount of bitumen coated (wt%) on various samples	64
Figure 3-3: Cyclohexane absorption curves of Sample A at two bitumen film thicknesses and two cyclohexane relative saturation points (? – is there a word missing here? Seems there should be a word here)	65
Figure 3-4: Fitting of the double-first-order kinetics model into the absorption data for Sample A with 108 nm film thickness: (a) – 90% cyclohexane saturation; (b) – 20% cyclohexane saturation. Black curves signify experimental data	66
Figure 3-5: Rate constants k_1 and k_2 as determined by fitting the double-first-order kinetics model to the absorption curves of all samples	69

Figure 3-6: Absorption diffusion coefficient of cyclohexane in bitumen: solid symbols indicate cyclohexane relative saturation 90%, open symbols – 20% cyclohexane relative saturation; Sample A – black; Sample B – red; Sample C – blue 70

Figure 3-7: Solubility of cyclohexane in bitumen: solid symbols indicate cyclohexane relative saturation 90%, open symbols – 20% cyclohexane relative saturation; Sample A – black; Sample B – red; Sample C – blue 70

Figure 3-8: A bare spherical glass bead with a diameter of 3 mm (right) and a similar-sized glass bead coated with a layer of bitumen (left) using a rotary evaporator. The amount of coating was ~ 0.2 wt% or ~ 1 μm thick. 76

Figure 3-9: Schematic representation of an IGA system..... 79

Figure 4-1: Schematic flow chart of a non-aqueous bitumen extraction process..... 81

Figure 4-2: SA absorption curves. Dashed lines - samples with 0.5 wt% bitumen and solid lines - samples with 2 wt% bitumen 90

Figure 4-3: SB absorption curves. Dashed lines - samples with 0.5 wt% bitumen and solid lines - samples with 2 wt% bitumen 90

Figure 4-4: The initial mass uptake rates of SA and SB samples at 25 oC as a function of the measured bitumen content (error bars represent standard deviation) 93

Figure 4-5: The initial mass uptake rates of additional SA and SB samples at 25 oC coated with different amounts of bitumen (error bars represent standard deviation)..... 93

Figure 4-6: The fine content dependence of measured diffusion coefficient of cyclohexane in SA and SB samples at 25 oC (error bars represent standard deviation) 94

Figure 4-7: Diffusion coefficients of cyclohexane in SA and SB samples at 25 °C with comparable bitumen film thicknesses (error bars represent standard deviation)..... 95

Figure 5-1: Selected absorption curves for samples exposed to cyclohexane vapor at 20% and 90% RS in the carrier gas.....	106
Figure 5-2: Desorption curves for the selected saturated samples obtained from the absorption experiments shown in Figure 7-1.....	107
Figure 5-3: Relative mass release curves of the SA sample coated with bitumen films with thicknesses over two orders of magnitude from 51 nm – 6,500 nm. The samples were saturated at 90% RS of cyclohexane prior to the desorption measurements	112
Figure 5-4: Initial rates of relative mass uptake for 90% (filled legends) and 20% RS (open legends) samples	113
Figure 5-5: Initial rates of relative mass release for 90% (filled legends) and 20% RS (open legends) samples	114
Figure 5-6: Absorption diffusion coefficients for 90% RS (filled legends) and 20% RS (open legends) samples	115
Figure 5-7: Desorption diffusion coefficients for 90% RS (filled legends) and 20% RS (open legends) samples	115
Figure 5-8: The initial mass release rates of SD and SE samples.....	120
Figure 5-9: The fine content dependence of measured diffusion coefficient of cyclohexane in SD and SE	120
Figure 5-10: Desorption diffusion coefficients of cyclohexane in SD and SE samples with comparable bitumen film thicknesses.....	121

List of Tables

Table 2-1: Main oil sand components.....	15
Table 2-2: Alberta bitumen-water-solids ratio.....	20
Table 3-1: Amount of bitumen coated on various substrates (wt%). ^a Soxhlet solids after the Dean Stark extraction with no bitumen added (the sample still contains a small amount of residual bitumen).....	61
Table 3-2: Particle size distribution of the gangue.....	77
Table 4-1: Composition of SA (borosilicate glass) and SB (kaolin clay) samples	86
Table 4-2: Calculated surface weighted film thicknesses of bitumen films coated on SA and SB samples	89
Table 4-3: Initial mass uptake slopes of all SA and SB samples	91
Table 4-4: Measured diffusion coefficients at various bitumen film thicknesses of SA and SB samples.....	96
Table 5-1: Samples with estimated bitumen film thicknesses	104
Table 5-2: Initial relative mass uptake rates for all samples exposed to a 90% RS of cyclohexane in the carrier gas and the initial relative mass release rates of the corresponding saturated samples	108
Table 5-3: Initial relative mass uptake rates for all samples exposed to a 20% RS of cyclohexane in the carrier gas and the initial relative mass release rates of the corresponding saturated samples	109

Table 5-4: Initial absorption diffusion coefficients for samples exposed to a 90% RS of cyclohexane and the initial desorption diffusion coefficients of such saturated samples110

Table 5-5: Initial absorption diffusion coefficients for samples exposed to a 20% RS of cyclohexane and the initial desorption diffusion coefficients of such saturated samples110

Table 5-6: Initial rates of relative mass release in samples SD and SE 119

Table 5-7: Measured desorption diffusion coefficients at various bitumen film thicknesses of SD and SE sample 121

Chapter 1

Problem statement

1.1 Broad problem statement

It is not going to be a surprise to anyone to hear that today's worldwide trend in economy is based on the shift towards so-called 'green and sustainable' future when it comes to energy generation and all the aspects of our lives connected with energy. A considerable amount of money has been invested in the development of newer and cleaner energy technologies worldwide, including in Canada [1]. For instance, the development of Green Infrastructure is listed among the five priority investment streams [2]. No need to deny, Canada has been doing a good job in the past years in the renewable energy market, contributing 3% to the world's total renewable energy generation of 79,092 PJ (10^{15} Joules), placed Canada on the 7th position in the world renewable energy generation ranking in 2017, being a second country in the world after China in hydro energy production and listed top-10 in such categories as solar, wind, and liquid biofuels [3].

The numbers look promising indeed and the future of Canada's renewable energy industry seems bright and positive amid multiple environmental problems and significant climate change issues. However, there is another side of the energy industry in Canada which has been becoming less attractive to the general public in the past few years.

According to the data provided by the Canada Energy Regulator, 4.8 million barrels per day (MMb/day) of crude oil was produced in Canada in 2018 (3.6 MMb/day of which was exported), which showed a 61% increase in production since 2010 and placed Canada fourth in the world ranking of crude oil production [4]. In addition, Canada has one of the largest crude oil reserves

in the world as of 2018 (after Venezuela and Saudi Arabia) and, despite all the social and political discussions, is expected to increase its crude oil production by about 50% by 2040 [5]. It is also important to keep in mind that the production of crude oil in Canada is not evenly distributed across the country. Alberta, Saskatchewan, and Newfoundland produce almost 97%, and 27% of refineries are located in Alberta [4].

As per year 2018, Alberta’s production was 3.91 million barrels per day of crude oil, which accounted for 87% of the total Canadian production that year [6]. See Figure 1-1 for the past 10-year dynamic of conventional fossil fuels production in Alberta.

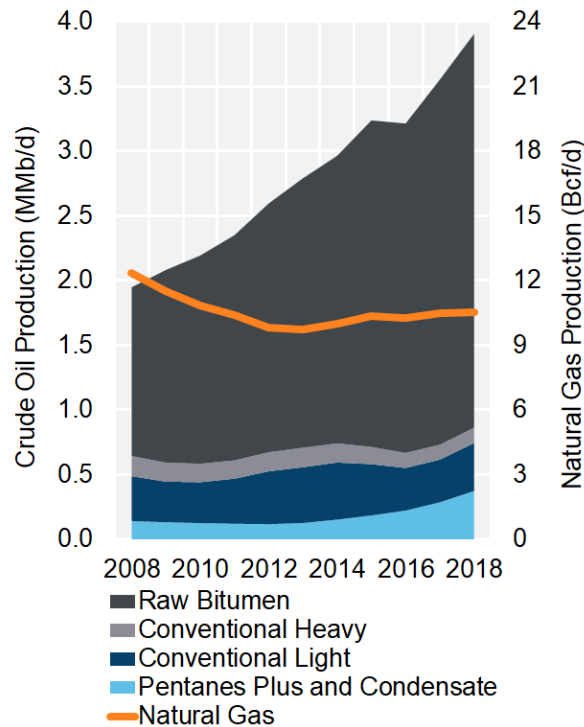


Figure 1-1: Production of conventional fossil hydrocarbons in Alberta since 2008 (Reproduced from Canada Energy Regulator with Non-Commercial reproduction Permission: https://www.cer-rec.gc.ca/glbl/mprntntc-eng.html#s5_2_1)

Although the numbers seem relatively small compared to the world production scale, the crude oil energy sector remains significant for the economies of both Canada and Alberta. Even though the role of petroleum-based fuel in the generation of electric energy in Alberta is extremely low

(<0.1 %) [6], the role of crude bitumen in petrochemical industry cannot be underestimated. The upgrading capacity of Alberta's facilities is estimated at around 1.46 million barrels per day. The products of these refineries are widely used in various branches of petrochemical industries. Although many are controversial due to widely discussed environmental reasons, some of them, such as polypropylene [7], are essential for manufacturing high-demand medical equipment such as face masks and shields [8]. Polypropylene manufacturing is set to be expanded in Alberta; a new petrochemical propane dehydrogenation and polypropylene production complex is expected to open in Fort Saskatchewan in late 2021 [9]. Hence, given that the demand for medical equipment is something that can grow exponentially within a very short period of time and that general manufacturing demands might show an "over-the-roof" growth as we might expect upon the end of the current pandemic, there is no reason to forecast any collapse of the crude oil production industry worldwide even amidst the current oil prices crisis.

Thus, it becomes more and more obvious that the global production of crude oil will most likely end either upon the total depletion of oil reserves on our planet or due to some major climate disaster. As one can tell, the likelihood of either the former or latter happening any time soon is negligible. Therefore, our main problem and task as chemical engineers is addressing all the current issues and challenges that the oil industry has in order to achieve the most efficient and sustainable (as much as possible) recovery, processing, refinery, and consumption of all types of crude oil and petroleum-based chemicals to minimize their impacts on the climate and the life of future generations.

1.2 Specific problem statement

The most abundant source of crude and heavy oil, called bitumen, in Alberta is oil sands (also referred to as Athabasca oil sands). Alberta's proven oil reserve (ranked third in the world) contains about 170 billion barrels [10]. Such a huge reserve possesses significant potential for the development of the chemical industry and a tremendous amount of job opportunities.

However, the recovery of crude oil from oil sands has been extensively questioned by various political, social, and scientific communities—often for good reason. Let us look at why oil sands ore became such a stumbling block for the energy industry. For the sake of introduction, I will not go deep into the explanation of the composition of bitumen and solid particles in oil sands in this chapter. These topics will be covered in-depth in the following chapters. Here, in Chapter 1, I will only give enough general information to describe the problem.

Oil sands are a naturally occurring mixture of solid particles made up of sand and clays, water, and bitumen [11]. The composition of oil sands may vary based on the location they are extracted from but in general the bitumen content is about 4 – 18 wt% [12]. Bitumen is the most valuable component of an oil sands ore. Bitumen recovered from the oil sands is a heavy, viscous crude that is dark brown to almost black. Its components can be divided primarily into two groups with respect to their solubility in alkane solvents (such as pentane, hexane, and heptane): maltenes (soluble) and asphaltenes (insoluble), with the latter having the greatest fraction of molecular weight [12]. The main method employed these days for bitumen recovery from oil sands is based on the process developed by Dr. Karl Clark, who worked at the University of Alberta in the 1920s [13]. I will not stress much of your attention on the method itself as it is not the main objective of my study. In a few words, the oil sands mixture is crushed and treated with hot water or steam to form a slurry, which is pumped down through the pipelines to the

conditioning facility where the slurry undergoes different separation steps. Multiple studies and reviews were done and published in different years on the Clark hot water extraction method (CHWE) [14–21].

As one can reasonably assume, the method developed a century ago might not have considered various aspects of the process, that seemed very casual back in the days but became a challenge today. And indeed, there are multiple issues accumulated within last century after the hot water extraction method was implemented for bitumen recovery. One of the first significant drawbacks of the CHWE method is that it consumed a huge amount of thermal energy: it required approximately 2.5 m³ of hot water per barrel of bitumen recovered [12]. Heating these large amounts of water required a large input of thermal energy which caused excessive carbon dioxide emissions (approximately 0.044 tonne CO₂ per barrel of bitumen produced). Another noticeable issue was that CHWE consumed a huge amount of fresh water. To make up for water trapped in the fine tailings, it takes approximately 3-4 barrels per barrel of crude oil produced [22]. Of course, repetitive freshwater withdrawal might have negatively impacted the local fauna in rivers and lakes.

Finally, one of the biggest issues that we all hear about more and more frequently has become so-called tailings and, associated with that, tailing ponds. This issue gained a very significant impact to the point that it has become an argument in the hands of politicians and it shows that the problem actually exists and needs to be addressed [23]. Tailings are what remains after bitumen is extracted. They are composed mostly of sand, clay, slit, water, and some leftover bitumen. Tailings are stored in ponds that are expensive to construct and maintain and not as efficient. The reason for this is, although most of the tailings get separated from water and settle down to the ponds' bottom relatively soon, the fine tailing particles, predominantly clays, stay in

the floating state forming the colloidal suspension [24,25]. As a result, water cannot be reclaimed, and the tailing ponds essentially become massive mud storage spaces that keep expanding year after year. Multiple analyses and studies have been done on tailings treatment in order to address the challenges of the ponds and find a way to settle the fine particles [17,26,27]. Since the hot water extraction was not the objective of the study, there will be no further detailed explanation on this topic.

Given all the aforementioned drawbacks of the currently used crude oil extraction method and keeping in mind that the total recovery of bitumen from low grade ores can be as low as 60% [15], one can reasonably argue that the CHWE method is not the best option for either the economy or the environment. Hence, assuming the production of crude oil is essential for Canadian and Albertan economies and for the petrochemical industry, the current method needs to be improved to develop a more robust, efficient, and sustainable way of processing the oil sands ore. Given the overall growth of oil production in the past years and expected growth in coming years, this task becomes critical.

It is important to note that currently there is no commercially available alternative to the hot water-based extraction method. All the approaches and methods mentioned here are only studied in labs or pilot scale plants. In order to reduce the environmental impact from the CHWE extraction process, researchers in different universities and companies have been working on so-called non-aqueous extraction (NAE) methods. The main idea of the NAE process is to replace water with organic solvents for bitumen extraction in such a way that the solvent can be recovered and reused once the extraction is complete and the residual solids can be deposited back into the mining sites.

The NAE process itself is not new and has been known for over 60 years [28]. Within this time period, multiple researchers have attempted to use various solvents and combinations of solvents, such as benzene, toluene, gasoline, coal tar naphtha, petroleum naphtha, trichloroethylene, and kerosene [28–34]. Plenty of NAE methods have been examined: in Solvent-Alone Extraction (SAE) [35], the oil sands ore is introduced to a solvent or a solvent mixture that completely replaces water; Solvent Extraction Spherical Agglomeration (SASE) [36] when the solvent is mixed with water, Ionic Liquid Assisted Solvent Extraction (ILASE) [37], and Switchable Hydrophilicity Solvent Extraction (SHSE) [38,39].

In the current research, the focus was only on the residual solids from the SAE process. Although the process might vary slightly from one SAE setup to another, the general idea is similar. At the beginning of the process, oil sands are introduced to some solvent to allow for the dissolution of bitumen into the solvent (recycled or fresh). This step is called digestion. The mixture is further subjected to a multistep process to achieve a liquid-solid separation in separation vessels. The product (liquid bitumen solution in solvent) is further treated to remove the fine particles and bitumen is recovered from supernatant liquid by distillation. The solid fraction from separation vessels (wet gangue) is dried to recover solvent that can be further recycled in the process and the solid dried residual is discharged from the process (and referred to as “dry gangue” or simply “gangue”). This process will also be discussed in the upcoming chapters.

As all the bitumen was removed (or at least the vast majority of it), one can reasonably assume that the most obvious thing to do with the gangue would be to return it to where it was taken from, i.e., to deposit it back to the mining site. However, there is an issue associated with it which is why no non-aqueous extraction process has ever been done commercially in large-scale crude oil production, regardless of how good the bitumen recovery was. The problem has always

been the residual solvent in the dry gangue. It was impossible to simultaneously achieve a high bitumen recovery rate and good residual solvent recovery from the gangue. It wasn't just that the recovery of solvent from wet gangue was not perfect [40] but the dry gangue at the very end of the process also retained some solvent. The main reason was the gangue that still contained some bitumen after bitumen extraction (0.5 wt% - 2 wt%); this leftover bitumen was able to trap solvent which had a concentration of up to 0.1 wt% – 0.5 wt% in the dry gangue.

Previous studies at the University of Alberta showed that cyclohexane, if used as a solvent in the SAE process, yields the best results in terms of oil recovery and solvent recovery capabilities [40]. At the same time, the most promising process of solvent removal should reach the lowest concentration of solvent in the residual dry gangue at 260 ppm [41]. Since the NAE is not commercialized, there are no official government-imposed regulations. However, in the currently used extraction method, there is a regulation that permits the solvent losses to be up to four volumes of solvent lost per 1000 volumes of bitumen produced [15]. Some research groups were able to lower down this number to three volumes of solvent lost per 1000 volumes of bitumen produced [40]. The conversion of this number to the NAE-base gangue results in 260 mg of residual solvent per one kilogram of gangue, or, in other words, 260 ppm (based on a 10 wt% bitumen content ore) [40,42].

The information provided up to this point should provide a clearer picture of the challenges facing the oil-and-gas industry/the bitumen-removal process/whatever. There are still multiple questions to be answered. What exactly happens with solvent when it is trapped in the leftover bitumen in the dry gangue? What is the mechanism of solvent transport within the leftover bitumen fraction? Does the amount of bitumen in the gangue affect the solvent removal rate? Why does it take so long (and how long does it take, exactly) for solvent to escape the bitumen in

dry gangue? Can we achieve solvent removal from the dry gangue to as low as 260 ppm without using extra energy (i.e., without increasing the temperature or using fans to pass air through what)?

As it was already mentioned, many research groups across the country and at the University of Alberta are working hard on solving these and many other challenges associated with NAE methods. This research is the description of my humble contribution to a better understanding of the underlying mechanisms of residual solvent mass transport in leftover bitumen in dry gangue. Hopefully the research will help to move all of us closer to solving this problem, which will enable us to take the process of bitumen production from oil sands to a considerably new level of environmental decency and sustainability.

1.3 Scope and objectives

First, it is important to establish the boundaries of the project. The area of NAE of bitumen from oil sands ores is very broad and the scope for the research needs to be determined clearly. In the current research, it was attempted to study the dynamics and mechanisms of cyclohexane transport in residual bitumen in the by-product material, called dry gangue, after the bitumen extraction process in which cyclohexane was used as an extracting solvent. The method of choice was gravimetric analysis in which the relative mass uptake/release of cyclohexane was measured as a function of time. The reason for the choice of the main method for the research was the access to the full set of relative mass uptake/release curves. It gives not only the opportunity to carry out the required calculations of diffusion coefficients, but also a close look at the dynamics of relative mass change of the samples during the entire experiment. The

collected mass uptake/release curves, in fact, possessed even more valuable information about the potential mechanisms of cyclohexane transport in the residual bitumen.

In spite of the challenges inherent in the NAE process, a number of objectives was achieved, which we will address in the following chapters :

1. In Chapter 2, a brief review will be given an insight into the chemistry of Athabasca oil sands and bitumen. Then, the NAE process and current research will be discussed. Lastly, Chapter 2 will include an introduction to the sorption process. The theory of intermolecular interactions, solubility, and mass uptake theory will be reviewed in detail.
2. The first significant observation done in the current research was the thickness dependency of the diffusion coefficient of cyclohexane in nanoscale bitumen films. This observation will be described in Chapter 3
3. Chapter 4 will provide insight into how particle size distribution and surfaces with different degrees of hydrophilicity affect the relative mass uptake rates and diffusion coefficients.
4. Chapter 5 will include a discussion of desorption kinetics and their potential mechanisms.
5. The last chapter, Chapter 6, will include a summary and suggestions for future work.

Chapter 2

Literature review

2.1 Oil sands: origin, terminology, and composition

2.1.1 A few words about the origin of petroleum

Before going deeper into the experimental data, it is important to provide a brief insight into what petroleum is, since my work focused on the oil sands. As mentioned in Chapter 1, the significance of crude oil today is great, and the variety of petrochemicals made from it is huge [43]. Figure 2-1 shows a petrochemical “tree” with some of the materials that can be obtained from oil [44].

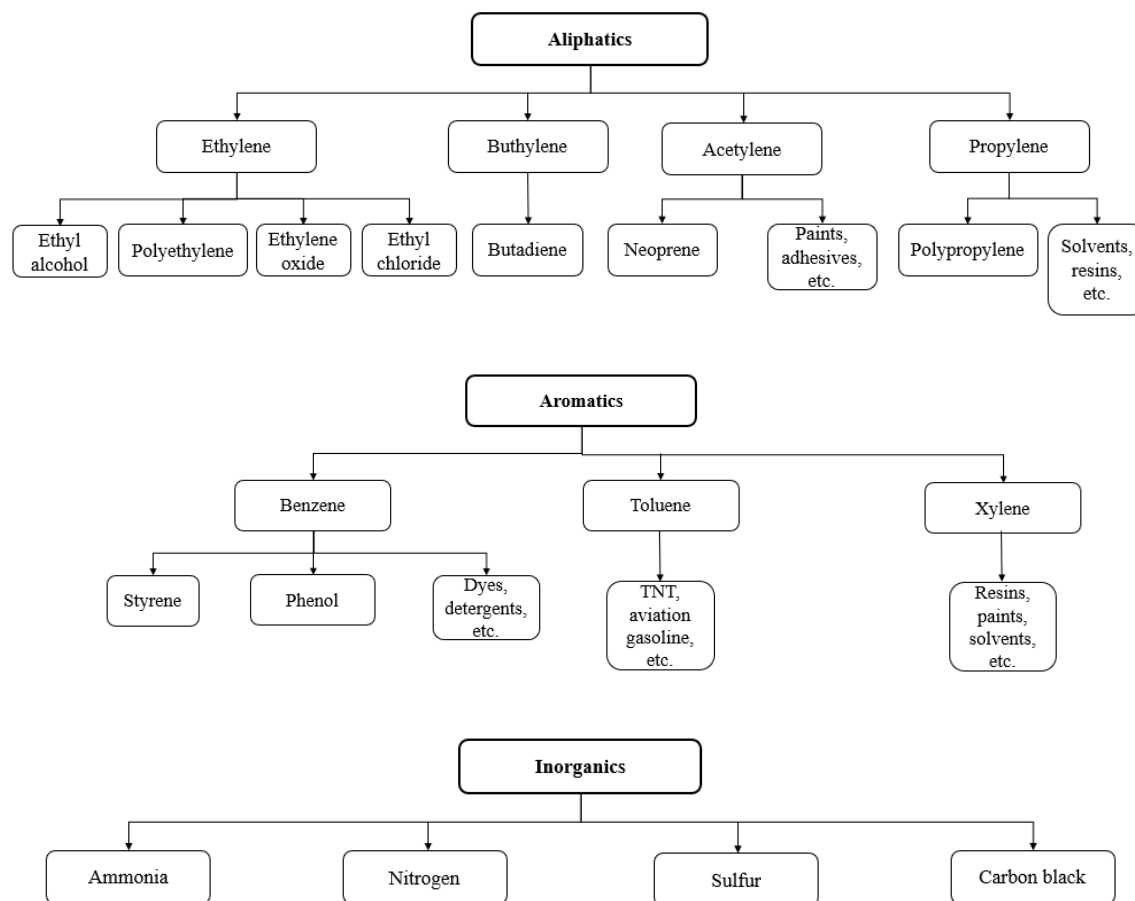


Figure 2-1: Schematic “tree” of petrochemicals (adopted from Strausz [43])

The generally accepted theory of what? is that all the commonly known organic fossil fuels such as oil, natural gas, coal, tar, and kerogen (a precursor of oil) are the result of the accumulation of organic matter and debris, mostly living organisms that collected their energy and carbon source using a photosynthetic reaction, an essential reaction of natural carbon source (sugar) generation on our planet [44]. This organic debris subjected to water, dead and living microorganisms (aerobic and anaerobic), and minerals, under certain mild temperature and pressure conditions it was exposed to for hundreds of millions of years, has converted into what we know today as fossil fuels [45].

Up till now we have used the terms oil (also crude oil) and bitumen (also source bitumen) interchangeably. In fact, this is not quite correct. Crude oil is derived from source bitumen. However, crude oil and source bitumen are chemically different due to their migration within rock formations called reservoirs [44]. Because polar molecules have a higher affinity to the rock surface, the oil has a lower fraction of asphaltenes and polar resins, has less high molecular weight components, and more hydrocarbons than bitumen [46,47].

There are multiple processes taking place in the original oil (thermal, biological, physical, etc.) that may change the chemical composition of the oil and alter its final chemical and physical properties [44]. For instance, in reservoirs that are very deep, hence having elevated temperatures, the high molecular weight fractions undergo changes resulting in the release of gas, occurrence of lower molecular weight fractions, and condensates. Therefore, the deeper stored oil might become more light. This is called the thermal effect [48]. The processes do not take place one at a time but rather are known to happen simultaneously. Changes caused in oil due to thermal changes result in what is called a “de-asphalting” effect, in which the gas released

upon the thermal decomposition of high molecular weight components dissolves in the oil, resulting in the precipitation of asphaltenes and resins. This amplifies the thermal effect.

The presence of aerobic and anaerobic microorganisms cause certain biological processes called biodegradation. If conditions are favorable, biodegradation can occur very quickly, decreasing saturated hydrocarbons and the aromatic fraction while increasing the number of polar resins and the asphaltenes fraction [49,50]. Although biodegradation is restricted to the depth of the oil reservoir [51,52], the Albertan oil sands are affected by this process as most of the ores are located around 600-900 meters deep [44]. Another less severe effect that changes the chemical composition of oil is the water washing when the most polar, low-molecular-weight compounds are washed away by water at the interface upon contact [44].

The results of different thermal and biological effects might be severe and change the structure of oil dramatically. In fact, the Albertan oil sands, which are mined from the Western Canadian Sedimentary Basin [53], provide an example of such changes. Although the precursor to Alberta oil is associated with the type of oil rich in *n*-alkanes, the bitumen in oil sands is basically missing any *n*-alkanes due to extensive biological and water washing effects [54].

2.1.2 Composition and properties of oil sands

Oil sands are a naturally occurring type of ore rich in bitumen. In most cases they consist of sand, bitumen, fines, colloids, clay organics, water, minerals, gases, carboxylic acids, humin, and humic acids [55,56]. The term oil sands is generally interchangeably used with tar sands and bituminous sands, although it is the latter term that is technically correct [44]. In the literature, and for the sake of this study, we define fines as particles that pass a 325-mesh sieve (<44 μm) and consist of mineral clays, silt, quartz, and heavy minerals.

Naturally, oil sands are an ore in which the sand particles are bound together by bitumen and disperse when the bitumen is removed. The main properties used for oil sands characterization are porosity, heat conductivity, permeability, specific heat, chemical composition of each component, and micro- and macrostructure. The porosity of Alberta oil sands ore was estimated to be in the range of 25% - 40% with the average values to be 25-35% [57]. Porosity is essentially a void volume between the grains capable of holding the liquid, bitumen, or water. The liquid fraction by weight is generally the same for Athabasca oil sands ore and is about 20 wt%. Hence, there is an inverse relationship between the water and bitumen contents: the more bitumen in the ore, the less water it has and vice versa. The oil sands ore can be classified by the bitumen amount in it: a low-grade ore contains 6-9 wt%, an average-grade ore contains 9-12 wt%, and a high-grade ore contains more than 12 wt% [44]. The highest-grade ore (~18.6 wt% bitumen) contains the lowest amount of water and fines. The grade also affects the recovery rate, which increases with the increasing grade of the oil sands. The general breakdown of oil sands composition can be found in Table 2-1 [55]. The special feature of Alberta oil sands is the water film layer separating the sand particles from the bitumen layer, allowing the property to easily break up in presence of hot water, which is used as the main recovery process. For this reason, the oil sands is called “water wet” [44].

The mineral composition of the most mineable oil sands affects the overall pH of the ore in the upper layers of the sites. Studies have shown that the mineral composition of the sand is mostly (>90%) composed of quartz, muscovite, mica, and fine-grained sedimentary rock called “chert” [57]. Figure 2-2 summarises the composition of minerals in the sand. The fine fraction appears to contain mostly clays, predominantly kaolinite, illite, and chlorite [57]. The size distribution

curves for high-grade (~15 wt%) and low-grade (~7 wt%) ores exhibit peaks at 180 μm and 90 μm, respectively [56,57].

Table 2-1. Main oil sands components (Adopted from Strausz [44,50,55])

Organics	Water	Salts	Minerals	Gases
Bitumen	Hydration: <ul style="list-style-type: none"> ○ Lattice ○ Surface film 	Soluble in water	Sand	Dissolved in bitumen
Humin, Humic acids	Unbonded: <ul style="list-style-type: none"> ○ Pendular ring ○ Retained in fines clusters 	Insoluble in water	Silt	Dissolved in water
Fulvic acids		Surface adsorbed ions	Clay	Free in structure
Aliphatic carboxylic acids (chemisorbed)		Ions in water	Colloids	
Insoluble organic-noncrystalline inorganic complex (IONCI)			Heavy minerals	

Plenty of other organic matter insoluble to solvent has also been identified in the oil sands, such as humin, humic acids, carboxylic acids, and ketones. [58,59]. Some of this organic matter naturally belongs to bitumen and has the same biological origination, while there is also organic matter in the bitumen that has nothing to do with bitumen itself and probably originated and resided in the rock formations. This solvent-insoluble matter, when adsorbed on inorganic charged polar surfaces, makes this surface hydrophobic with good oil-wetting characteristics.

Surfaces with characteristics like this become more bound to bitumen than to water, which makes the water separation of bitumen quite challenging. In a low-grade ore, where the fine particles content is high, the fine particles might be coated, which makes the recovery efficiency lower than in high-grade ores [44,59].

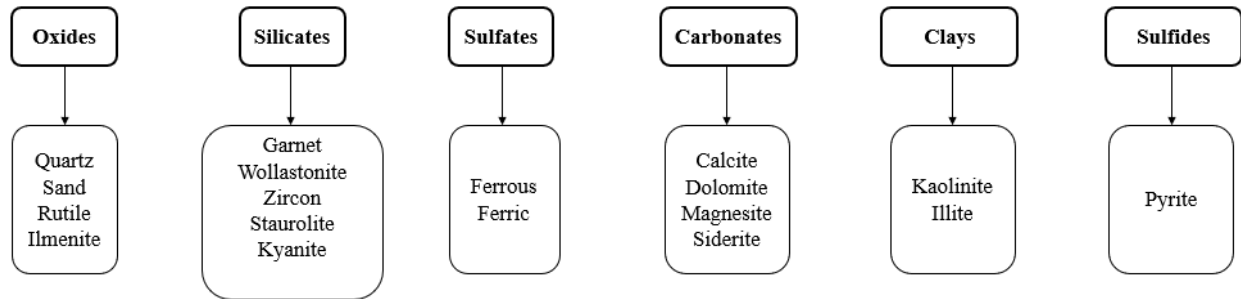


Figure 2-2: Mineral composition of Alberta oil sand (adopted from Sanford [43,59])

Previous studies of the microscopic structure of oil sands ores have proposed different models; however, they all had some common characteristics such as “connate water,” a layer of water approximately 10 nm thick surrounding each sand particle and located at the bitumen-sand interface [60]. This model was able to explain the surface characteristics of oil sand and the water content retained permanently in the ore. It was proposed that the connate water is presented in three forms: 1) as pendular rings in the contact points of sand particles; 2) retained in fines; and 3) as a thin layer covering up to 70% of the particle surface, in which stability was explained by the disjoining pressure as a result of attractive London dispersion forces and repulsive force caused by an electric double layer [44,60,61]. In the case of low-grade ores with high fine particles content, the situation becomes more complicated due to the water presence in fine particles clusters and because of the inorganic-humic species presented in water as colloidal particles in connate water; and as a coating matter on the particles’ surfaces, therefore promoting adhesion of bitumen to the particle [59,60].

To better understand the structure of oil sands and their chemical composition and behavior, it is important to consider the interfacial interactions that govern the behavior of oil sands and their components. Oil sands are a very complex multiphase system and are strongly affected by the nature of interactions between the molecules and between surfaces, or in the interfaces within it. The interfacial phenomena are not the main goal of the study, but it is important to mention at least briefly such parameters as surface/interface tension and zeta potential.

Interfacial tension is the force acting on the molecules in the boundary layer between two phases. In the case of liquids, it tends to reduce the surface area to a minimum [61]. In general, the force acting in the boundary between two liquids is called interfacial tension, while the one acting between the liquid and gas phases is called surface tension. The visualization of surface tension is called the capillary effect; the liquid propagates within a small tube (capillary) and the contact angle between the walls of the capillary and the liquid determines the wettability. If the contact angle is less than 90° , the condition is called water-wet, while if the contact angle is above 90° the condition is oil-wet. Alberta oil sand is generally water wet with the exception of when the extraction is solvent-based [44]. The conditions at which the bitumen was extracted also affect surface tension properties since the different amount of surfactants (presented in the water layer) might be different in the extracted bitumen [62,63]. In low molecular weight fractions and *n*-alkanes, the surface tension increases as the molecular weight increases. The effect of increasing temperature on surface tension is to reduce the surface tension [44].

Because interfaces are generally charged, the properties at the interface are governed by the phenomena occurring within a short range from the interface. Since there is a water layer (~10 nm thick) covering the sand particles, the colloidal particles suspended in the layer might significantly affect the behavior in the bitumen, especially if the bitumen film is also extremely

thin. This behavior can be explained by the interfacial zeta potential and electric double layer phenomena. For more in-depth background on this theory, there is plenty of literature available [61,64].

2.1.3 Chemical composition of bitumen

The major elements of conventional crude oil are carbon and hydrogen. Their fractions are 79-87% and 9.5-14% respectively. Lower amounts of such elements as sulfur (trace-8%), oxygen (0-2%), and nitrogen (trace-1.7%) are also detectable along with traces of some metals [44].

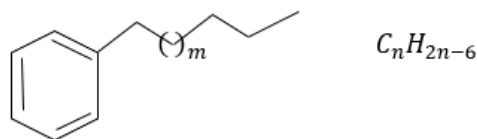
The majority of crude oils consists of hydrocarbons, molecules made of hydrogen and carbon only. Light oils generally have a higher content of hydrocarbons (up to 80% by weight) while heavy oils have a lower hydrocarbon content and higher heteroatoms content. For instance, Athabasca bitumen has a hydrocarbon content of approximately 35-45% by weight [44,50].

The most abundant chemicals in most types of petroleum are [44]:

- Alkanes (paraffins, acyclic molecules, aliphatic), which are open-chain hydrocarbons with a saturate fraction. Alkanes contain only single bonds
- Cycloalkanes (alicyclic molecules, naphthene), which are cyclic aliphatic hydrocarbons
- Aromatics (arenes), which are cyclic hydrocarbons with alternating single-double bonds

In terms of molecular weight, bitumen is the heaviest form of petroleum. A microbiologically degraded substance, bitumen is a dark brown to brown-black dense, viscous hydrocarbon, with a density on average around 1 g/cm³ and a viscosity of 10⁴ mPa·s. It occurs in nature as an oil sand ore in an unseparated form from sands and rocks. It contains a large amount of heteroatoms and nitrogen, oxygen, and sulfur compounds along with metals in various forms of migrabitumens and kerogen [49]. The ratio of main compounds, such as paraffins, cycloalkanes, and aromatics,

varies from one site to another. These compounds in many cases exist not in a pure form but rather as a combination of groups, for example as alkylbenzenes [44]:



The classification of oils comes from a conventional gradation based on the most used characteristics, such as specific gravity, density, viscosity, molecular weight, and boiling point. The classification is generally ordered as follows: conventional light oil, conventional medium oil, heavy oil, extra heavy oil, and bitumen (i.e., bitumen is the heaviest) [65]. In general, bitumen is a complex heterogeneous mixture of various types of hydrocarbons as well as other types of molecules, some of which are in solution state, while others can be presented as colloidal dispersion. The latter poses a significant challenge in determining a chemical composition and affects the recovery techniques and properties of the final product.

One of the first conventional methods of composition analysis of bitumen was developed by Syncrude [66] and involves a toluene and isopropyl alcohol blend to recover both bitumen and water. Further studies showed that methylene chloride was a better option [67,68]. The typical oil-water-solids ratio for Alberta oil sands is shown in Table 2-2 and was first obtained and published by Suncor and Syncrude [69,70].

Table 2-2. Alberta bitumen-water-solids ratio (Adopted from Wallace [44,69,70])

	Oil sands grade		
	High	Medium	Low
Bitumen, wt%	14.6 ± 2.2	11.6 ± 1.7	8.9 ± 4.7
Water, wt%	1.5 ± 11.7	3.6 ± 7.2	4.7 ± 5.8
Solids, wt%	84.2 ± 0.4	85.0 ± 0.6	86.7 ± 0.3

The elemental composition of Alberta bitumen, determined with a standard CHNS method, doesn't vary significantly from one reservoir to another [44]:

Carbon	83.1 ± 0.5%
Hydrogen	10.3 ± 0.3%
Nitrogen	0.4 ± 0.1%
Oxygen	1.1 ± 0.3%
Sulfur	4.6 ± 0.5%

The presence of nitrogen and oxygen are attributed to the microbial presence and activity that the distribution of these is not even in the bitumen. The least polar fractions (saturated) contain the least amount of oxygen and nitrogen while the most polar subfractions and asphaltenes tend to contain the most of the heteroatoms [50]. An understanding of bitumen's chemical structure is crucial since eventually bitumen's properties are determined by its composition. For instance, the viscosity of bitumen is mostly determined by the fraction and composition of its heaviest fraction (asphaltene), while the properties of asphaltene are governed by the types of functional groups (polar or nonpolar) presented in it and the types of bonds established between the groups [44,47].

When talking about properties of bitumen, such as transport and thermodynamic properties specifically, it is important to introduce a broad classification of bitumen into major compound classes. The presence of each class and its proportion in the whole bitumen sample will be a determining factor in how the bitumen behaves. The first class is asphaltenes. Asphaltenes can be separated with low molecular weight alkane solvents and is the highest molecular weight fraction of bitumen containing the majority of heteroatoms, polar groups, and has a tendency to molecular aggregation [44,50,65]. This gives asphaltene different solubility properties than the rest of the bitumen. Asphaltene can be separated by precipitation from the toluene solution by adding *n*-pentane or *n*-heptane. The deasphaltinated bitumen is generally referred to as maltene [44].

Another class of what? is interchangeably called “resins” or “polars,” neither of which are completely correct. This class is defined as a part of maltenes that is adsorbed to clays. And the last two classes eluded from the solution ‘saturates’ and ‘aromatics’ [71–73]. Figure 2-3 summarises the classification.

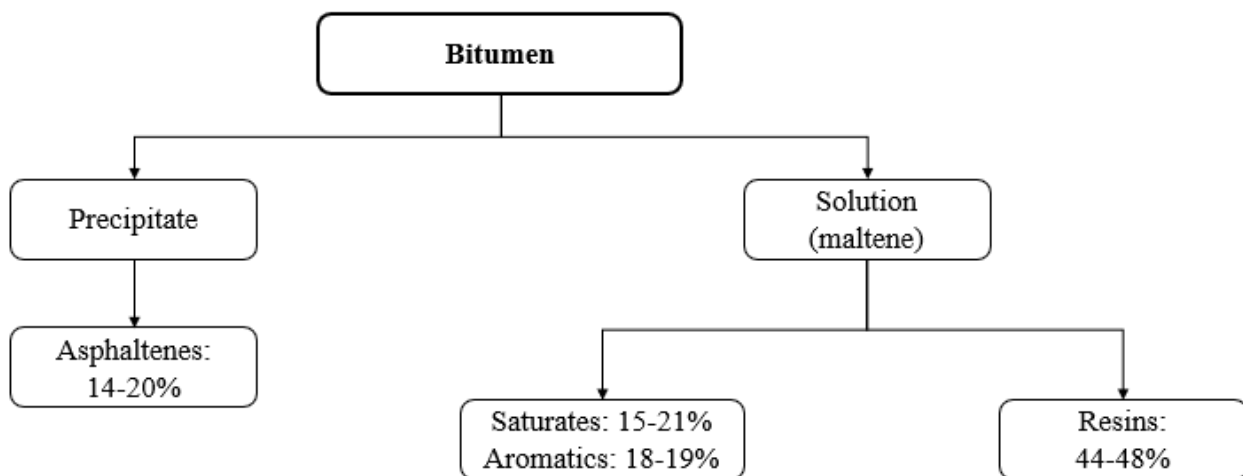


Figure 2-3: Class composition of Alberta bitumen as used by Syncrude (Adopted from Strausz [43,74])

As one can see from this chapter, oil sands in general and bitumen specifically are very complex systems to evaluate. The properties and behavior of bitumen itself and its interactions with other substances are extremely hard to predict and even harder to study. Multiple experiments have been done during the last few decades to understand the composition and underlying structure of bitumen and its components; however, it is has yet to be completely studied and understood. For more information about the chemistry and composition of Alberta bitumen, one can refer to the literature in this chapter [74–79].

2.2 Solvent extraction

Now that we have discussed the composition and properties of Alberta oil sands, it is time to look at the non-aqueous extraction (NAE) process. NAE is not a new idea and it has been studied since 1960-70s [12]. In this chapter, we will pay attention mostly to the solvent alone extraction (SAE) type of NAE since it is the residual material after SAE is of the primary concern in our study. Other types of NAE techniques were mentioned in Chapter 1. Each method is discussed in detail in the literature [12,33,37,38].

2.2.1 Procedure background

The anhydrous extraction of bitumen from oil sands received close attention initially due to its high efficiency and low operation cost and has been carefully looked at since approximately 1963 [80]. Since then, scientists have tried to evaluate various parameters such as residential time, solids weight fraction, stirrer speed, and solvent types, to develop a procedure that could be successfully implemented commercially [81]. Figure 2-4 depicts a schematic representation of an oil sand aggregate described in Chapter 2 [81]. This aggregate was commonly used in early NAE literature.

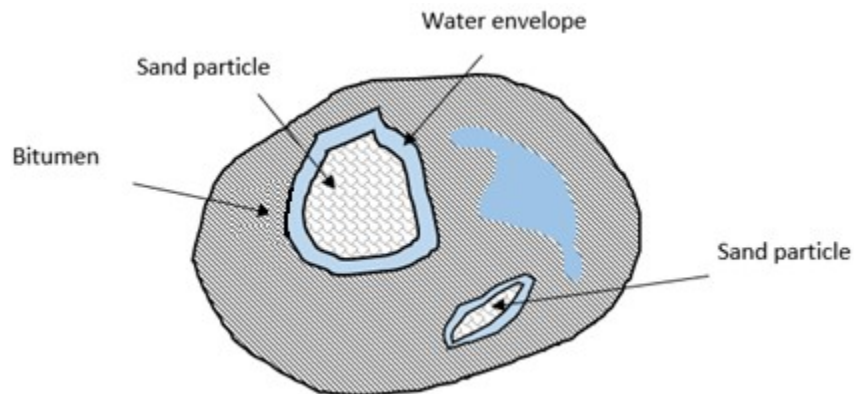


Figure 2-4: Oil sand aggregate schematic (adopted from Cormack [82])

One of the first flow sheets proposed for NAE contains an extraction stage, a washing stage (three subsequent), and a solvent recovery unit. Figure 2-5 show a simplified flow chart of the process [80].

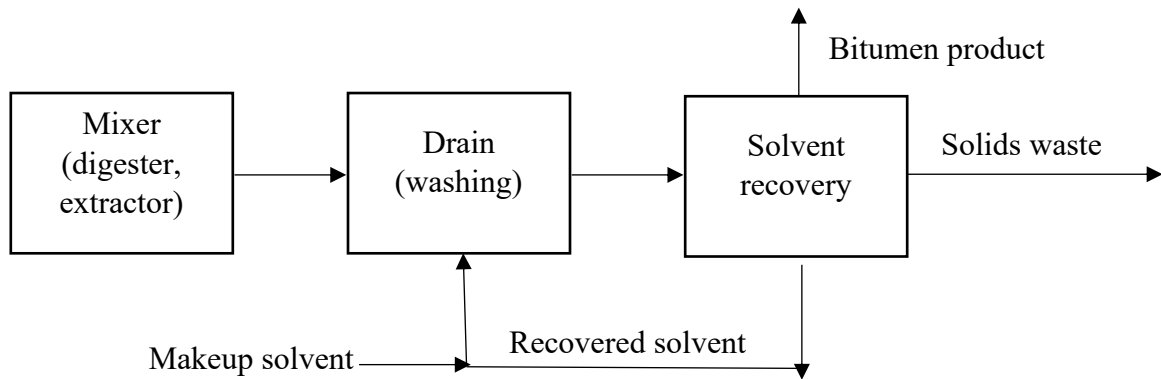


Figure 2-5: A simplified scheme of a NAE process (adopted from Cottrell [81])

To optimize the process, multiple other parameters have been evaluated and different experimental and theoretical approaches have been taken [80–82].

2.2.2 Choice of solvent

Despite all of the research and optimization attempted on NAE, it was suggested that the primary criterion for a good extraction process is the choice of solvent. The solvent should be capable of dissolving most of the bitumen fractions, including asphaltene (the polar fraction of bitumen) [83]. In the early stages of the NAE development, Raymond tested both low boiling point solvents (toluene, xylene, benzene, etc.) and high boiling point solvents (kerosene, petroleum naphtha, coal tar naphtha, etc.) and suggested adopting high boiling point solvents (less volatile) to avoid significant loss of solvent during the extraction process [83].

Since a high boiling point solvent recovery appeared to be problematic from the solvent recovery perspective, researchers started to make attempts at using low boiling point solvents. Hanson

[84] was one of the first to use toluene which was pre-heated. Later, Blaine [31] achieved a solvent recovery with less than 0.5% of solvent lost by using trichloroethylene. In an attempt to agglomerate the sands and fines, Meadus [36] added some water to naphtha and was able to achieve a recovery rate of bitumen that was around 95%.

The first attempt to use a rotary mixer was made by Leung and Phillips [82]. According to their study, the mass transfer of solvent into bitumen is crucially important in the early stage of the NAE process. They also discovered that the mass transfer into the bitumen is higher for solvents with higher aromaticity and lower boiling points. Later, Wu and Dabros [85] summarized these studies and suggested that the ideal solvent is one that has a high bitumen solubility (with respect to as many bitumen fractions as possible). It should have a low boiling point for the sake of recovery, and ideally has poor mass transport properties into the bitumen.

Lately, a significant contribution to the development of the NAE method was made by the Institute of Oil Sands Innovation (IOSI) at the University of Alberta [35,40,86] in terms of the solvent alone extraction process with 95% recovery rates achieved. The schematic flowchart of the multistage process developed by the IOSI group is provided in Appendix A (Figure A1).

Multiple solvents were evaluated as well as mixtures of solvents. OISI researchers studied the recovery of bitumen using each solvent/mixture. Based on the recovery rates as well as migration of fines into the product bitumen stream, Nikakhtari et al. concluded that cyclohexane fits best as a single solvent for NAE [40]. Later, Pal et al. [35] suggested that the precipitation of asphaltene from bitumen needs to be dealt with. They proposed that the mixture of solvents can yield a higher recovery because of the solubility of asphaltene in such mixtures [87]. They also

discovered that mixing cyclohexane with *n*-hexane gave the highest recovery because the solubility parameters of the two gases are comparable.

2.2.3 Recent study and commercialization issues

The main barrier to commercializing the current NAE process is that there is frequently/often a solvent recovery problem. However, it should be pointed out that there is another major issue associated with the potential commercialization: the fine solids that migrate into the bitumen during the extraction process. Nonetheless, it is most desirable that the generated residual solids can be deposited back to the mining site, thus reclaiming the land and territory where the ore mining took place. However, the residual dry solids, the dry gangue, retain some solvent. The concentration of this solvent was lowered to the minimum number of 260 ppm using the most advanced technique based on stationary bed drying [41]. What we discovered is that due to the presence of residual bitumen and bitumen-nonrelated organic matters discussed in Chapter 2, the solvent tends to have some affinity to the residual solids and hence cannot be completely removed without extra energy input, which puts the economical advantage of the entire method of extraction to a sufficient doubt. Until recently, there have been no attempts to study the kinetics of solvent transport in the residual bitumen. Noorjahan et al. [42] attempted to study and understand the mechanisms of cyclohexane transport in Athabasca asphaltenes. Natural Resources Canada carried out similar studies [88].

Noorjahan et al. was the first group to study the diffusion of organic solvent in residual bitumen [42]. They studied the diffusion process of cyclohexane in Athabasca asphaltenes coated on silicon wafers. They used a spray-coating technique. The film was around ~5 microns thick. With a gravimetric analyser, they measured the mass change of the samples over time. On

average, the saturation time of a sample was a few days. As will be explained later, in our study, samples subjected to similar conditions were saturated within hours. The reason for the apparent time difference in the experiments is that Noorjahan et al. used asphaltenes only, the most polar fraction, while cyclohexane is a nonpolar solvent and the mass transfer was apparently extremely slow. The mass uptake curves collected in the Noorjahan et al. [42] study suggest that after a rapid initial linear relative mass uptake (minutes scale) there was a nonlinear relative mass uptake that lasted for a few days.

Based on the assumption of diffusion being the limiting mechanism, Noorjahan et al. evaluated the diffusion coefficient values by solving the equation (1) using the method of lines:

$$\frac{\partial C}{\partial t} = \frac{\partial}{\partial x} \left(D_{AS}(C) \frac{\partial C}{\partial x} \right) = D_{AS} \frac{\partial^2 C}{\partial x^2} + \frac{dD_{AS}}{dC} \left(\frac{\partial C}{\partial x} \right)^2 \quad (1)$$

In equation (1), c is the concentration of solvent in asphaltenes, t is the time, x is the coordinate, and D_{AS} is the diffusion coefficient. The analysis in their study was to determine whether existing models fit the experimental data, specifically the Double-First-Order (DFO) kinetics model and Weibull model.

The DFO model introduces a two-step process [89]:

$$\frac{M_t}{M_\infty} = \varphi(1 - e^{-k_1 t}) + (1 - \varphi)(1 - e^{-k_2 t}) \quad (2)$$

where φ is the fraction of the total mass of solvent taken by the first mechanism, and k_1 and k_2 are the rate constants of the first and second mechanisms, respectively. This model assumes that after the fast initial interfacial mass uptake there is a second mechanism related to the lower rate constant [90].

Another model considered in the Noorjahan study was the Weibull model:

$$\frac{M_t}{M_\infty} = 1 - e^{-(kt)^\zeta} \quad (3)$$

Where k is the rate constant and ζ – parameter related to viscoelastic relaxation time [91].

The experimental data collected by Noorjahan et al. [42] fit reasonably well in the DFO model and even better in the Weibull model. Although fitting was not the main objective of the study, important observations were made, suggesting that there are at least two mechanisms involved in transporting cyclohexane in asphaltene film and that the asphaltene film may undergo some structural changes. In the experimental studies described in the current document, we took the aforementioned observation further and carried out studies to evaluate the structural changes that could take place in bitumen (not just the asphaltene fraction) nano-scale films, changes that could affect the rate constants upon absorption and desorption.

2.3 Sorption and mass uptake theory

As previously mentioned, the amount and rate of cyclohexane recovery from the gangue depend on the thermodynamics and kinetic processes involved [41]. So far, we have discussed the composition of oil sands and bitumen and the current NAE methods and types of solvents involved. Now that we know that cyclohexane is the preferred solvent in our study, it is important to take a better look at the processes that occur upon the transport of cyclohexane in the gangue. It is worth pointing out that most of the residual cyclohexane is dissolved in the bitumen that is adsorbed on the gangue particles (sand and clay particles). The transport of cyclohexane through the bitumen film surface exposed to the air is attributed to its dissolution

(absorption) and evaporation (desorption) which are purely thermodynamic processes. However, the transport of cyclohexane in the bitumen film is a diffusion process.

In this chapter, we will discuss the theoretical aspects of solution thermodynamics first, followed by the diffusion process. Finally, we will discuss the mass uptake theory and the corresponding experimental methods that we used in this work. But first, we start with intermolecular interactions to better understand why cyclohexane vapor can establish an interaction with bitumen in the first place.

2.3.1 Some information about intermolecular forces

Intermolecular forces and energy

The internal energy of a molecular system is the sum of its kinetic and potential energy of all molecules in that system. Kinetic energy, clearly, comes from the molecular motion while potential energy is the manifestation of the forces acting between the molecules [92]. The intermolecular force, F , acting between two molecules located at a distance r , apart, is related to the potential energy, Γ , as follows:

$$F = -\frac{d\Gamma}{dr} \quad (4)$$

And Γ in this case is related to the amount of work needed to be done to separate two molecules from distance r to infinity [92,93]. In the case of attractive forces, when work must be done on the system, potential energy is negative.

Because of the electrostatic interactions between the molecules, intermolecular forces arise, and they can be either attractive or repulsive depending on the intermolecular distance. There is a rigorous theory behind each class of forces. Let us briefly consider the most significant theories

and introduce some important terms [92]. Covalent, ionic, and metallic are known as chemical forces [64], while van der Waals forces (weaker than chemical ones) are generally referred to as physical interactions. The most common van der Waals forces are dipole-dipole, dipole-induced dipole, and dispersion forces (also known as Keesom, Debye, and London dispersion forces), respectively [92].

The attractive forces in electrically neutral molecules arise from a dipole moment. From basic chemistry, it is known that in some molecules, some atoms are more electronegative than others, thereby creating a net negative charge around more electronegative atoms and a net positive charge around less electronegative atoms. The molecules with both net positive and net negative charges are called dipoles [94]. And dipoles can carry a dipole moment:

$$\mu = el$$

where l is the distance between the positive and negative charges, e is the charge, and μ is the dipole moment that has a commonly accepted unit called a Debye. And consequently, all molecules that carry a dipole moment are referred to as polar molecules, while those with no dipole moment or a very small one are called nonpolar [92,94].

Dipole-dipole forces

When two dipoles are found together at a distance r , the electric fields of the molecules will act in such a way to align them, leading to a strong interaction, while kinetic energies will act to move them around randomly. Hence, an attractive or repulsive force will arise, and the potential energy can be estimated as [95]:

$$\overline{\Gamma}_{ij} = -\frac{2}{3kT} \frac{\mu_i^2 \mu_j^2}{r^6} + \dots \quad (5)$$

Dipole-induced dipole forces

When a nonpolar molecule approaches a polar molecule, the electric field of the latter affects the nonpolar molecule in such a way that it generates a displacement of electrons in a nonpolar molecule, thereby creating a dipole moment. As a result, an attractive force arises, known as a Debye force (named after Debye, who first estimated it) [92,95]:

$$\overline{\Gamma}_{ij} = -\frac{\alpha_i \mu_j^2}{r^6} \quad (6)$$

In equation (6), α_i is called the polarizability of a molecule i (nonpolar), a characteristic of how easily the electrons can be displaced by the electric field of a polar molecule.

Because in the current study we evaluate the interaction of cyclohexane, a solvent considered to be nonpolar, with bitumen films which involves mostly interaction of nonpolar entities, it would be beneficial to take a closer look at this type of intermolecular interaction.

This type of intermolecular interaction involves polarization – a phenomenon that occurs when the electric field from the nearby molecules induces the dipole in the molecule [61]. Since all molecules can be polarized, the strength of the induced dipole moment u_{ind} is proportional to the electric field, E , and the coefficient of proportionality is called polarizability:

$$u_{ind} = \alpha E$$

In nonpolar molecules, polarizability comes from the displacement of the negatively charged electron cloud away from the positively charged nucleus in the presence of an electric field.

London dispersion forces

There are also interactions that are significant in understanding the mechanisms of intermolecular interactions, known as dispersion forces, acting between molecules without permanent dipoles [96]. This type of force is a non-additive, short distance force and acts at an Angstrom order of magnitude (up to a nanometer scale). It not only brings molecules together but also tends to align them [61]. London dispersion forces can be either attractive or repulsive and do not follow the general power law.

The dispersion forces are quantum mechanical in nature. The background theory of these forces is rigorous and complex, yet not quite relevant to the scope of our study. Intuitively, the following explanation can be used to give insight into this type of force. A nonpolar molecule has a time-average dipole moment equal to zero. However, at any given instance, this molecule can be considered to have an instant dipole carrying a dipole moment with a certain direction. The presence of this dipole moment gives rise to an electric field that induces a dipole moment by shifting an electron cloud in the neighboring molecules. This, in turn, aligns the neighboring molecules and produces a dipole moment in them [61].

Hence, all three intermolecular forces briefly discussed above are considered van der Waals forces. The interactions are not the main objective in our research, but if you wish to learn more, there is plenty of literature available on the topic [61,64,96]. Now that we have a better understanding of the types of intermolecular interactions, we can have a closer look at the solution theory, since it turned out to be a very important concept for understanding processes and mechanisms involved in the experiments that will be described in subsequent chapters.

2.3.2 Solution theory

Ideal solution

Let us briefly start with some important terms, fugacity and activity, before we introduce the ideal solution concept. To express chemical potential in terms of a “real world” equivalent, G. N. Lewis, who considered the pure ideal system, derived the expression for ideal gas [97]:

$$\left(\frac{\partial \mu_i}{\partial P}\right)_T = v_i$$

Replacing this expression in an Ideal Gas Law and integrating at constant temperature yields the expression for an ideal gas system that undergoes an isothermal process from initial pressure P_0 to P [97]:

$$\mu_i - \mu_i^0 = RT \ln \frac{P}{P_0} \quad (7)$$

To account for the non-ideality of any system, whether it is a gas, liquid, or solid, Lewis introduced a term called fugacity, f :

$$\mu_i - \mu_i^0 = RT \ln \frac{f}{f_0} \quad (8)$$

where μ_i^0 and f_0 are the arbitrary values, but once one is chosen, the other is fixed. Hence, fugacity is equal to the pressure in a pure ideal gas while in a mixture of ideal gases it is equal to the partial pressure, $y_i P$, where y_i is a mole fraction of component i .

The relation $\frac{f}{f_0}$ in equation (8) Lewis called activity, a , the meaning of which is to point out how active the component is at a given state relative to its standard state (note the relation was

derived for the constant temperature process; therefore, the temperature of the current state must be the same as the temperature of the relative state, while the same is not necessarily true for composition) [97]. Let us keep the concept of activity in mind, as we will use it in Chapter 5.

In an ideal solution, therefore, the fugacity of each component is proportional to its concentration at constant temperature and pressure:

$$f_i^L = k_i x_i$$

where x_i is the mole fraction of the i^{th} component, and if the relation is valid for the entire range of compositions ($x_i = 0..1$), then the solution is called ideal [97].

Regular solution concept

The original statement about the concept of solubility dates back to 1916 when Hildebrand [98] assumed that in the solution, molecules should be “sufficiently alike” and under the same forces in the solution as they are in a pure state. He came to this conclusion when he was looking at the nature of deviations from Raoult’s law. He also showed that the deviations increase with increasing changes in internal pressure. To distinguish between the ideal solution and the regular solution, Hildebrand developed a theory stating that in regular solution the entropy change due to change in volume is zero [99]. The correction for an entropy change due to irregularity was given as:

$$\left(\frac{\partial S}{\partial V}\right)_T = \left(\frac{\partial P}{\partial T}\right)_V$$

In other words, the Gibbs free energy change in an ideal solution is purely due to the entropy change of mixing, while in regular solution, the enthalpic term arises from the breaking

intermolecular interactions between solvent and solute and the establishment of new solute-solvent interactions [100].

The Gibbs free energy upon mixing two components can be written as:

$$\bar{F}_1 - F_1^0 = \bar{H}_1 - H_1^0 - T(\bar{S}_1 - S_1^0) \quad (9)$$

And at the same time:

$$\bar{F}_1 - F_1^0 = RT \ln \left(\frac{f_1}{f_1^0} \right) = RT \ln a_1 \quad (10)$$

where f is fugacity and a is activity

If the solution is ideal, $\bar{H}_1 - H_1^0 = 0$, and $(\bar{S}_1 - S_1^0) = -R \ln x_1$ and hence

$$\frac{f_1}{f_1^0} = a_1 = x_1$$

which is a manifestation of Raoult's law, and therefore the deviation from ideality (Raoult's law) can be related to the magnitude of the enthalpy change of mixing [98,101]. For the solution or mixing process to take place, it is required that the Gibbs free energy change of mixing is negative [100]. Given that entropy change is always a positive value, it is important that the enthalpy change of mixing is as low as possible, ideally $\Delta H_m \leq T\Delta S_m$.

Later, Hildebrand introduced an important parameter, the solubility parameter, to account for mixing substances with different intermolecular forces which are quantified as [101] the square root of energy of vaporization per unit volume:

$$\delta = \left(\frac{\Delta E^v}{V} \right)^{1/2} \quad (11)$$

This solubility parameter became a crucial factor in studies on the determination of the most suitable solvent for NAE [35,40].

In 1931, Scatchard published a significant study in which the relation of enthalpy (heat) of mixing to solubility parameters was derived [102]. The following assumptions were made: a) mutual energy of two molecules only depends on the separation distance between them but not their relative orientation; b) the distribution of molecules is random; c) the change of volume upon mixing at constant pressure is zero.

The cohesive energy of 1 mol of a mixture of two components, 1 and 2, could be written according to Scatchard [102]:

$$-E_m = \frac{c_{11}V_1^2x_1^2 + 2c_{12}V_1V_2x_1x_2 + c_{22}V_2^2x_2^2}{x_1V_1 + x_2V_2} \quad (12)$$

For pure components, $c_{11} = -E_1/V_1$ is the cohesive energy density (similar expression for

component 2). At regular temperatures, when the vapor is ideal, $-E_m$ was identified by

Scatchard with the energy of vaporization, $c_{11} = E_{vap}/V_1$, and therefore the equation (12) could

be transformed into:

$$-E_m = (x_1V_1 + x_2V_2)(c_{11}\phi_1^2 + 2c_{12}\phi_1\phi_2 + c_{22}\phi_2^2) \quad (13)$$

And the energy of mixing then was obtained:

$$\Delta E_M = (x_1V_1 + x_2V_2)A_{12}\phi_1\phi_2 \quad (14)$$

The further assumption $A_{12} = (c_{11}^{1/2} - c_{22}^{1/2})^2$ yields the equation:

$$\Delta E_M = (x_1 V_1 + x_2 V_2) \phi_1 \phi_2 (\delta_1 - \delta_2)^2 \quad (15)$$

This important equation signifies that in order to have the lowest heat of mixing, ideally the solubility parameter values of the two mixing components should match or their magnitudes should have values as close as possible [100–102]. Overall, getting back to the original statement of this subchapter, the solubility parameters take into account the intermolecular interactions, cohesive energies, and internal pressures of pure components. Hence, matching the solubility parameters of two different substances may be the basis for an assumption of two “alike” systems from the perspective of an intermolecular interaction.

2.3.3 Diffusion and mass transfer

Diffusion

The mass transfer process is the basis of a wide variety of industrial processes. Its application can be observed but not limited to absorption, desorption, humidification, different types of distillation, leaching, extraction, drying, dyeing, adsorption, fixed bed separation, membranes, and crystallization [103]. Diffusion is closely related to mass transfer and has been a topic of a significance for a long time [100]. To better understand the results and conclusions of the experimental work presented in the current dissertation, let us take a closer look at the diffusion process and its background theory.

Firstly, let us point out that, while solution is an entirely thermodynamic process, diffusion is a kinetic process. There are different variations of defining the term diffusion. One is that diffusion is a type of motion of an individual component through a mixture due to a concentration gradient. Another [104] is that molecular diffusion or molecular transport is a transfer (movement) of individual molecules in a fluid due to a random motion of those molecules.

Crank's definition [105] suggests that diffusion is the process in which matter is relocated from one part of the system to another one by means of a random molecular motion.

In fact, it was noticed that the motion of an individual molecule in the solution is random [105]. When the molecules in a solution move independently of each other (dilute solution), they collide only with the solvent molecules. Hence, each collision results in a random direction of molecular motion. That motion can be in the direction of the lower concentration or the higher one. Generally, the motion of a single molecule can be described with a "random walk" model [100,105,106], which means the root mean square of the distance travelled can be calculated, it is almost impossible to predict the direction.

Although it is hard to say in which direction a single molecule is moving, it was noticed that the molecular ensemble moves from the higher concentration regions to the lower concentration regions. In fact, it appears that it is the concentration gradient that moves the molecules in such a way and in certain directions that it averages the concentration of the molecules throughout the medium and the concentration gradient no longer exists [103]. The most common type of diffusion encountered in chemical engineering is the diffusion driven by a concentration gradient [107]. In the mixing process, the initial mass transport process is identified by the motion characteristics of turbulent flow and is called eddy diffusion [103].

Basic mathematical theory and Fick's first law

In 1855, while working on diffusion experiments, German scientist Adolf Fick noticed what he thought was an apparent similarity between conductive heat transfer and mass transport [108]. He had an idea that the rate of transfer of a substance diffusing in a medium per unit area of a cross-section was proportional to the normal to the cross-section concentration gradient

[105,108]. This idea resulted in a mathematical manifestation of the equation known as Fick's first law:

$$J = -D \frac{\partial C}{\partial x} \quad (16)$$

where J is the rate of transfer per unit area of cross-section (in some literature it is used as the molar flux of diffusant, J), C is the concentration of diffusant, x is the special coordinate measured as a normal to the cross-section plane in the direction of diffusion, and D is the diffusion coefficient (in chemical engineering textbooks, it is called volumetric diffusivity) [103–105] and has a unit of $(length)^2 (time)^{-1}$.

Fick's second law

Fick's first law does not provide any information about the time change of concentration. When the conservation of mass law is applied, the time-dependent concentration can be obtained [100]. The equation for a transient diffusion process in a medium is known as Fick's second law. To obtain this equation, let us consider a rectangular-shaped unit volume, the sides of which have the following dimensions: $2dx$, $2dy$, and $2dz$, and are parallel to the axes of Cartesian coordinates as in Figure 2-6.

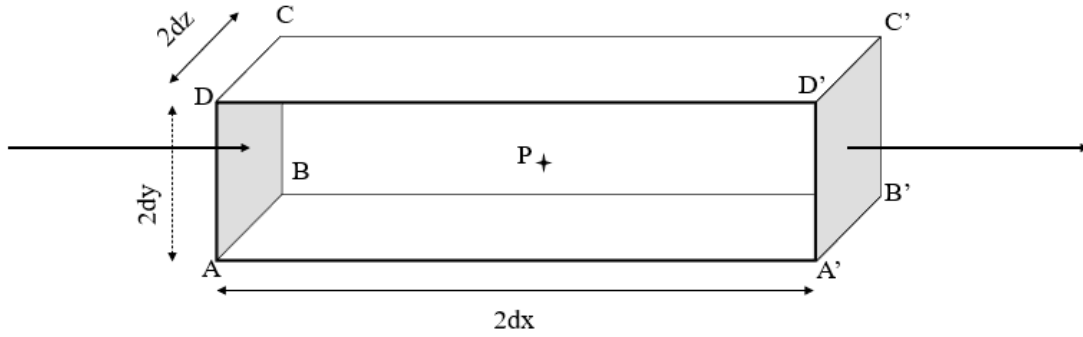


Figure 2-6: Unit volume element (adopted from Crank [107])

The center of the unit volume element is point $P(x, y, z)$. $ABCD$ and $A'B'C'D'$ are the faces of the rectangular volume that is perpendicular to the x axis.

The diffusing substance enters the element through the left face ($ABCD$) with the coordinate $x - dx$ (since the total length is $2dx$, the left face is at $x - dx$, and the right face is at $x + dx$) with the rate:

$$4dydz \left(J_x - \frac{\partial J_x}{\partial x} dx \right) \quad (16')$$

Here J_x is the rate of transfer through the plane containing P .

Similarly, the rate of the substance leaving the unit volume through the face $A'B'C'D'$ is:

$$4dydz \left(J_x + \frac{\partial J_x}{\partial x} dx \right) \quad (16'')$$

The net contribution to the rate of increase of the diffusant in the unit volume is given as:

$$4dydz \left(J_x - \frac{\partial J_x}{\partial x} dx \right) - 4dydz \left(J_x + \frac{\partial J_x}{\partial x} dx \right) = -8dx dy dz \frac{\partial J_x}{\partial x}$$

In a similar manner, one can obtain for all the other faces:

$$-8dxdydz \frac{\partial J_y}{\partial y} \text{ and } -8dxdydz \frac{\partial J_z}{\partial z},$$

where $8dxdydz$ is the volume of the element. But at the same time, the time-rate change of concentration of the diffusant is:

$8dxdydz \frac{\partial C}{\partial t}$, and we can obtain the expression:

$$-8dxdydz \frac{\partial J_x}{\partial x} + \left(-8dxdydz \frac{\partial J_y}{\partial y}\right) + \left(-8dxdydz \frac{\partial J_z}{\partial z}\right) = 8dxdydz \frac{\partial C}{\partial t}$$

or

$$\frac{\partial C}{\partial t} = -\left(\frac{\partial J_x}{\partial x} + \frac{\partial J_y}{\partial y} + \frac{\partial J_z}{\partial z}\right)$$

In the latter expression, the right-hand side can be rearranged using Fick's first law from equation (16). In a system where the diffusion coefficient depends on the concentration of the diffusant, for example, inhomogeneous systems, equation (17) becomes [105,108]:

$$\frac{\partial C}{\partial t} = \frac{\partial}{\partial x} \left(D \frac{\partial C}{\partial x}\right) + \frac{\partial}{\partial y} \left(D \frac{\partial C}{\partial y}\right) + \frac{\partial}{\partial z} \left(D \frac{\partial C}{\partial z}\right) \quad (17)$$

Equation (17) is known as Fick's second law. When D is independent of concentration, equation (17) becomes:

$$\frac{\partial C}{\partial t} = D \left(\frac{\partial^2 J_x}{\partial x^2} + \frac{\partial^2 J_y}{\partial y^2} + \frac{\partial^2 J_z}{\partial z^2}\right) \quad (18)$$

For the one-dimensional diffusion case, equation (18) is reduced to the following equation:

$$\frac{\partial C}{\partial t} = D \frac{\partial^2 J_x}{\partial x^2} \quad (19)$$

The reason we introduced the Fick's second law in such detail is that this equation is a basis equation for the mass uptake theory. This theory is one that is commonly used to determine numerical values of diffusion coefficients. It requires a solution of PDEs arising from Fick's second law. Let us therefore look at how one can estimate the values of a diffusion coefficient.

2.3.4 Diffusion coefficient types

In mass transfer problems, as suggested by Fick's law, it is important to know the diffusion coefficient. The best estimation of the diffusion coefficient is experimental measurements. If such data is available, it should be used directly [100,103].

However, there are different types of diffusion coefficients, each with a different meaning and requiring a different experimental technique to measure it. The diffusion coefficient used in Fick's first law is a mutual diffusion coefficient. It gives a quantitative estimation of how fast species A moves in a medium made up of species A and B when the concentration gradient exists. Hence, the mutual diffusion coefficient is a characteristic of a non-equilibrium system and is exactly what we measured in our experimental section [100].

In an equilibrium system, if the concentration of one component is at infinite dilution, it is also possible to estimate the diffusion coefficient of such a component. In this case, it is called the tracer diffusion coefficient and is essentially a measure of the mobility of species A in a medium made up of species B when the concentration of species A is so low that the mobility of A is only affected by the molecules of species B surrounding it [100,106].

Another important type of diffusion worth mentioning is self-diffusion, which is also an equilibrium property and signifies the mobility of a molecule of species A due to a thermal motion in a pure component A [100].

In practice, there are a few ways to have an order of magnitude estimation of the diffusion coefficient. For instance, to estimate the diffusivity of a gas in air, the diffusion coefficient was found to be proportional to the product of the average molecular velocity and mean free path in the air [103]:

$$D \cong \frac{1}{3} \bar{u} \lambda \quad (20)$$

In certain industrial processes, such as membrane separation, drying, and adsorption, the gaseous substance moves in a porous medium with a pore size (~ 2 to 50 nm) smaller than the molecular mean free path and undergoes multiple collisions with the pore walls. The diffusion process is known as Knudsen diffusion and the diffusion coefficient is called Knudsen diffusivity, D_K [103,104]:

$$D_K = 9,700r \sqrt{\frac{T}{M}} \quad (21)$$

Here, T is the absolute temperature of the system, M is the molecular weight of the diffusant, and r is the pore radius.

For systems with intermediate sized pores ($\sim 10^2$ nm), one needs to take into account collision with the pore walls, other molecules, and the combined diffusivity, the latter of which can be found using the mutual diffusion coefficient (D) [103]:

$$\frac{1}{D_{pore}} = \frac{1}{D} + \frac{1}{D_K} \quad (22)$$

Because the mean free path of the molecules in liquids is orders of magnitude smaller than in gases, the diffusivity of substances in liquid can be up to four to five orders of magnitude smaller than that in the gas phase. The theory of diffusivity in liquid is not as advanced as for gases, and most data comes from experiments. However, a theoretical approach was derived to predict the diffusivity of large spherical molecules at low concentrations in a solution. In such an approach, the molecules and medium are assumed to experience drag forces and be continuous, respectively. The corresponding equation is called the Stokes-Einstein equation [100,103,106]:

$$D = \frac{kT}{6\pi r_0 \mu} \quad (23)$$

In this equation, T is the absolute temperature, r_0 is the molecular radius, and μ is the viscosity of the medium.

For solutes with a smaller molecular weight ($M < 400$), the diffusion coefficient values are greater than those estimated by equation (23) because the drag is less. The proper correlation was made by Wilke-Chang [109]:

$$D = 7.4 \times 10^{-8} \frac{(\psi_B M_B)^{1/2} T}{\mu V_A^{0.6}} \quad (24)$$

where V_A is the molar volume of the solute in the liquid phase, ψ_B is the association parameter of the solvent, and M_B is the molecular weight of the solvent.

2.3.5 Diffusion coefficient estimation and measurement

In the next few paragraphs, a simple description of the theoretical background of Fick's second law solution is given. Although there are dozens of books about Fick's law, we narrowed the topic to the plane sheet only as it is the main geometry of interest in the experimental studies to follow. However, there is still a theory for any geometry that might be employed in the diffusion experiments.

Steady State

Permeation method

One of the simplest methods in terms of experimental setup and mathematical approach is a permeation method at steady state conditions. In this experiment, diffusion takes place in a plane sheet (membrane) with thickness l . Surfaces with coordinates $x = 0$ and $x = l$ are subjected to constant concentrations of diffusant C_1 and C_2 , respectively. After some time, the steady state is established, for which the concentration of the permeant is constant across the sheet. With the assumption that diffusivity is constant, Fick's second law becomes [110]:

$$\frac{d^2C}{dx^2} = 0 \quad (25)$$

Proper integration with known values of concentration at boundaries yields:

$$\frac{C - C_1}{C_2 - C_1} = \frac{x}{l} \quad (26)$$

From equation (26) concentration, C , has a linear dependence from x , and the flow rate, J , is:

$$J = -D \frac{dC}{dx} = D \frac{(C_1 - C_2)}{l} \quad (27)$$

Since the concentrations C_1 and C_2 are known, one can simply estimate the value of the diffusion coefficient from the single measurement of the flowrate, which is the same across all the sections.

In those cases, when the diffusant is in the gas phase, the concentrations might not be known. In this case, gas pressures p_1 and p_2 , known at both sides of the sheet, can be used. The flowrate then becomes:

$$J = P \frac{(p_1 - p_2)}{l} \quad (28)$$

In this case, the constant P is known as permeability. Within the membrane, the relationship between the permeant concentration and external gas pressure can be considered linear [110]:

$$C = Sp$$

where S is the solubility, this leads to a famous relation:

$$P = DS \quad (29)$$

In cases in which the diffusion coefficient varies with the concentration, the value calculated from the abovementioned method and the estimated flowrate corresponds to the average value for the entire plane sheet thickness [111]:

$$J = -D \frac{\partial C}{\partial x} = \text{constant}$$

And the flowrate after integration:

$$J = \frac{D_I(C_1 - C_2)}{l}$$

where D_I is the mean value:

$$D_I = \frac{1}{C_1 - C_2} \int_{C_2}^{C_1} D dC$$

Non-steady State (time lag)

Sorption method

Before we start looking at the numerical evaluations which look rigorous due to the overwhelming amount of mathematical expressions, it is worth pointing out that all of the expressions one can find in this sub-chapter were obtained by various scientists by solving Fick's second law for certain scenarios, with certain assumptions and boundary conditions. All such solutions eventually became a very important tool in diffusivity studies. Later, John Crank did a great job putting all the findings together and organizing them in a logical order. Therefore, all the credits for the derivation and solution of these equations go to the original publications' authors.

Consider the same plane sheet as in part *A*. Let us start with one of the first important solutions of Fick's second law for a non-steady-state case with constant surface concentration and variable initial distribution within the sheet. This was made by Barrer [112], Carslaw and Jaeger [113], Jacobs [114], and Jost [115] in different years in the middle of 20th century. The solution in the form of a trigonometric series is as follows:

$$\begin{aligned}
C &= C_1 + (C_2 - C_1) \frac{x}{l} \\
&+ \frac{2}{\pi} \sum_1^{\infty} \frac{C_2 \cos n\pi - C_1}{n} \sin \frac{n\pi x}{l} \exp(-Dn^2\pi^2 t/l^2) \\
&+ \frac{2}{l} \sum_1^{\infty} \sin \frac{n\pi x}{\pi} \exp(-Dn^2\pi^2 t/l^2) \int_0^l f(x') \sin \frac{n\pi x'}{l} dx
\end{aligned} \tag{30}$$

The next problem solved was the case in which the initial distribution in the sheet was uniform (C_0) and both surface concentrations were the same. This is a common case for absorption/desorption by a membrane. The initial concentration in the region $-l < x < l$ is uniform and is equal to C_0 . Both surfaces are kept at the same constant concentration C_l . In this case the solution of equation (30) becomes:

$$\frac{C - C_0}{C_l - C_0} = 1 - \frac{4}{\pi} \sum_{n=0}^{\infty} \frac{(-1)^n}{2n+1} \exp\left\{-\frac{D(2n+1)^2\pi^2 t}{4l^2}\right\} \cos \frac{(2n+1)\pi x}{2l} \tag{31}$$

Let us then introduce two parameters: M_t is the the amount of diffusant in the sheet at a given instance (at time t); M_∞ is the the amount of diffusant in the sheet at infinite time. Then the equation (31) becomes:

$$\frac{M_t}{M_\infty} = 1 - \sum_{n=0}^{\infty} \frac{8}{(2n+1)^2\pi^2} \exp\left\{-\frac{D(2n+1)^2\pi^2 t}{4l^2}\right\} \tag{32}$$

At a short time, the solution to equation (32) is:

$$\frac{M_t}{M_\infty} = 2 \left(\frac{Dt}{l^2}\right)^{\frac{1}{2}} \left\{ \pi^{-\frac{1}{2}} + 2 \sum_{n=1}^{\infty} (-1)^n \operatorname{ierfc} \frac{nl}{\sqrt{Dt}} \right\} \tag{33}$$

Equations (32) and (33) can be solved graphically for Dt/l^2 and D can be obtained from the sorption time curves as done by Jason and Peters (1973) [116].

Finally, the following scenario is the most relevant for our experimental situation described in this work. In this scenario, the plane sheet with thickness l with an initial uniform concentration of C_0 has a different surface concentration. One face of the sheet, say $x = 0$, has the concentration C_1 , while the other face, $x = l$, has the concentration C_2 . Before the steady state is established, there is a finite period of time when the concentration in the sheet changes. This change of concentration was deduced from equation (30) by Barnes in 1934 and given by [105,117]:

$$\begin{aligned}
C = C_1 + (C_2 - C_1) \frac{x}{l} \\
+ \frac{2}{\pi} \sum_1^{\infty} \frac{C_2 \cos n\pi - C_1}{n} \sin \frac{n\pi x}{l} \exp(-Dn^2\pi^2 t/l^2) \\
+ \frac{4C_0}{\pi} \sum_{m=0}^{\infty} \frac{1}{2m+1} \sin \frac{(2m+1)\pi x}{l} \exp\{-D(2m+1)^2\pi^2 t/l^2\}
\end{aligned} \tag{34}$$

One can notice that as $t \rightarrow \infty$, the concentration C takes a linear expression given in equation (26) [105].

Again, if we introduce M_t and M_∞ as we did previously, then the following expression can be obtained:

$$\frac{M_t}{M_\infty} = 1 - \frac{8}{\pi^2} \sum_{n=0}^{\infty} \frac{1}{(2n+1)^2\pi^2} \exp\left\{-\frac{D(2n+1)^2\pi^2 t}{l^2}\right\} \tag{35}$$

Equation (35) looks similar to equation (32), with the correction that in equation (32) l stands for half-thickness, while in equation (35), l indicates the whole thickness of the plane sheet [105].

The diffusant escapes the sheet through the surface $x = l$ per unit area at a rate

$$-D \left(\frac{\partial C}{\partial x} \right)_{x=l}$$

And then, integrating equation (34) with respect to t , one can obtain an expression for the total amount of diffusant, Q_t , which passed through the plane sheet per time t :

$$Q_t = D(C_1 - C_2) \frac{t}{l} + \frac{2l}{\pi^2} \sum_1^{\infty} \frac{C_1 \cos n\pi - C_2}{n^2} \{1 - \exp(-Dn^2\pi^2 t/l^2)\} \\ + \frac{4C_0 l}{\pi^2} \sum_{m=0}^{\infty} \frac{1}{(2m+1)^2} \left\{ 1 - \exp\left(-\frac{D(2m+1)^2\pi^2 t}{l^2}\right) \right\} \quad (36)$$

Daynes (1920) [118] and Barrer (1951) [112] used this equation to develop a graphical method for diffusion coefficient estimation. In the most common experimental setup, the initial concentration of diffusant in the sheet and at one of the surfaces is zero (C_0 and C_2). For this situation, equation (36) becomes:

$$\frac{Q_t}{lC_1} = \frac{Dt}{l^2} - \frac{1}{6} - \frac{2}{\pi^2} \sum_1^{\infty} \frac{(-1)^n}{n^2} \exp\left(-\frac{Dn^2\pi^2 t}{l^2}\right) \quad (36')$$

At $t \rightarrow \infty$, equation (36) simplifies to:

$$Q_t = \frac{DC_1}{l} \left(t - \frac{l^2}{6D} \right) \quad (36'')$$

If Q_t plotted against time, t , the plot has an intercept, L , with the time axis given by:

$$L = \frac{l^2}{6D} \quad (37)$$

In the permeation method, L is generally referred to as a time lag. With time, the method described here becomes a basis method of diffusivity, solubility, and permeability estimations [105].

Experimental methods of measurement

It is pertinent to start this section by commenting on the methods described by Crank [105,110]. Although, as was previously mentioned, the mathematical theory described in Crank's book still stands and is commonly used as a basis for experimental and graphical estimations, it needs to be kept in mind that the book was published in the middle of the 20th century. Clearly, experimental tools have moved on significantly and the devices Crank et al. describe in their book [110] are probably not used anymore. However, the techniques (not to be mistaken with devices), such as mass uptake, sorption-desorption, NMR, IGC, and some others, are still widely used. Here, we only consider the techniques relevant for our experimental study.

Sorption experiment

Most of the methods are based on the assumption that the diffusion coefficient is constant. This is not necessary true in some cases, and the value of the diffusion coefficient obtained from these experimental studies signifies the mean value of the entire process [105]. One of the first experimental methods described dates to 1933 [119] and 1928 [120].

The experiments are based on the vapor uptake by a plane sheet with thickness l . The sheet is suspended in the constant temperature and pressure environment with a constant permeant vapor

concentration. The weight change with time is measured. As we previously showed, the appropriate solution of Fick's second law for this scenario is given by equation (35). The method is based on half mass uptake. The value of t/l^2 for which $M_t/M_\infty = 0.5$ can be written as:

$$\left(\frac{t}{l^2}\right)_{1/2} = -\frac{1}{\pi^2 D} \ln \left\{ \frac{\pi^2}{16} + \frac{1}{9} \left(\frac{\pi^2}{16}\right)^9 \right\} \quad (38)$$

And the diffusion coefficient can be relatively accurately estimated as:

$$D = \frac{0.04919}{\left(\frac{t}{l^2}\right)_{\frac{1}{2}}} \quad (39)$$

Which means that if the half-time of the sorption process can be experimentally determined or observed, the average value of the diffusion coefficient can be found using equation (39). If \bar{D}_s and \bar{D}_d are average diffusion coefficients determined upon absorption and desorption using equation (39), respectively, then the average \bar{D} value can be approximated as $\frac{1}{2}(\bar{D}_s + \bar{D}_d)$.

Initial rates of absorption and desorption

The average diffusion coefficient can also be determined from the initial slope of the sorption curve (when it has a linear part) [121]. At early stages, $t \rightarrow 0$, equation (33) becomes:

$$\frac{M_t}{M_\infty} = \frac{4}{\sqrt{\pi}} \left(\frac{Dt}{l^2} \right)^{\frac{1}{2}} \quad (40)$$

Plotting the relative mass uptake rate, $\frac{M_t}{M_\infty}$, as a function of $(time)^{1/2}$, the slope of the initial linear part of the graph is equal to $\frac{4}{\sqrt{\pi}} \left(\frac{D}{l^2} \right)^{\frac{1}{2}}$ and the value of the average diffusion coefficient can be estimated.

Another possible method of analysis is plotting $\frac{M_t}{M_\infty}$ versus $\left(\frac{t}{l^2} \right)^{1/2}$. Then the initial gradient

$R = \frac{d\left(\frac{M_t}{M_\infty}\right)}{d\left(\left(\frac{t}{l^2}\right)^{1/2}\right)}$ can be estimated and the average diffusion coefficient value is determined as:

$$\bar{D} = \frac{\pi}{16} R^2 \quad (41)$$

These two approaches, based on our experience, yield the same results for diffusion coefficient values. However, these values might be different from those obtained using equation (39). The reason is that the assumption of a linear sorption curve is not always valid for $M_t/M_\infty = 0.5$.

Chapter 3

Thickness Dependence of the Diffusivity and Solubility of Cyclohexane in Nanoscale Bitumen Films

3.1 Abstract

Diffusivity and solubility of cyclohexane in nanoscale bitumen films coated on hydrophilic substrates at ambient conditions was studied using a gravimetric analyzer. Three substrates were used and they were Sample A – monodisperse spherical glass beads, Sample B – polydisperse spherical glass beads mixed with polydisperse irregular shape kaolin clay particles, and Sample C – irregular shape residual solids generated from a solvent extraction process of an oil sands ore. All of the above samples had a mean diameter of $150\ \mu\text{m}$. Diffusion coefficients were determined based upon the initial rates of cyclohexane absorption when bitumen coated samples at various amounts (thicknesses) were exposed to a carrier gas with cyclohexane vapors at two levels of relative saturations (RS) and they were found in the range of $10^{-18} - 10^{-16}\ \text{m}^2/\text{s}$. A double-first-order kinetics model fits well to the absorption data, suggesting that there exists a concentration gradient of polar (or nonpolar) bitumen molecules in the nanoscale films. This is because the hydrophilic substrates attract the relatively polar fraction of bitumen molecules to the region close to the substrates and the nonpolar fraction resides in the region near the free surface. As a result, the measured diffusion coefficients exhibited positive thickness dependence when the thickness of the bitumen films was at the nanoscale. The molecules near the substrates tended to diffuse slower than those in the free surface region. However, diffusivity was insensitive to the cyclohexane RS. On the other hand, the measured solubility of cyclohexane in the nanoscale bitumen films exhibited no thickness dependence but strong cyclohexane RS dependence. These results suggest that solubility is not affected by the inhomogeneous

distribution of bitumen molecules in the nanoscale films and that it follows more or less Henry's law.

3.2 Introduction

In a variety of industrial and environmental remediation processes, removal of organic solvent is a necessary step. For example, in the polyethylene industry, for the safety reason, residual solvent in the freshly made polyethylene pellets needs to be removed before they are transported to the customer sites. In typical soil remediation processes, solvent is removed to minimize the negative impact on the environment. Recently, our group has been developing a process that cyclohexane is used to extract bitumen from oil sands ores and this process generates waste materials, hereafter referred to as gangue, that contain mainly solid particles (coarse sand particles and fine clay particles) and a small amount of residual bitumen[86,122,123].

Cyclohexane, which is also in the gangue, needs to be removed for obvious environmental and process economics reasons. The amount of residual bitumen in the gangue is generally in the range of 0.5 – 2 wt%. Despite such a small amount, it was found that the residue bitumen significantly reduces the removal rate of cyclohexane [86] and that one of the rate controlling steps is the diffusion of cyclohexane in the residual bitumen.

Given the amount of bitumen in the gangue, it is interesting to note that the thickness of bitumen film on solid residue could be at the nanometer scale. Interestingly, there are a number of studies suggesting that thermal, mechanical, transport and absorption properties including diffusion coefficient in nanoscale polymer films are thickness dependent[124–133]. This is because for nanoscale films, there exists a near-substrate layer slowing down the rate of diffusion [124]. For example, the effect of substrate chemical structure was evaluated and showed to have an impact on the diffusivity of water in poly (vinyl pyrrolidone) nanofilms [134]. The confinement effect

was also evaluated for the transport of water in thin Nafion films [128]. This led to the speculation that the diffusivity of solvent in nanoscale bitumen films would also be thickness dependent. It was also previously reported that the spontaneous formation of water droplets at the oil/substrate interface might occur in the presence of water or humid environment [135–137]. This effect was not considered in the current study and requires a separate rigorous experimental study.

Nevertheless, experimental studies of the diffusion of organic solvents in bitumen films are scanty. Using a gravimetric technique, Noorjahan *et al.* [42] measured the diffusion coefficients of a couple of solvents in asphaltene (the most polar fraction of bitumen) films. However, the effect of thickness was not evaluated. A couple of previously reported studies attempted to determine the diffusion coefficients of volatile solvents in bulk bitumen and the values for cyclohexane were estimated to be $\sim 3 \times 10^{-12} \text{ m}^2/\text{s}$ [138,139]. Most of the measurements were done on well-defined geometries, plane sheet in particular. Given that gangue particles have irregular shapes, we are interested in studying whether the shape of gangue particles compared to particles with well-defined geometry (e.g., sphere) but with comparable mean diameter would yield different diffusion coefficients. In this regard, we are interested in three samples. The first one is monodisperse spherical glass beads with a diameter of 150 microns. The second sample contains large spherical glass beads and fine, irregular shape kaolin clay particles with an overall mean diameter of 150 microns. The final sample is the gangue with a mean particle size of 150 microns. A gravimetric technique will be used to study the diffusivity of cyclohexane in the aforementioned substrates with different amounts of coated bitumen at ambient conditions. Since solubility can be readily obtained from the experiments, we will report such results as well.

3.3 Theory on the measurement of diffusion coefficient

One of the oldest methods for the experimental determination of diffusion coefficient is based on the rate of uptake of a diffusing component by a plane sheet [105,110,140]. In these experiments, a plane sheet with thickness l is placed in an environment with known ratio of carrier gas to solvent vapor at constant temperature and pressure and the mass change of the plane sheet is monitored as a function of time. The solution for the diffusion equation for this configuration is given by [40]:

$$\frac{M_t}{M_\infty} = 1 - \frac{8}{\pi^2} \sum_{m=0}^{\infty} \frac{1}{(2m+1)^2} \exp\{-D(2m+1)^2\pi^2 t/l^2\} \quad (42)$$

where M_t – mass of vapor absorbed at time t , M_∞ - equilibrium mass of vapor absorbed. When the value of $\frac{M_t}{M_\infty}$ is equal to 0.5 which occurs at the initial stage in many cases, equation (42) can further be approximated as follows:

$$\left(\frac{t}{l^2}\right)_{1/2} = -\frac{1}{\pi^2 D} \ln \left\{ \frac{\pi^2}{16} - \frac{1}{9} \left(\frac{\pi^2}{16}\right)^9 \right\} \quad (43)$$

and the diffusion coefficient can be found approximately with:

$$D = 0.049/(t/l^2)_{1/2} \quad (44)$$

It is important to mention that equation (42) is valid under the assumption that as soon as the plane sheet is in contact with the vapor, the concentration at the free surface is equal to the equilibrium concentration (M_∞) and remains unchanged thereafter. This leads to the situation that the mass uptake is linearly proportional to the square root of time at the initial absorption stage.

It has been observed that the initial stage diffusion coefficient can be calculated by plotting the relative mass uptake as a function of the square root of time. At the early stage, the plot has a

linear shape and thus the initial stage constant diffusion coefficient can be calculated directly from the slope of the plotted line [110]:

$$\frac{M_t}{M_\infty} = \frac{4}{\pi^{1/2}} \left(\frac{Dt}{l^2} \right)^{1/2} \quad (45)$$

Plotting $\frac{M_t}{M_\infty}$ against $(t/l^2)^{1/2}$ yields the curve that is a straight line at the initial part with the slope R. This slope, R, of a linear part (i.e., the early stage) of the curve can be determined as:

$$R = \frac{d(M_t/M_\infty)}{d(t/l^2)^{1/2}} \quad (46)$$

Then, the early-stage absorption diffusion coefficient at initial time is calculated as:

$$D = \frac{\pi}{16} R^2 \quad (47)$$

It is worth saying that equations (42) to (47) are only valid when the plane sheet has uniform thickness. This can also be applied to the cases that the material is coated on a solid support with well-defined geometries with uniform thickness [105,110,141].

However, films, especially in naturally occurring materials such as oil sands ores, are not always coated on plane sheet geometry and the curvature of film surface might occur. This can bring up a question whether it is reasonable to consider a nanoscale film coated on a micron scale spherical or irregular shape particle as a plane sheet. For instance, when a film has a spherical shape with an internal diameter a and external diameter b , it, hence, has thickness $l = b - a$. The total uptake of the diffusing substance in the spherical wall is given by Crank [105]:

$$\frac{M_t}{M_\infty} = 1 - \frac{6}{\pi^2(a^2+ab+b^2)} \sum_{n=1}^{\infty} \left(\frac{b \cos n\pi - a}{n} \right)^2 \exp\{-Dn^2\pi^2 t/(b-a)^2\} \quad (48)$$

For the case of diffusion through the spherical wall the amount travelling through the spherical surface is:

$$\frac{Q_t}{4\pi ab(b-a)c_1} = \frac{Dt}{(b-a)^2} - \frac{1}{6} - \frac{2}{\pi^2} \sum_{n=1}^{\infty} \frac{(-1)^n}{n^2} \exp\{-Dn^2\pi^2 t/(b-a)^2\} \quad (49)$$

However, according to Crank [105], the case when $\frac{b}{a} = 1$ is defined as a plane sheet, and $b/a \geq 4$ is a hollow sphere, so it does not seem unreasonable to consider the bitumen nanoscale films used in the present work which had thicknesses below 1.25 microns as plane sheets since b/a is approximately 1 due to the fact that the spherical particle size used as a solid support is orders of magnitude larger than the film thickness. Regarding the irregular shape particles, when their size dimensions were converted into an equivalent diameter using the concept of sphericity, such particles also satisfied the above plane sheet requirement.

3.4 Results and discussions

SEM

Scanning electron microscopy images of Samples A, B and C before and after bitumen coating are shown in Figure 3-1a, 3-1b, and 3-1c respectively. Since the thicknesses of the bitumen films and the size of the particles differ by orders of magnitude, it is impossible to see the bitumen films, which are in the nanoscale in these images. However, given the uniform coating achieved on similar particles, it was assumed that the bitumen film was evenly coated on all samples. As can be seen in Figure 3-1(b), after bitumen coating, some fine clay particles in Sample B attach to the surface of large sand particles. Figure 3-1(c) clearly shows that the shape of the particles in Sample C is irregular. Although bitumen may not be coated uniformly on the edges of such particles, it is also assumed that the film thickness is uniform in order to calculate the corresponding diffusion coefficients.

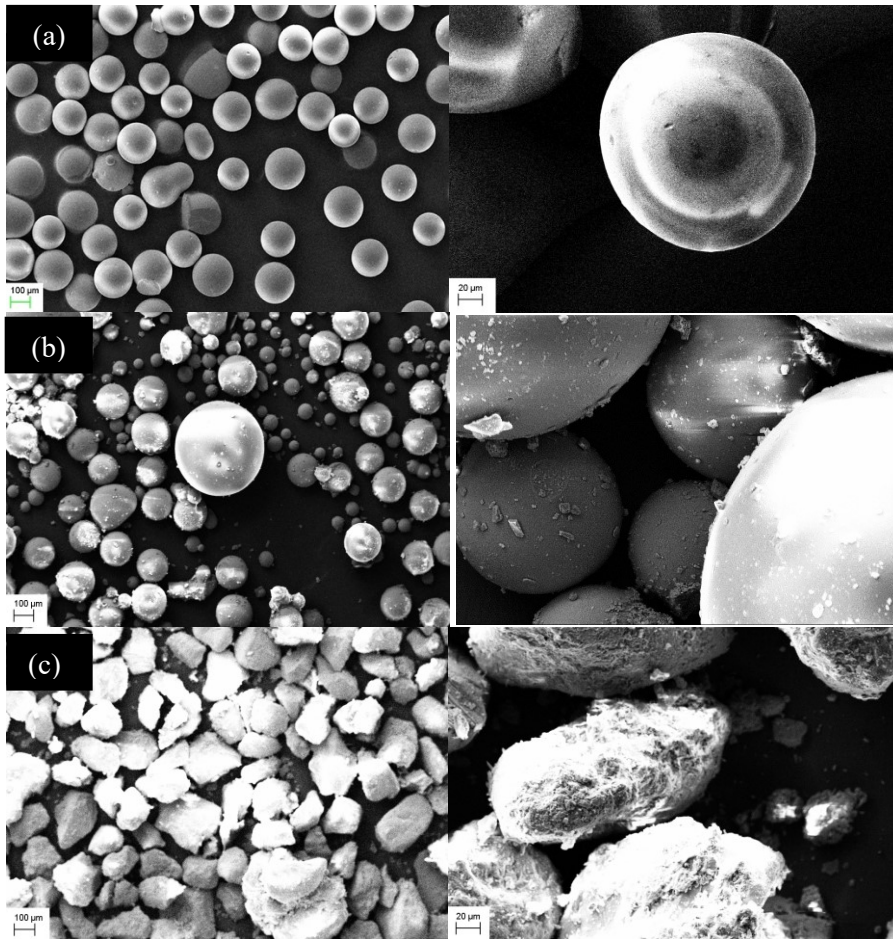


Figure 3-1: SEM images. Left images represent the particles before coating (scale bar = 100 μm); right images show the particles after coating (scale bar = 20 μm): (a) – Sample A; (b) – Sample B; (c) – Sample C

CHNS Analysis

The CHNS analysis was used to determine the actual amount of coated bitumen on the samples.

The results are shown in Table 3-1.

Table 3-1. Amount of bitumen coated on various substrates (wt%). ^a Soxhlet solids after the Dean Stark extraction with no bitumen added (the sample still contains a small amount of residual bitumen), n = 5

Sample A	0.20 ± 0.02
	0.74 ± 0.04
	1.10 ± 0.07
	1.14 ± 0.10
	2.23 ± 0.65
Sample B	0.11 ± 0.01
	0.54 ± 0.04
	0.88 ± 0.11
	0.98 ± 0.12
	2.55 ± 0.69
Sample C	0.62 ± 0.09^a
	0.78 ± 0.00
	1.01 ± 0.19
	1.86 ± 0.10
	2.06 ± 0.12

In general, the mass of the bitumen actually coated on the particles was approximately half of the bitumen that was initially used for the coating process. This is attributed to the unavoidable loss of bitumen that coated on the walls of glassware. However, the range of the bitumen actually coated (i.e., 0.5-2 wt%) corresponds to that observed in gangue obtained from the solvent extraction process [142]. The “average thickness” of each sample was calculated as thickness on particles of each mass fraction “weighted” against the total surface area of the sample calculated based upon the surface area of particles in each mass fraction. The details of the average thickness calculations are given below.

To calculate the thickness of Sample A, we first estimated the number of glass beads: based on spherical geometry the volume of one particle was calculated. Then the mass of one particle was found as a product of volume and borosilicate density. To estimate the total amount of particles in monodisperse sample the total sample mass was divided by the mass of one particle. The mass

of bitumen on each glass bead was determined based on the assumption that bitumen was evenly distributed among the glass beads. Using the estimated mass of bitumen on each particle (from the bitumen content analysis) and known bitumen density at room temperature, we then calculated the volume of bitumen on each glass bead (spherical shape), thereby the bitumen film thickness.

In the case of Samples B, the average thickness was calculated as follows: the sample with known average bitumen content was separated based on the particle sizes using four sieves (500 μm , 212 μm , 150 μm , and 45 μm). Then, the average bitumen content was measured on each size fraction using the CHNS analyser, each size fraction sample was repeated five times and the average value was calculated. For instance, for the sample with 0.54 wt% average bitumen content, it was found that the average bitumen content on particles with diameter 500 μm and larger was 0.39 wt%; that with diameter 212 μm was 0.48 wt%; that with 150 μm was 0.61 wt%; and that with 45 μm and smaller was 0.89 wt%. Then, as mentioned before, the average thickness on each size fraction was calculated by finding the volume of bitumen on each glass bead. Using the estimated number of beads of each size in the sample, the total surface area of all beads and the surface area provided by each size fraction of beads were estimated. For instance, it was found that the surface area of beads with size 45 μm and smaller accounted for almost 30% of total surface area of the sample even though the weight fraction of such fine particles was only around 5%. Then, the average thickness weighted by the area fractions was calculated: “surface average thickness” was found as a summation of thickness of bitumen on particles of one size multiplied by the fraction of surface area these particles account for in the total sample area. This procedure was then repeated for the remaining four coating ratios and the average thickness was calculated for each sample.

Similarly, the thickness was estimated for Sample C. However, due to the shape of the particles being irregular, the equivalent diameter was calculated using the sphericity, Φ_s [103], defined as surface-volume ratio of a sphere divided by surface-volume ratio of an irregular particle as given in equation (50):

$$\Phi_s = \frac{s_{sphere}/v_{sphere}}{s_{irregular}/v_{irregular}} \quad (50)$$

Assuming that volumes of particles with the same apparent size (i.e., passed the same sieve) is approximately the same, we end up with:

$$\Phi_s = \frac{s_{sphere}/v_{sphere}}{s_{irregular}/v_{irregular}} \cong \frac{s_{sphere}}{s_{irregular}} \approx \left(\frac{D_{sphere}}{D_{irregular}} \right)^2 \quad (51)$$

Here, D is diameter of the particle. Therefore, as suggested by equation (51), the ratio of diameter of the sphere and its corresponding diameter of irregular shaped particle is equal to the square root of sphericity, which was chosen to be 0.65 (tabulated for crushed glass or flint sands)[103] and the diameter of spherical particle was calculated as a product of irregular shape particle diameter and the square root of 0.65. This means that for the particle with an irregular shape, as in Sample C, the equivalent diameter of the spherical particle is smaller. Calculated thickness values for all samples are summarized and plotted in Figure 3-2.

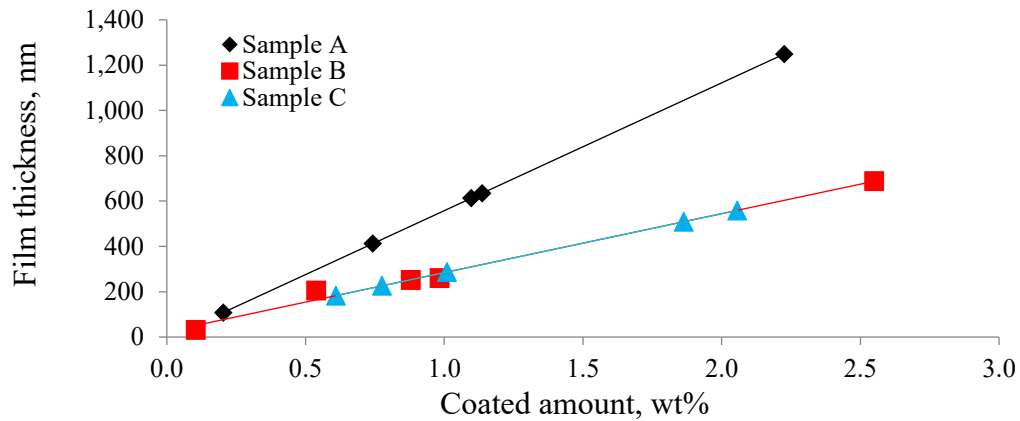


Figure 3-2: Calculated bitumen film thickness based upon the amount of bitumen coated (wt%) on various samples

Gravimetric Absorption Analysis

To determine the diffusion coefficients and solubility of cyclohexane for all fifteen samples, the corresponding absorption curves were obtained. For the illustration purpose, only the absorption curves for Sample A at the lowest and highest bitumen film thicknesses and two cyclohexane RS – 20% and 90% are shown here (see Figure 3-3). The rest of the absorption curves are shown in the Appendix B section (see Figures B1, B2, and B3). As Figure 3-3 shows, the initial rate of absorption (the initial slope), regardless of the RS, decreases with increasing bitumen film thickness and higher cyclohexane RS yields shorter time for reaching equilibrium. The cyclohexane RS dependence is consistent with the concept of Henry’s Law that solubility increases with increasing partial pressure of the solvent involved. However, the first observation deserves some explanation.

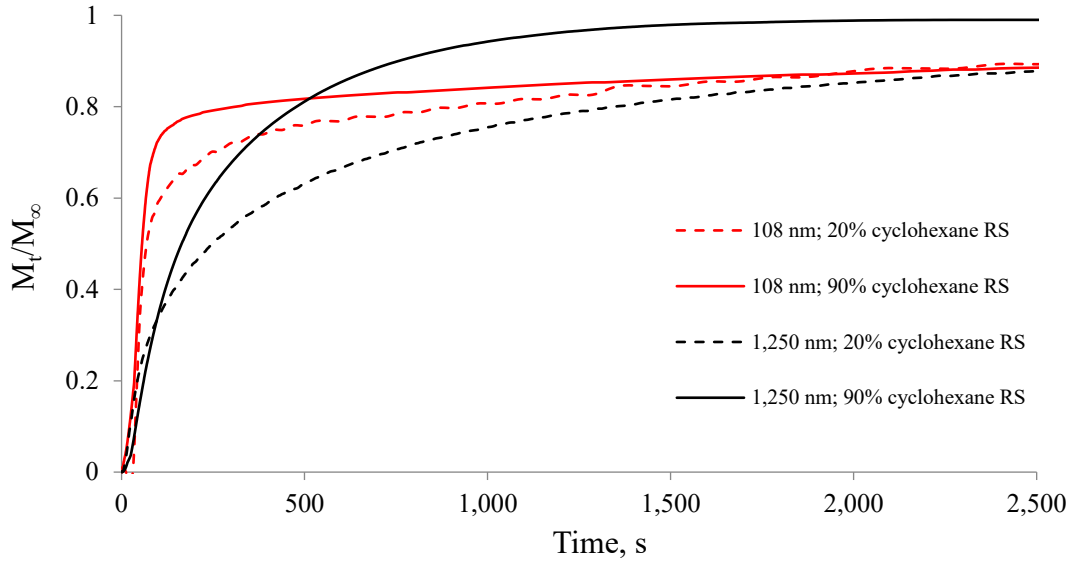


Figure 3-3: Cyclohexane absorption curves of Sample A at two bitumen film thicknesses and two cyclohexane relative saturation

To get insights into the above absorption curves, two models were attempted to fit into the mass uptake data: Weibull relaxation model and double-first-order kinetics model [89,122,126,143]. Weibull model (equation (51)) with a relaxation parameter ζ related to the relaxation time of viscoelastic materials [143,144] was previously found to be a good fit for data for water absorption in polymers:

$$\frac{M_t}{M_\infty} = 1 - e^{-(kt)^\zeta} \quad (51)$$

It appeared that the Weibull model, which assumes only one stage of diffusion, does not fit well to the present experimental data, suggesting that there exists more than one diffusion mechanism involved in the absorption process. On the other hand, the double-first-order (DFO) kinetics model (equation (52)) shows a much better fit of the experimental data which suggests that there are two kinetic mechanisms involved in the uptake of cyclohexane by the nanoscale bitumen film:

$$\frac{M_t}{M_\infty} = (1 - \phi)(1 - \exp(-k_1 t)) + \phi(1 - \exp(-k_2 t)) \quad (52)$$

Here, ϕ is the mass fraction of the bitumen in which diffusion takes place by the first mechanism, k_1 and k_2 represents the rates of the mass uptake at the initial and final stages of absorption, respectively. The fitting was done to all samples. Fitting of DFO kinetics model to all samples is shown in Figure B4 in the Appendix B section. For convenience, only the lowest and the highest bitumen film thicknesses for Sample A are shown. Figure 3-4 shows the DFO kinetics model fit into the experimental data. Black lines represent experimental data while the red lines are those for the DFO kinetics model.

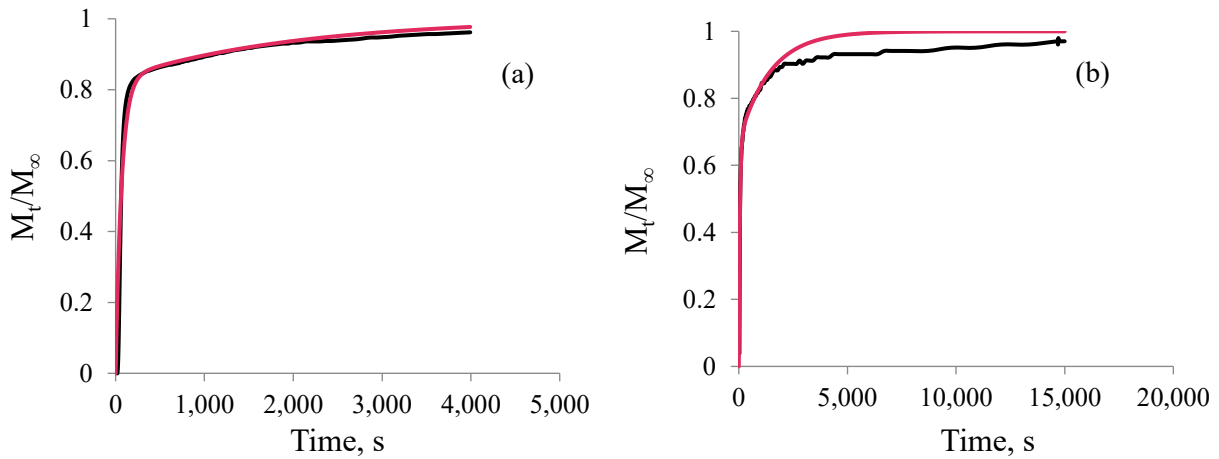


Figure 3-4a: Fitting of the double-first-order kinetics model into the absorption data for Sample A with 108 nm film thickness: (a) – 90% cyclohexane saturation; (b) – 20% cyclohexane saturation. Black curves signify experimental data

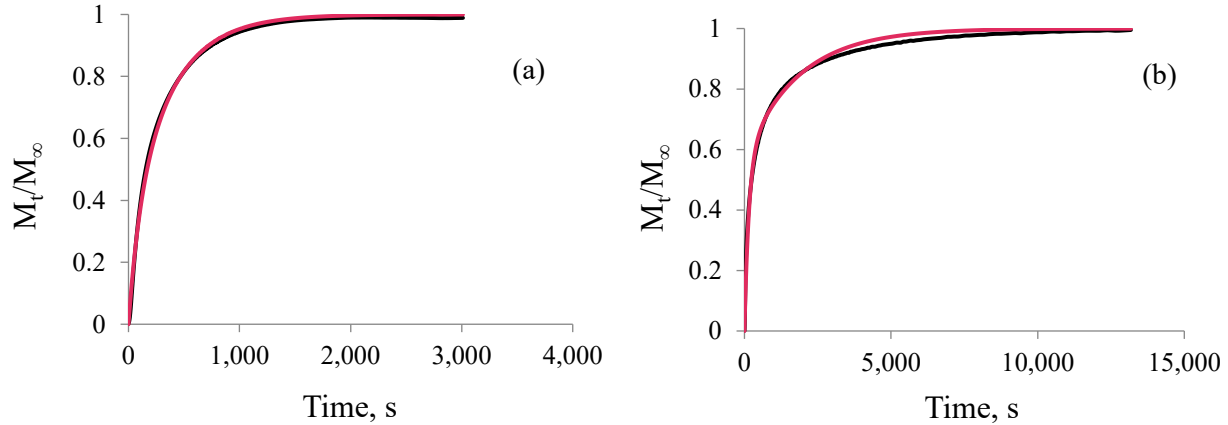
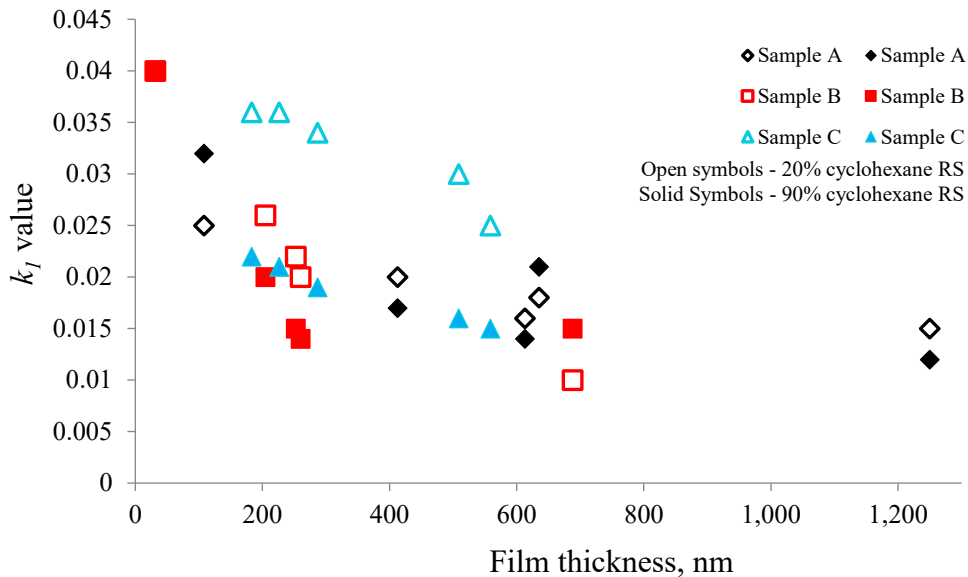


Figure 3-4b Fitting of the double-first-order kinetics model into the absorption data for Sample A with 1,250 nm film thickness: (a) – 90% cyclohexane saturation; (b) – 20% cyclohexane saturation. Black curves signify experimental data

All k_i values for fitted absorption curves of Samples A, B and C are respectively summarized in Tables B1, B2, and B3 of the Appendix B section and are plotted in Figure 3-5. All k_i values plotted as a function of thickness in one plot are shown in Figure B5. It is clear from Figure 3-5 that k_1 (initial absorption rate) decreases while k_2 (final absorption rate) increases with increasing bitumen film thickness. Since the initial dissolution rate is used to determine the diffusion coefficients, let us explore the thickness dependence of k_1 . First, it is worth pointing out at the outset that bitumen is a chemically inhomogeneous material. Bitumen consists of four class fractions, namely saturates, aromatics, resins and asphaltenes (known as SARA in the petroleum industry) [44]. For example, bitumen used in the present work contains by weight about 10.3% saturates, 5.3% aromatics, 62.3% resin and 22.2% asphaltenes. And such fractions exhibit a range of polarity with the asphaltenes fraction being the most polar. Given that substrates used in this work is hydrophilic, it is believed that most polar molecules (e.g., asphaltenes) are attracted to the substrate surfaces while the relatively nonpolar molecules (e.g., saturates) tend to reside in regions near the free surface. This naturally generates a concentration gradient of polar (or nonpolar) molecules in the film thickness direction. It should be emphasized that the

concentration gradient does not signify a phase separation from a thermodynamics perspective. Since k_1 is the largest for the thinnest film and cyclohexane is nonpolar, the thickness dependence of k_1 suggests that the concentration of nonpolar molecules near the free surface regions of the thinner bitumen films is higher than those of the thicker bitumen films. On the other hand, the concentration of polar molecules near the substrate surface of thinner bitumen films should be higher than those of the thicker films. This leads to a slightly positive thickness dependence of k_2 . This is because the dissolution process taking place in the final stage involves the dissolution of cyclohexane into a relatively polar environment in the region near the substrate surface.



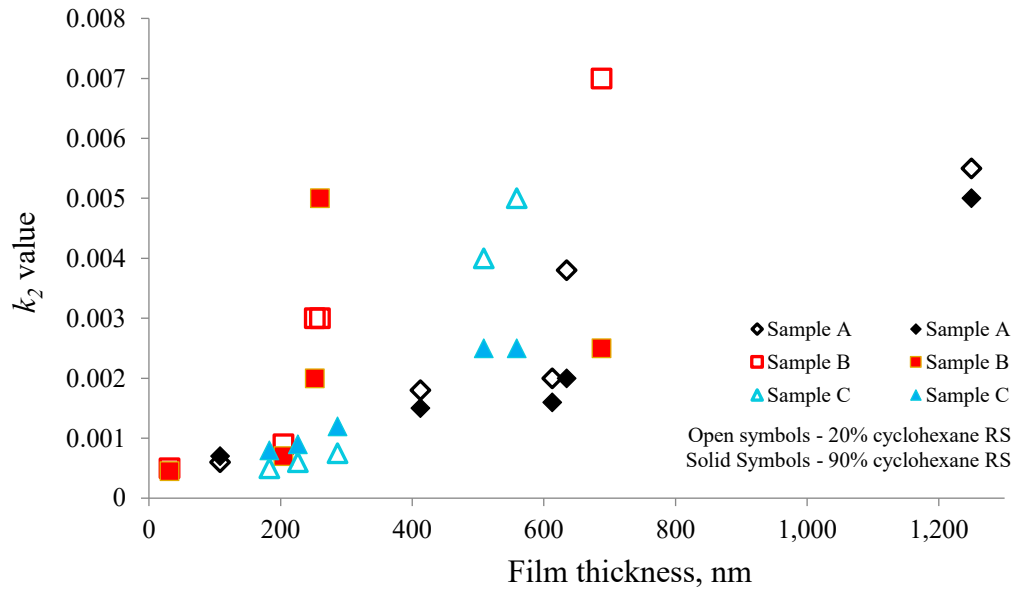


Figure 3-5: Rate constants k_1 and k_2 as determined by fitting the double-first-order kinetics model to the absorption curves of all samples

The average diffusion coefficients and the equilibrium solubility of cyclohexane at different bitumen film thicknesses are shown in the Appendix B section (see Tables B4, B5, and B6). The results are also plotted against bitumen film thickness and are shown in Figures 3-6 and 3-7.

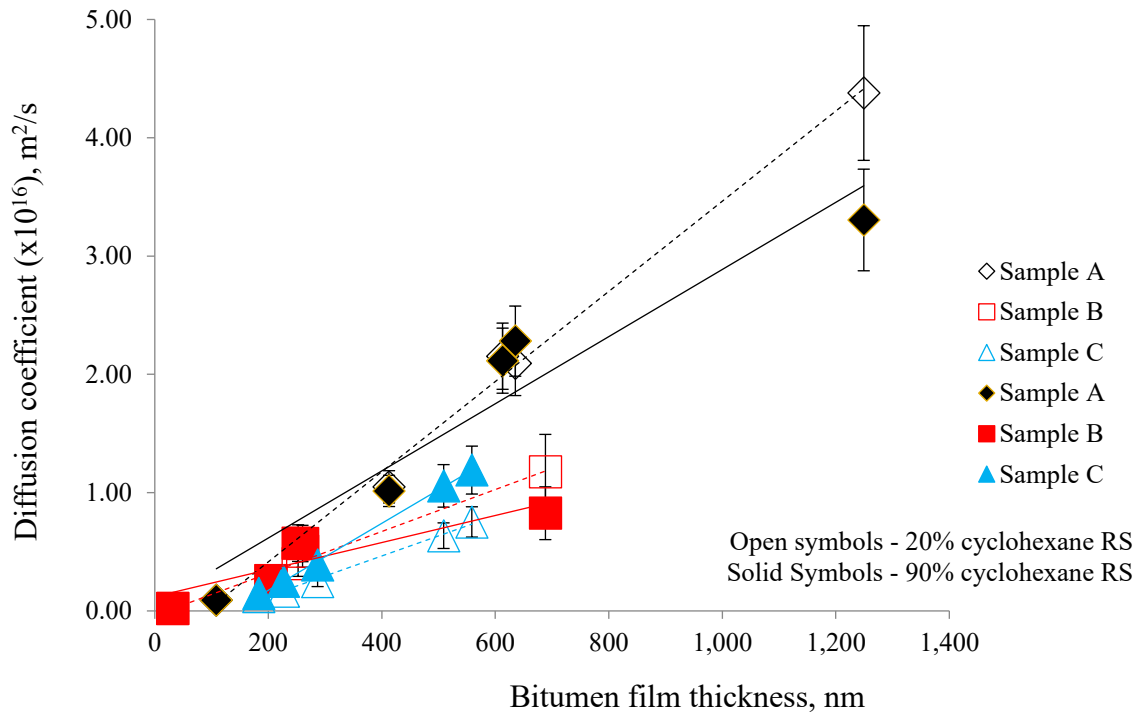


Figure 3-6: Absorption diffusion coefficient of cyclohexane in bitumen: solid symbols indicate cyclohexane relative saturation 90%, open symbols – 20% cyclohexane relative saturation; Sample A – black; Sample B – red; Sample C – blue

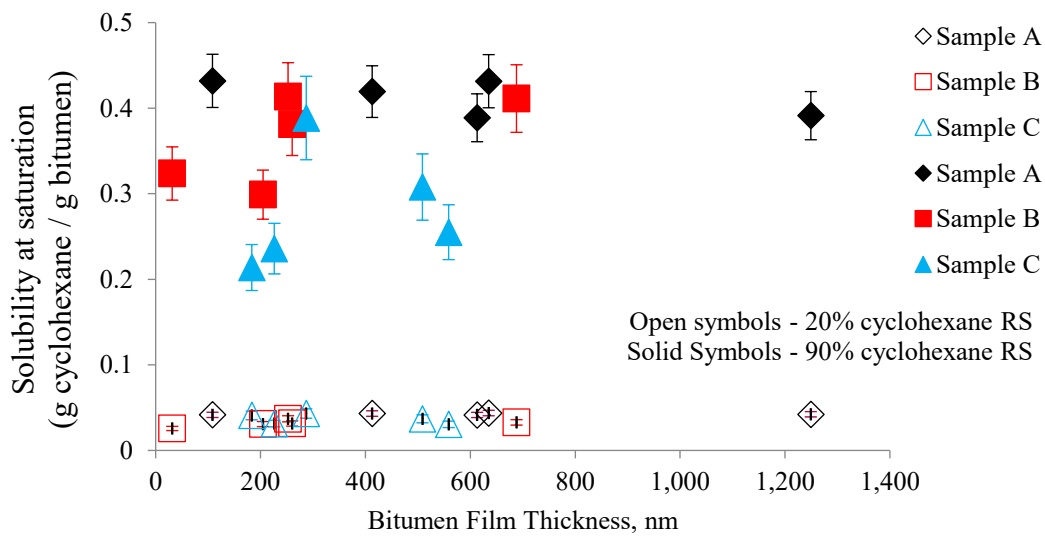


Figure 3-7: Solubility of cyclohexane in bitumen: solid symbols indicate cyclohexane relative saturation 90%, open symbols – 20% cyclohexane relative saturation; Sample A – black; Sample B – red; Sample C – blue

Obviously, the measured diffusion coefficient exhibits thickness dependence but essentially no RS dependence while the solubility data exhibits the opposite behavior. Let us discuss the diffusivity behavior first. Unlike the observed thickness dependence of k_1 , diffusion coefficient increases with increasing bitumen film thickness. According to equation (45), the one we used to determine the diffusion coefficient, which shows explicit positive thickness dependence.

However, there is also an indirect thickness dependence term in the equation and that is the mass uptake term. The mass uptake term (M_t/M_∞), as quantified by k_1 , exhibits a negative thickness dependence. Such opposite thickness dependence in equation (4) suggests that when a film is very thick (k_1 becomes relatively small), the diffusion coefficient would be thickness independent as observed experimentally [125]. However, when the bitumen film thickness is at the nanoscale (i.e., k_1 becomes relatively large and is in the order of 10^{-2}), the diffusion coefficient shows an overall positive thickness dependence.

The above discussion alludes that the substrate chemical properties could affect the diffusion in nanoscale bitumen films. This speculation was reported for polymer films [125,134]. Despite both polymers [125] and bitumen exhibited the thickness dependence effect, the underlying molecular mechanisms may be different. First, polymers are chemically homogeneous substances while bitumen is not. Unlike the case of polymers, diffusion of cyclohexane in bitumen is a complex process that takes place in a mixture of chemically different species. Secondly, the molecular weight of polymers is significantly higher than the molecular weight of bitumen (up to hundreds of thousands of Daltons versus up to only hundreds of Daltons for bitumen).

The measured diffusion coefficient appeared to be dependent on particles size distribution (Figure 3-6). At a given thickness, the measured diffusion coefficient of Sample A was higher

than that in Samples B and C. The effect is more pronounced at high film thickness. This is due to the fact that the average thicknesses of Samples A, B and C were different with Sample A having the thickest films.

As the calculations show, the measured diffusion coefficients are of the order of $\sim 10^{-16}$ m²/s which indicates an extremely slow diffusion process. However, such slow rates of diffusion were previously reported by Kokes and Long [145] in their study of organic vapors diffusion in polyvinyl acetate. In that study, the diffusion coefficients were estimated to be 0.48×10^{-16} m²/s and 1.3×10^{-15} m²/s for benzene and acetone, respectively. Kokes and Long attributed such observation to the strong interactions present in the systems as quantified by the Flory-Huggins interaction parameters. The evaluation of the Flory-Huggins interaction parameters might be also informative for further understanding of the solvent-bitumen interaction of our systems.

Unlike the diffusion coefficient, the solubility did not exhibit thickness dependency but showed a strong cyclohexane RS dependence. The cyclohexane RS dependence seems to be consistent with the concept of Henry's Law that solubility increases with increasing partial pressure of the solvent involved [146]. However, in this work, it is not sure whether such dependence is linear or not as only two RSs were used. While the saturation concentration values seem to be almost the same for all three samples at 20% cyclohexane RS, the results for 90% RS seem a bit more disperse, in particular, Sample C exhibits slightly lower values. There is no obvious reason for it; however, we believe that this might be due to the irregular shape geometry of the particles in Sample C. The irregularity of the shape might create capillaries impermeable for cyclohexane but still containing some bitumen accounted for in thickness calculations.

3.5 Conclusion

In this study, the thickness dependence of the diffusivity and solubility of cyclohexane in nanoscale bitumen thin film coated on particles with different shapes and size distribution was studied at ambient conditions using a gravimetric technique. A good fitting of the double first order kinetics model to the experimental data suggested that there existed a concentration gradient of polar (or nonpolar) bitumen molecules in the film thickness direction with higher concentration of more hydrophilic molecules near the hydrophilic substrates (slower diffusion) and more hydrophobic molecules near the free surface (faster diffusion). This led to the observation of the thickness dependence of diffusion coefficient in nanoscale bitumen films. The diffusion coefficient was observed to increase with increasing thickness of the bitumen film. It appeared that relative saturation of cyclohexane in vapor phase had no effect on measured diffusion coefficient. Monodisperse particles (Sample A) yielded higher diffusivity compared to the polydisperse particles (Samples B and C). This is because the mean bitumen film thickness of Sample A was higher than those of Samples B and C. The measured values of diffusion coefficients at the initial absorption stages were found to be in the range of $10^{-18} - 10^{-16} \text{ m}^2/\text{s}$. Unlike diffusion coefficient, the saturation concentration of cyclohexane in nanoscale bitumen films appeared to have no thickness dependence; however, a strong relative cyclohexane vapor saturation dependence was observed. The solubility of cyclohexane in bitumen films was not affected by the concentration gradient present in the nanoscale films but only by the partial pressure of cyclohexane in the carrier gas.

3.6 Experimental section

Materials

The gangue was collected after the non-aqueous extraction (Dean-Stark extraction) described elsewhere in literature [142] using oil sands rich grade ore that was provided by Imperial Oil. The ore contained $11.5 \pm 0.6\%$ bitumen content by weight. ACS certified cyclohexane was purchased from Fischer Chemical. Spherical borosilicate glass beads (standard sizes: 425-600 μm , 150-212 μm , $\leq 160 \mu\text{m}$) were purchased from Sigma Aldrich, U.S.A. Standard test sieves no. 35, 70, 100 were purchased from Fischer Scientific, U.S.A. standard testing sieve no. 325 was purchased from Advantech Manufacturing. Pure kaolin clay (irregular shape clay particles) with size $<45 \mu\text{m}$ was purchased from ACROS Organics. Nitrogen, the carrier gas, was purchased from Praxair (99.999% purity).

Samples Preparation

As mentioned, three types of particles were of interest in the present work and they were all coated with bitumen at various bitumen-particles weight ratios: Sample A – monodisperse spherical glass beads with a size of 150 μm , Sample B: polydisperse spherical glass beads (600 μm – 45 μm) were mixed with fine ($<45 \mu\text{m}$) glass beads and fine kaolin clay ($<45 \mu\text{m}$) particles. Fine kaolin clay to fine glass beads weight ratio was 45:55 respectively. As in the original gangue the mean particle size by weight in Sample B was 150 μm . Sample C – reconstituted gangue composed of irregular shape particles with a mean diameter of 150 μm by weight.

Sample A

The purpose of preparing Sample A is to create a reference sample containing monodisperse particles with spherical geometry that represents the gangue particles. Considering the fact that

gangue contains essentially particles with irregular shape and that the concept of sphericity is used to quantify their size, we decided to use spherical particles as the reference particles [103].

Given that the weight average diameter of the real gangue sample was approximately 150 μm , spherical borosilicate glass beads with a diameter 150 μm (monodisperse) and a particle density 2.26 g/cm^3 were used. Figure 3-8 shows two glass beads with a diameter of 3 mm with and without coated bitumen. The coated glass bead had approximately 0.2 wt% of bitumen. The coating was carried out using a rotary evaporator Heidolph Hei-VAP Core. Bitumen was first dissolved into cyclohexane and the solution with concentration of 0.05 g bitumen/1 mL of cyclohexane was mixed with glass beads (monodisperse) in a round flask so that the calculated mass of bitumen was 0.5 wt% of the mass of glass beads. The round flask was connected to the aforementioned rotary evaporator so that the cyclohexane was slowly evaporated. The evaporation of solvent was carried out at a speed of 40-60 rpm and 55 °C for approximately 6 hours followed by the vacuum drying at 60 °C for four hours. The reason for using rotary evaporator was that bitumen films with uniform thickness would be obtained. This was previously achieved in our lab by using the rotary evaporator for coating on glass beads [147].

Thickness was controlled by varying the amount of bitumen solution added to each sample before rotary evaporation. For a given sample of particles, at the start, we arbitrarily added 1 mL of bitumen solution to it. After the rotary evaporation and vacuum oven conditioning, the amount of bitumen settled on the particles was calculated (mass difference before and after). After the thickness was calculated as described below, we estimated the amount of bitumen solution needed to be added to achieve the desired range of thicknesses.

The CHNS analysis was later done to determine the actual mass of bitumen coated. Nonetheless, it appeared that the bitumen was evenly coated on the entire glass bead.



Figure 3-8: A bare spherical glass bead with a diameter of 3 mm (right) and a similar sized glass bead coated with a layer of bitumen (left) using a rotary evaporator. The amount of coating was ~ 0.2 wt% or ~ 1 μm thick.

Sample B

This sample was composed of two broad classes of particles. They were spherical borosilicate particles ($45\ \mu\text{m} - 600\ \mu\text{m}$) and fine particles ($<45\ \mu\text{m}$) made up of fine kaolin clay mixed with fine glass beads [40,142]. To mimic the gangue characteristics, for Sample B, we mixed the aforementioned types of particles with a particle size weight distribution and weight average diameter similar to those of real gangue. To do so, we mixed borosilicate glass beads of various sizes, $45\ \mu\text{m}$ to $600\ \mu\text{m}$ (glass beads were also sieved to separate them by size) using the same weight ratios of different sizes as found in gangue and given in Table 3-2. For the fine particles, 55% of the required amount was “modeled” by the glass beads with less than $45\ \mu\text{m}$ diameter and the rest 45% was “modeled” by using fine kaolin clay particles. The ratio 55:45 was used from the previously reported fine particles composition [40]. Kaolin clay was sieved on a $45\ \mu\text{m}$ sieve and the clay particles passed the sieve were collected and used as the model of fine particles which are reported to clays, predominantly kaolin. The coating procedure was the same as that was used for Sample A. Again, SEM imaging and CHNS analysis were done for the sample characterization.

Sample C

The residual solids after the Dean Stark procedure was divided in small portions, placed on weigh dishes, and left overnight in a fume hood. After drying in a fume hood, the gangue was

placed into a vacuum oven at 60 °C for 4-6 hours to remove any traces of solvent that could have potentially left in the residual solids. The vacuum dried gangue was then collected and sieved through four standard testing sieves (500 µm, 212 µm, 150 µm, and 45 µm). The approximate size distribution by weight is given in Table 3-2 and the corresponding weight average diameter was calculated. One noteworthy point is that the Dean Stark procedure did not remove all bitumen (Table 3-1).

Table 3-2. Particle size distribution of the gangue

Size	wt%
>500 µm	7.4
500 µm >...>212 µm	11.3
212 µm >...>150 µm	50.5
150 µm >...>45 µm	25.1
<45 µm (fines)	5.7

The same coating procedure as used for Sample A was used. The resultant sample was subjected to SEM and CHNS analysis.

Experimental Methods

Scanning Electron Microscopy

SEM images were obtained on a Zeiss Sigma Field Emission – Scanning Electron Microscope (FE-SEM). The beam voltage was set to 10 kV and the working distances were in the range of 5-15 mm. An in-lens detector was used.

CHNS Analysis

A Thermo-Scientific Flash 2000 CHNS/O Analyzer was used to determine the bitumen contents of all samples. For each sample (i.e., Samples A, B and C), there were five bitumen contents

prepared. As a result, there were a total of fifteen samples. For each sample, the bitumen content measurement was repeated five times and the corresponding average value is reported.

Gravimetric Absorption Analysis

Mass uptake was measured using the Hiden Isochema intelligent gravimetric analyzer (IGA). The experiment setup and operation protocols are described elsewhere [42]. Figure 3-9 shows a schematic setup for the instrument. The temperature of experiments was set to 25 °C. The temperature was chosen to be as close as possible to the normal ambient temperature and at the same time high enough to avoid condensation of cyclohexane on the sample surface. The pressure was set to the atmospheric pressure 1 atm. Both temperature and pressure were controlled throughout the entire experiment. The temperature was controlled by a water bath temperature controller. First, the sample was subjected to an 8-hour conditioning when the sample was retained in a carrier gas (N₂) environment at constant flowrate 100 mL/min to remove any residual volatile compounds and impurities before the experiment as suggested by previous observations and experiments [42]. Then in the next step cyclohexane was introduced into the carrier gas stream at a RS of interest (20% or 90%) one value of RS at a time. This was done to compare if there could be any variations in the diffusion coefficients in low and high RS cases. 20% and 90% RS were limited by the instrumentation to avoid condensation. Change of mass of the sample, which was measured by a microbalance with accuracy of $\pm 0.1 \mu\text{g}$ was monitored as a function of time. All experiments were repeated at least three times.

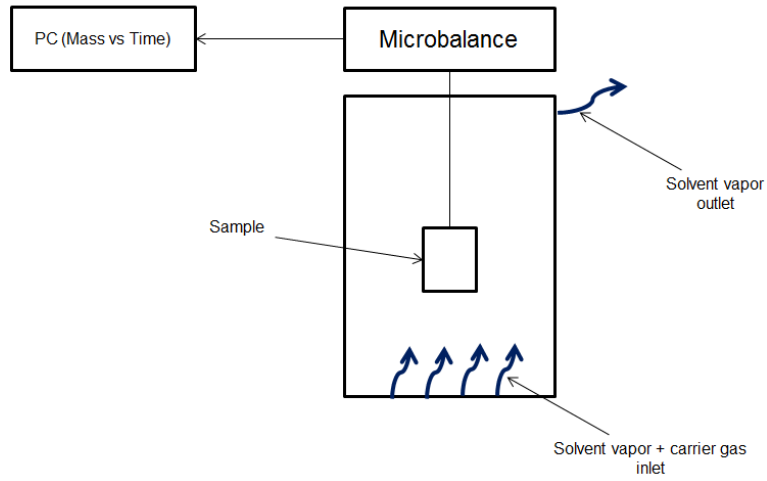


Figure 3-9: Schematic representation of an IGA system

Chapter 4

Initial mass uptake dynamics and diffusivity of cyclohexane vapor in nano-scale bitumen films coated on substrates with different degrees of hydrophilicity

4.1 Abstract

Absorption of cyclohexane vapor into thin bitumen films with 0.5 wt% and 2 wt% bitumen coated on samples containing large spherical particles made up of borosilicate glass and fine particles with different chemical compositions (borosilicate glass versus kaolin clay) was studied using a gravimetric technique. Samples containing glass fines and clay fines are denoted as SA and SB, respectively. Fines refer to the particles with sizes less than 45 μm and their concentration varied from 5 to 20 wt% in SA and SB. The results clearly showed that the chemical composition of the fines significantly affected the cyclohexane initial mass uptake rate and that this rate exhibited a negative bitumen content dependence with the dependence of SA much stronger than that of SB. This is because glass (SA samples) is much more hydrophilic than clay (SB samples). As a result, SA rendered a stronger concentration gradient of the polar bitumen molecules in the film thickness direction than SB, thereby stronger negative bitumen content dependence. Diffusion coefficients were estimated using the cyclohexane initial uptake rates and the surface area average film thicknesses of the samples and were found that the diffusion coefficient increased with increasing bitumen content (i.e., film thickness) in both SA and SB cases. Varying fines content did not have any effect on the cyclohexane initial mass uptake rate. It was found that increase in the fines content decreased the bitumen film thickness, thereby decreasing the diffusion coefficient that is offset by the increase in the amount of cyclohexane dissolved at the interface.

4.2 Introduction

Removal of organic solvents from products and waste streams is an important step in many manufacturing processes from economic and environmental points of view. Over the past couple decades, there has been a renewed interest in a process that uses cyclohexane for the extraction [86] of bitumen from oil sands ores [40,148]. A simplified version of such a non-aqueous extraction process is given in Figure 4-1.

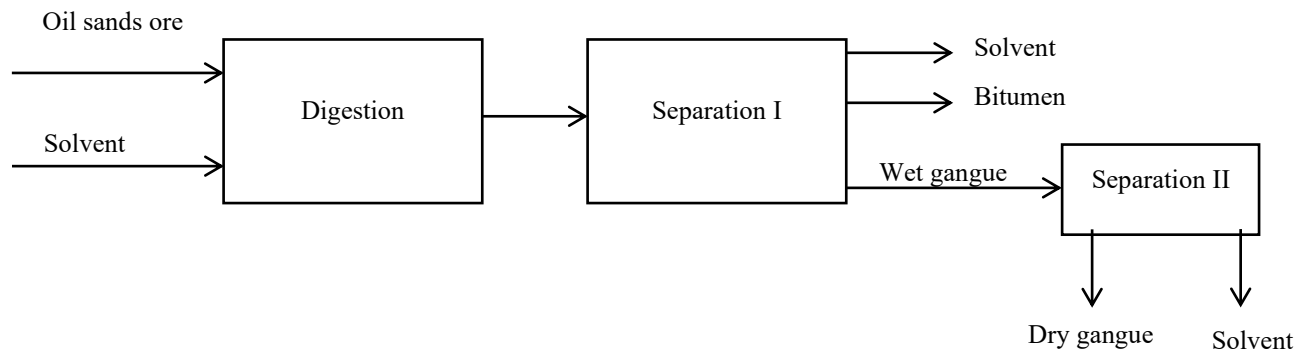


Figure 4-1: Schematic flow chart of a non-aqueous bitumen extraction process.

Here, the crushed oil sands ore is mixed with the solvent in a digester to allow the dissolution of bitumen into the solvent. The mixture of bitumen solution and solid particles are then fed into the first set of separators where the separation of all the fractions occurs resulting in the three streams: liquid solvent, bitumen, and so-called wet gangue. The wet gangue essentially contains liquid solvent and a small amount of residual bitumen entrapped within the pores in between the solid particles. The wet gangue is then fed to the second separation unit to recover more solvent and the reject stream is so-called dry gangue. The dry gangue typically contains about 0.5 – 2 wt% of residual bitumen and 0.1 – 0.5 wt% solvent [12,40].

The reason that non-aqueous extraction process has not yet been commercialized is that it generates a significant amount of dry gangue (referred to as ‘gangue’ hereafter). For obvious environmental reasons, such gangue cannot be deposited back into the mining sites due to high concentrations of cyclohexane. It is believed that a successful solvent recovery process needs to reduce the concentration of the solvent down to at least 260 ppm[42]. It is also economically beneficial to recover as much solvent as possible for further recycle and reuse in the same process.

The transport of solvent trapped within the gangue is a complex phenomenon; in the initial stage, or wet gangue, it involves the transport of liquid solvent through the pores to the sample surface due to capillary action and then evaporation at the surface. In the later stage (i.e., dry gangue), it involves the diffusion of the solvent vapor in the residual bitumen and then through the pores in the gangue to the gangue surface.

In our previous work [149], we evaluated the effect of the thickness of nano-scale bitumen film (i.e., bitumen wt% in the gangue) on the initial mass uptake rate and diffusion coefficient of cyclohexane in three types of samples: monodisperse spherical glass beads, polydisperse glass beads mixed with kaolin clay, and the actual dry gangue collected from the non-aqueous extraction process. We found that the initial mass uptake rate decreases with increasing bitumen content (film thickness) while the diffusion coefficient appears to increase with increasing film thickness. These observations led to the speculation that the mass transport of cyclohexane in bitumen nano-scale films is affected by the chemical composition of substrate material that the film is coated on. The subject was previously studied for polymers [89,125,127,134] and the results showed a correlation between sorption rates and the chemical properties of substrates.

However, to the authors' knowledge, the matter was not investigated for heterogeneous materials such as bitumen.

In the present work, the main focus was to evaluate whether the chemical properties of polydisperse substrates and the fines content would affect the initial solvent uptake or absorption rate and the corresponding diffusion coefficient. For the current experiments, we used a gravimetric technique to examine the mass uptake rate and determine the corresponding diffusion coefficient values in two samples: each one with chemically different types of fine particles, various fines contents, and different amounts of bitumen.

4.3 Theory

The simplest situation of gravimetric mass uptake of solvent vapor into the sample is the Fickian model. Fickian diffusion process mathematically can be expressed with the equation (53):

$$\frac{\partial c}{\partial t} = D \frac{\partial^2 c}{\partial x^2} \quad (53)$$

where D is the diffusion coefficient, c is the concentration, and x is the space coordinate.

The analytical solution of the equation (53) is derived by Crank (equation (54)) and given as [105,124,150]:

$$\frac{M_t}{M_\infty} = 1 - \frac{8}{\pi^2} \sum_{n=0}^{\infty} \frac{1}{(2n+1)^2} \times \exp\left[\frac{-D(2n+1)^2\pi^2 t}{l^2}\right] \quad (54)$$

where M_t and M_∞ are total masses of solvent absorbed into the sample at time t and at equilibrium, respectively. For a short period of time, equation (54) can be written in the form of equation (55):

$$\frac{M_t}{M_\infty} = \frac{2D^{1/2}}{l} \sqrt{t} \left[\frac{1}{\sqrt{\pi}} + 2 \sum_{n=1}^{\infty} (-1)^n \operatorname{ierfc} \frac{nl}{\sqrt{Dt}} \right] \quad (55)$$

Here, t is the time, and l is the thickness of the film. So, equation (55) at early stages for a constant D can further be approximated to equation (56)

$$\frac{M_t}{M_\infty} = \frac{4}{\sqrt{\pi}} \frac{D^{1/2}}{l} \sqrt{t} \quad (56)$$

In equation (56), if $\frac{M_t}{M_\infty}$ is plotted against $\left(\frac{t}{l^2}\right)^{1/2}$, the diffusion coefficient can be determined using equation (57) at the initial sorption stage as [105,110,150]:

$$D = \frac{\pi}{16} R^2 \quad (57)$$

where R is:

$$R = \frac{d(M_t/M_\infty)}{d(t/l^2)^{1/2}} \quad (58)$$

Here, R is the slope of the linear part of sorption curve at initial time period. As shown in equations (57-58), diffusion coefficient depends on the film thickness and the initial slope of the linear part of absorption curve that reflects the rate of mass uptake of solvent vapor by the bitumen film. Although, diffusion of cyclohexane exhibits a non-Fickian behaviour, the approach of estimation of diffusion coefficient at the initial stage and constant diffusion coefficient based on Fickian diffusion is widely accepted by the scientific community [89,151–154]

4.3 Materials and methods

Materials

Rich-grade oil sands ore was provided by Syncrude. Cyclohexane (ACS certified) for the bitumen extraction was purchased from Fisher Chemical. Borosilicate spherical glass beads were obtained from Sigma Aldrich and kaolin clay was provided by ACROS Organics. Standard test

sieves no. 35, 70, 100 were purchased from Fischer Scientific. Standard testing sieve no. 325 was purchased from Advantech Manufacturing. Nitrogen (99.999% purity) was provided by Praxair.

Methods

Sample preparation

Firstly, we collected gangue from the non-aqueous bitumen extraction process and sieved it through four sieves (500 μm , 212 μm , 150 μm , and 45 μm). It was found that fine particles (<45 μm) accounted for approximately 5 wt%. Then, based on the particle size distribution in the original gangue sample, two major types of samples were prepared for the current study. For convenience, we signify them as Sample A (**SA**) and Sample B (**SB**).

SA was prepared by mixing together only polydisperse borosilicate spherical glass beads at the same weight ratios as in the original gangue. For example, the composition of the original gangue was: 7.4 wt% particles with size $\geq 500 \mu\text{m}$, 11.3 wt% particles with size $\geq 212 \mu\text{m}$, 50.5 wt% particles with size $150 \geq \mu\text{m}$, 25.1 wt% particles with size $\geq 45 \mu\text{m}$, and 5.7 wt% of fine particles. Therefore, to prepare SA we mixed borosilicate spherical glass beads of each size fraction in the same wt% ratio as in the original gangue to obtain a polydisperse mixture of spherical borosilicate particles. Four types of SA were prepared each one having different wt% of fine particles. They are: SA with 5 wt% fines (mimicking the original gangue), SA with 10 wt% fines, SA with 15 wt% fines, and SA with 20 wt% fines.

The same approach was used to prepare SB. Unlike SA, where all size weight fractions were made of spherical borosilicate beads, in SB, we used fine kaolin clay for the fine particles (<45 μm) fraction. Kaolin clay powder was sieved through the no. 325 (45 μm) sieve and the content that passed through it was used as fine particles in SB. Similarly, four types of SB were prepared

each one with different fine weight ratio: SB with 5 wt% fines (mimicking the original gangue), SB with 10 wt% fines, SB with 15 wt% fines, and SB with 20 wt% fines.

The coating of samples with bitumen was carried out using the Heidolph Hei-VAP rotary evaporator. The reason for using rotary evaporator for coating is that it provides an even coating on all sides of the round-shaped particles and was used previously in our lab for this purpose [147]. The bitumen was dissolved in cyclohexane at concentration of 0.5 g/mL and added to the sample submerged in 50 mL of cyclohexane and evaporated at 50 °C at 40-60 rpm followed by vacuum drying in the vacuum oven for 4 hours at 60 °C. Each sample was coated with two bitumen contents: 0.5 wt% and 2 wt% that were chosen based on minimum and maximum documented bitumen wt% found in the gangue after the non-aqueous extraction process [40].

Therefore, a total of sixteen samples were prepared and their compositions are shown in Table 4-1.

Table 4-1. Composition of SA (borosilicate glass) and SB (kaolin clay) samples.

Sample	0.5 wt% Bitumen				2 wt% Bitumen			
	Fines content (wt%)				Fines content (wt%)			
SA (Borosilicate glass)	5	10	15	20	5	10	15	20
SB (Kaolin clay)	5	10	15	20	5	10	15	20

CHNS Analysis

The bitumen content in each sample was measured using the Thermo-Scientific Flash 2000 CHNS/O Analyzer. A standard soil reference with 7.5 wt% carbon content was used. Carbon

content measurement in each sample was repeated 5-7 times and the average value was used for bitumen film thickness calculation.

Gravimetric Analysis

Hidden Isochema Intelligent Gravimetric Analyser (IGA) with a built-in microbalance with accuracy of $\pm 1 \mu\text{g}$ was used for mass uptake experiments. The schematic image of the device setup was given elsewhere [42]. In each experiment, the sample (1.05-1.08 g) was added in a metal sample holding bucket and attached to a microbalance in the sample compartment of the IGA. Primarily to the mass uptake experiment the sample was pre-conditioned for 8 hours by introducing it to the pure nitrogen flow of 100 ml/min at 25 °C and 1 atm pressure. This was done to make sure all the impurities, moisture, traces of cyclohexane, and any absorbed micro particles are completely removed from the surface of bitumen film.

After the pre-conditioning stage, the cyclohexane vapor was introduced into the system at a relative saturation of 90%. The total flowrate (carrier gas + cyclohexane vapor) was kept at 100 ml/min. The temperature 25 °C was controlled by the water bath and total pressure of 1 atm was maintained within the entire experiment. The length of each experiment was 8 hours. This time was previously found to be sufficient for a full saturation of the bitumen with cyclohexane when the mass change was no more detected by the IGA's microbalance.

4.4 Results and Discussions

Bitumen Film Thickness

Two parameters are required to estimate the value of diffusion coefficient as per equations (57-58): film thickness and initial slope of the linear part of a mass uptake curve. After the polydisperse sample was coated with bitumen in the rotary evaporator, it was separated with

sieves based on the particle size into five fractions: 500 μm , 212 μm , 150 μm , 45 μm , and fines (<45 μm). Then, the bitumen content (i.e., mass) in each size fraction was measured using the CHNS analyzer. The thickness of bitumen film on particles of each of size fractions was calculated as follows: the total amount of bitumen on particles of a given size fraction was divided by the number of particles in the corresponding size fraction to determine the mass of bitumen on each particle. Then, using the bitumen density[155], we calculated the volume of bitumen on each particle and the film thickness was estimated from the film and particle geometry. This procedure was done for every particle size fraction.

After the thickness of bitumen film on particles of each size fraction was calculated, we estimated the total surface area in each sample provided by all the particles in the sample and the corresponding fraction (in %) of surface area provided by the particles of each size fraction. For example, in SA with 5 wt% fine particles, the particles with average size of 45 μm had the highest fraction of surface area (~51%) while in SB with 5 wt% fines, the fine particles contributed about 73% of total sample surface area. This difference is attributed to the fact that the average size of the fine particles in SA (borosilicate glass) is larger than that of SB (kaolin clay). Also, since the shape of kaolin clay particles is irregular, their surface area is larger compared to the spherical particles of the same size.

The surface average thicknesses of bitumen film in the whole sample were then calculated using equation (59) and are summarized in Table 4-2:

$$\text{Average Thickness} = \sum \text{Thickness}_i \times \text{Area Fraction}_i \quad (59)$$

where Thickness_i is the thickness of bitumen film on particles in the same size fraction and Area Fraction_i is the fraction of the surface area of such particles.

Table 4-2. Calculated surface weighted film thicknesses of bitumen films coated on SA and SB samples (n = 5).

Sample	Surface Average Film thickness, nm	
	0.5 wt% bitumen	2 wt% bitumen
SA (5 wt% fine)	339 ± 7%	892 ± 7%
SA (10 wt% fine)	294 ± 7%	882 ± 7%
SA (15 wt% fine)	250 ± 7%	801 ± 7%
SA (20 wt% fine)	240 ± 7%	750 ± 7%
SB (5 wt% fine)	114 ± 9%	469 ± 9%
SB (10 wt% fine)	96 ± 9%	319 ± 9%
SB (15 wt% fine)	83 ± 9%	277 ± 9%
SB (20 wt% fine)	67 ± 9%	242 ± 9%

Initial Mass Uptake

The mass uptake curves for both SA and SB samples at various fines contents were obtained and are shown in Figures 4-2 and 4-3, respectively. The initial slopes of the curves were then determined. Using such initial slopes along with the surface average film thicknesses from Table 4-2, the corresponding diffusion coefficients were calculated.

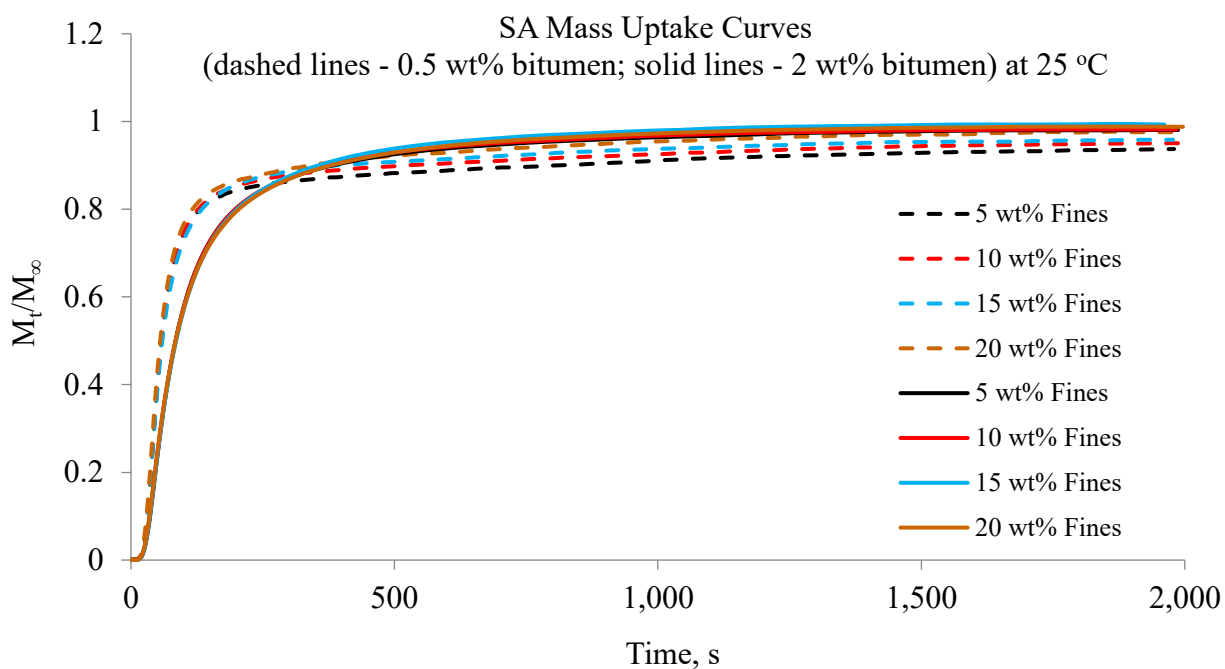


Figure 4-2: SA absorption curves. Dashed lines - samples with 0.5 wt% bitumen and solid lines - samples with 2 wt% bitumen

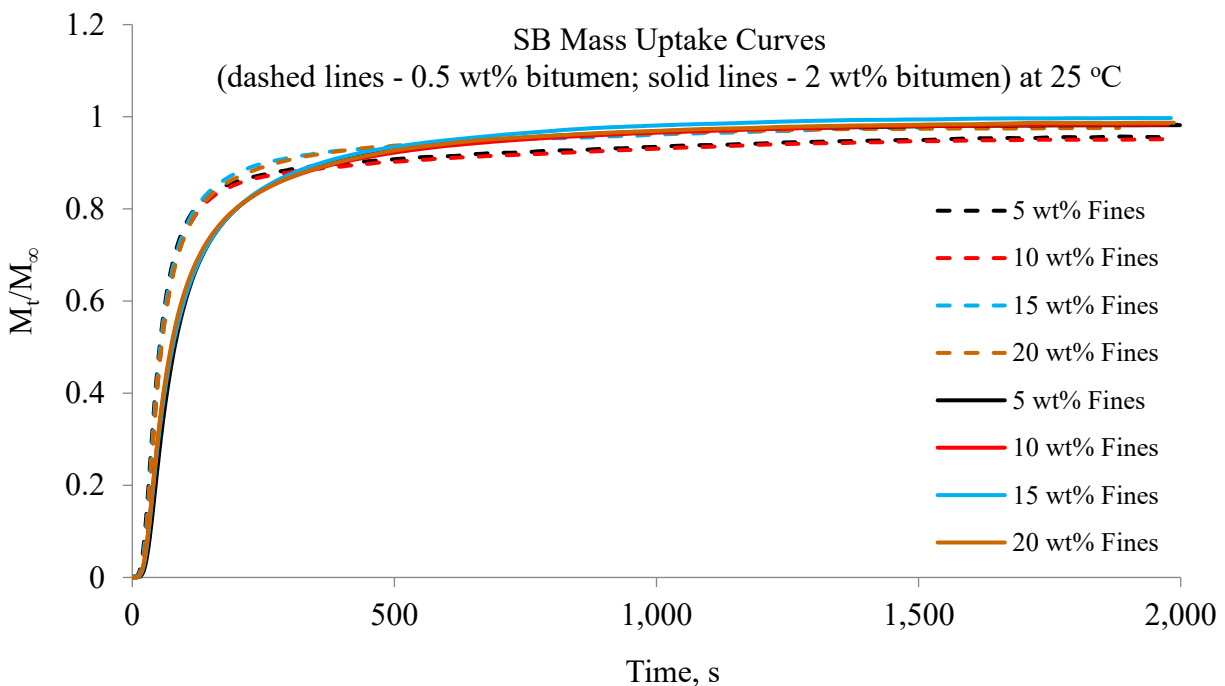


Figure 4-3: SB absorption curves. Dashed lines - samples with 0.5 wt% bitumen and solid lines - samples with 2 wt% bitumen

It can be seen from Figures 4-2 and 4-3 that the initial relative mass uptake rates for both SA and SB samples decrease as the bitumen content is increased. In other words, samples with lower bitumen contents reach the saturation faster than those with higher bitumen contents. However, the fines content appears to have no effect on the initial mass uptake rate. Table 4-3 summarizes the measured initial slopes (slopes of the linear part) of the mass uptake curves for all SA and SB samples. In Table 4-3, uncertainties were determined by standard deviation

Table 4-3. Initial mass uptake slopes of all SA and SB samples (n = 3)

Sample	Initial Mass Uptake Slope (s ⁻¹)	
	0.5 wt% bitumen	2 wt% bitumen
SA (5 wt% fine)	0.206 ± 0.003	0.119 ± 0.002
SA (10 wt% fine)	0.201 ± 0.003	0.116 ± 0.002
SA (15 wt% fine)	0.201 ± 0.003	0.117 ± 0.002
SA (20 wt% fine)	0.209 ± 0.003	0.114 ± 0.002
SB (5 wt% fine)	0.178 ± 0.004	0.132 ± 0.004
SB (10 wt% fine)	0.178 ± 0.004	0.131 ± 0.004
SB (15 wt% fine)	0.178 ± 0.004	0.130 ± 0.004
SB (20 wt% fine)	0.180 ± 0.004	0.133 ± 0.004

It is obvious that the chemical composition of the substrate (SA versus SB) exhibits a significant effect on the mass uptake rate. It is interesting to point out that the initial mass uptake rates of SA samples are higher than those of SB samples at 0.5 wt % bitumen while the trend reverses at 2 wt% bitumen. This shows that the negative bitumen content dependence of the initial mass uptake of the SA samples is much stronger than that of the SB samples. To understand the trends of the above data, we need to discuss the mass uptake mechanisms.

In general, there are three main mechanisms contributing to the mass uptake (i.e., absorption) process [89]: 1) mass transport from the solvent vapor phase into the interface of the film (a dissolution process), 2) diffusion of the solvent vapor from the interface into the bulk of the film, and 3) diffusion in the bulk [89,156]. In this work, it was the initial mass uptake rate that was evaluated. Literature suggests that the initial mass uptake depends essentially on the uptake rate at the interface (i.e., the dissolution process plus the diffusion from the interface into the bulk) [91,158]. Here, let us discuss the dissolution process first and the diffusion in the interfacial region later.

High mass uptake implies that solubility properties of bitumen molecules at the interface are similar to those of cyclohexane. Given that bitumen is a heterogeneous liquid in which molecules exhibit a wide range of polarity, a high concentration of bitumen molecules that are miscible with cyclohexane suggest that such bitumen molecules are likely to be non-polar and that relatively more polar bitumen molecules (e.g., asphaltenes) migrate to the substrate surface. Since borosilicate glass (SA samples, contact angle with water 25-32 degrees) is more hydrophilic than kaolin clay (SB samples, contact angle with water 77 degrees and higher)[157–160], it is expected that at a given film thickness, the concentration gradients of non-polar (or polar) bitumen molecules in the film thickness direction of SA samples are stronger than those of SB samples. And this difference manifested itself in the plot of the actual bitumen content dependence of the initial mass uptake rate (see Figure 4-4) and yielded a crossover at about 1 wt%.

Since the data shown in Figure 4-4 were obtained at only two bitumen contents, we prepared additional SA and SB samples with different amounts of bitumen using the procedure described

previously in this article to verify the observation shown in Figure 4-4. The results confirm the observation of Figure 4-4 and are shown in Figure 4-5.

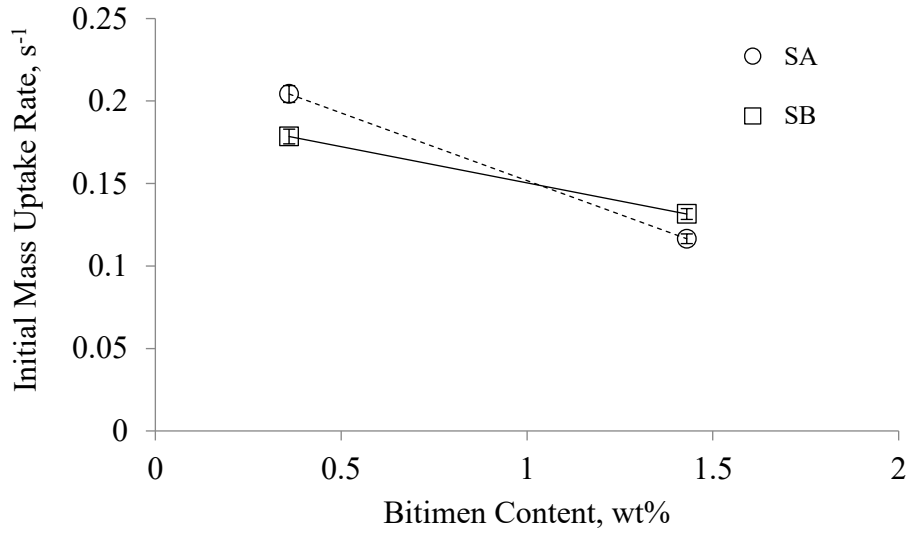


Figure 4-4: The initial mass uptake rates of SA and SB samples at 25 oC as a function of the measured bitumen content (error bars represent standard deviation)

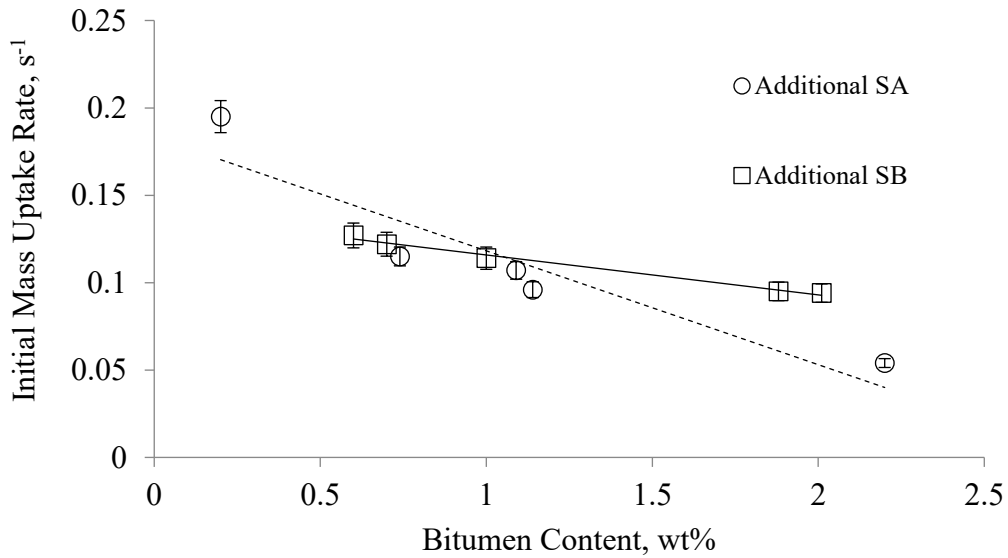


Figure 4-5: The initial mass uptake rates of additional SA and SB samples at 25 °C coated with different amounts of bitumen (error bars represent standard deviation)

According to Figures 4-4 and 4-5 it appears that in both cases, the lines intercept at approximately the same bitumen content (around 1 wt%) and more or less comparable mass uptake rates ($0.13 - 0.15 \text{ s}^{-1}$).

Diffusion Coefficients

Diffusion coefficients of all samples were estimated using equations (56-57) and are plotted as a function of fines content in Figure 4-6.

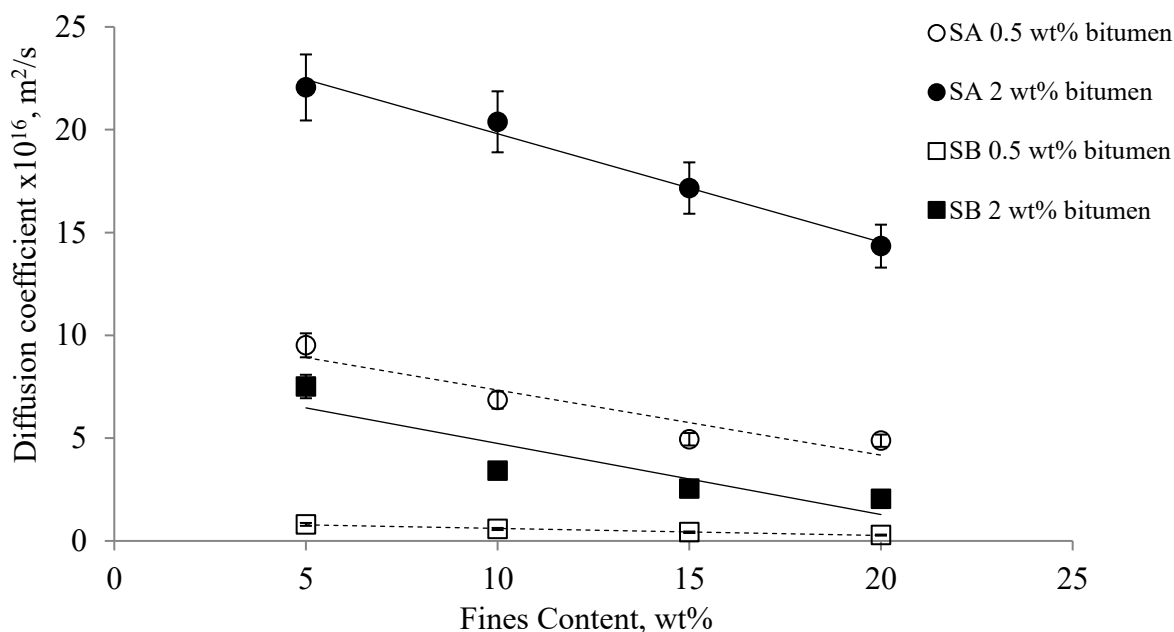


Figure 4-6: The fine content dependence of measured diffusion coefficient of cyclohexane in SA and SB samples at 25 °C (error bars represent standard deviation)

As shown in Figure 4-6, the diffusivity of cyclohexane in the bitumen thin film decreases with increasing fines content for both SA and SB samples. This is attributed to the fact that the mass uptake rate does not exhibit fines content dependence (see Table 4-3) and the surface average film thickness decreases with increasing fine contents (see Table 4-2). When the diffusion coefficient is plotted against the film thickness (Figure 4-7), it is clear that the diffusivity in the

SA samples is higher than that of the SB samples. Here, it is worth pointing out that only SA samples with 0.5 wt% bitumen and SB samples with 2 wt% bitumen share the same range of film thicknesses. Nonetheless, all diffusion coefficient values are summarized in Table 4-4 (uncertainties determined by standard deviation). At given bitumen film thickness, the difference in the diffusion coefficients must be due to the difference in the initial mass uptake rates. This shows that at 0.5 wt% bitumen content, cyclohexane not only dissolves more at the interface of the SA sample compared to SB sample as discussed earlier but also diffuses faster in the interfacial region.

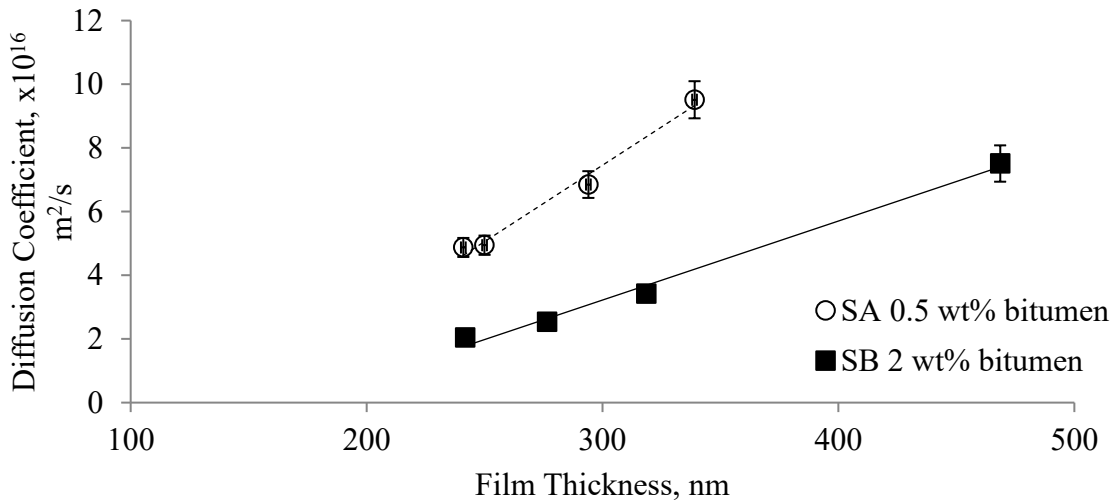


Figure 4-7: Diffusion coefficients of cyclohexane in SA and SB samples at 25 °C with comparable bitumen film thicknesses (error bars represent standard deviation)

Table 4-4. Measured diffusion coefficients at various bitumen film thicknesses of SA and SB samples (n = 3).

Sample	0.5 wt% bitumen		2 wt% bitumen	
	Thickness, nm	D, x10 ¹⁶ m ² /s	Thickness, nm	D, x10 ¹⁶ m ² /s
SA (5 wt% fine)	339	9.5 ± 0.5	892	22.1 ± 1.7
SA (10 wt% fine)	294	6.8 ± 0.5	882	20.4 ± 1.7
SA (15 wt% fine)	250	5.0 ± 0.5	801	17.2 ± 1.7
SA (20 wt% fine)	240	4.9 ± 0.5	750	14.3 ± 1.7
SB (5 wt% fine)	114	0.8 ± 0.05	469	7.5 ± 0.6
SB (10 wt% fine)	96	0.6 ± 0.05	319	3.4 ± 0.6
SB (15 wt% fine)	83	0.4 ± 0.05	277	2.5 ± 0.6
SB (20 wt% fine)	67	0.3 ± 0.05	242	2.0 ± 0.6

Fines Content Effect

Table 4-3 clearly shows that for both SA and SB samples, at a fixed bitumen content, the initial mass uptake rate is not sensitive to the fines content. Here, increasing fines content would decrease and increase the average pore size and the average film thickness, respectively. Given the particle size distribution of the fines used in this work, the average pore size is expected to be on the order of tens of microns [161]. Since the mean free path of cyclohexane molecules in dry air is less than 100 nm [162], which is significantly smaller than the average pore size, this suggests that the mass uptake of cyclohexane vapor should not be controlled by the Knudsen diffusion. Rather, it is determined by the dissolution rate at the interface and diffusion in the film thereafter. Given that the diffusion coefficient increases with increasing film thickness, it implies

that the cyclohexane dissolution rate at the interface must decrease with increasing film thickness. This is consistent with earlier finding that the concentration of non-polar bitumen molecules is higher for thinner films.

4.5 Conclusions

We used a gravimetric technique to evaluate the initial mass uptake and diffusivity of cyclohexane vapor in thin bitumen films coated on polydisperse samples containing both coarse and fine particles with the fine particles with different chemical compositions. Two types of samples were considered: SA composed of only borosilicate glass and SB composed of borosilicate glass and kaolin clay as the fines fraction (sizes less than 45 μm). SA and SB samples contained two levels of bitumen (0.5 and 2.0 wt%) as well as four levels of fines (5 – 20 wt%). The results showed a strong dependence of the initial cyclohexane mass uptake rate on the chemical composition of the fine particles and that borosilicate glass (SA samples) exhibited stronger negative bitumen content dependence than the kaolin clay (SB samples). This was due to the fact that borosilicate glass exerted a stronger concentration gradient of the polar (or non-polar) bitumen molecules in the film thickness direction. The diffusion coefficients based on the Fickian assumption at the initial stage of absorption experiment were estimated. SA samples yielded higher diffusion coefficients than SB samples as the surface average film thicknesses of SA samples are much higher than those of SB samples. Varying the fines content had no effect on the initial cyclohexane uptake rate. This is because increasing fines content decreases film thickness (i.e., decreases diffusion coefficient) that is offset by the increases in the concentration gradient (i.e., increases dissolution).

Chapter 5

Comparison between the kinetics of cyclohexane absorption and desorption for heterogeneous bitumen nanofilms

5.1 Abstract

We used a gravimetric technique to study the kinetics of cyclohexane absorption and desorption for bitumen films with thicknesses ranging from ~50 nm to ~1,000 nm by monitoring their relative mass uptake and relative mass release rates at 25 °C and 1 atm, respectively. In the absorption experiments, bitumen films were saturated with cyclohexane by exposing them to a carrier gas (nitrogen) containing cyclohexane vapor at two levels of relative saturation (RS) – 20% and 90% separately. These films were then used in the following desorption experiments. In general, the absorption rate was about two times faster than the desorption rate. Furthermore, the absorption rate exhibited a linear inverse film thickness dependence while desorption a non-linear one. The cyclohexane diffusivity in the films was found to have a linear positive film thickness dependence with it higher in absorption than that in desorption. The observations implied that amounts of cyclohexane dissolved and evaporated controlled the overall absorption and desorption rates, respectively, not the cyclohexane diffusivity. The inverse film thickness dependence of such rates was due to the decreasing influence of the hydrophilic substrate on the concentration gradient of bitumen molecules with different degrees of polarity in the films. It is interesting to note that mass uptake was observed in the early stage of the desorption experiments of the 20% RS samples, especially those with low bitumen coverages. This observation seemed to be a feature of nanoscale films. We speculated that cyclohexane evaporated into the carrier gas adjacent to the sample surface dissolved back into the bitumen film as a result of a cyclohexane concentration gradient reversal.

5.2 Introduction

Transport of small molecules through heterogeneous media is a topic of significant scientific and engineering importance since it takes place in processes such as drying, dyeing, packaging, gas leakage detection, separations of gases using polymeric membranes, and transport of air in soils and other porous media, to name a few [105,110].

Bitumen, appeared as a dark brown single-phase material, is actually a heterogeneous liquid that is mainly used as an energy source. Its heterogeneity is due to the fact that it consists of a wide variety of compounds with different chemical structures exhibiting a range of polarities from a relatively polar fraction to a non-polar fraction [44]. The main and the most abundant source of bitumen is the oil sands ores. Oil sands are a mixture of mineral solids (80-90 wt%), bitumen (4-18 wt%), and water [12,44]. Here, the mineral solids contain a wide range of size and chemical composition such as silicates and fine clays.

The currently used method of bitumen extraction, so-called Clark hot water extraction (CHWE) [12] has significant environmental and economic drawbacks: high greenhouse gas (GHG) emissions and energy consumption, large usage of fresh water, relatively low bitumen recovery, and the one that causes most concerns, a fast growth of tailing ponds [163]. To address these issues, over the last two decades, researchers have revisited an alternative method of bitumen extraction from oil sands ores, a so-called non-aqueous extraction (NAE) using cyclohexane [40,86,148]. In this multiple stage process, an oil sands ore is mixed with cyclohexane. The resulting desired product is a bitumen solution in which cyclohexane is the solvent while the by-product is a mixture of inorganic mineral particles, water, 0.5-2 wt% of residual bitumen and some cyclohexane (0.1-0.5 wt%) [12]. In the current article, this mixture is referred to as a “dry gangue” or simply “gangue”.

For the gangue to be deposited back into a mining site without imposing a significant environmental damage, the amount of residual solvent is expected to be no more than 260 ppm [42]. The number 260 ppm is the maximum acceptable value according to current promising technique [41,85]. The current average amount of residual cyclohexane reported (1,000 – 5,000 ppm) dramatically exceeds the permitted cyclohexane level and imposes challenges on potential commercialization of the NAE process. Another reason for the solvent recovery is the economic benefit as the recovered solvent can be recycled in the extraction process multiple times.

In our previous experimental studies, we showed that given the amount of bitumen in the gangue, normally in the range of 0.5 – 2 wt%, and the available surface areas of the mineral solids, the thickness of bitumen coated on the particles is likely to be on the nanoscale [149] and that there is a linear positive film thickness dependence of the initial relative cyclohexane mass uptake rate and of diffusivity in such nanoscale films. The observation was due to a concentration gradient of bitumen molecules with different degrees of polarity in the film thickness direction. We later showed that the surface hydrophilicity of substrate particles also exerts an impact on such concentration gradient and that more hydrophilic substrate results in a stronger linear inverse film thickness dependence of the initial relative mass uptake rate [164]. We also reported that the fine particles content does not affect the initial relative mass uptake rate although the cyclohexane diffusivity in the bitumen films was changed [164]. Nevertheless, the desorption process was not evaluated in the previous work. It is of great interest to compare the absorption and desorption processes in such systems, which is the focus of the present work. The literature on the desorption kinetics of chemically heterogeneous materials such as bitumen is scanty. Indeed, most of the desorption work has been carried out on chemically homogeneous polymer films [89,153,154].

It is noteworthy that desorption in bitumen is not just a reverse process of absorption. This is because the concentration gradients of bitumen molecules with different degrees of polarity within the nanoscale films at the outset of the desorption (saturated with cyclohexane) and absorption (no cyclohexane) processes are very different. As a result, diffusivities of cyclohexane during the absorption and desorption processes are conceivably different. Also, the chemical environments in which the dissolution and evaporation of cyclohexane in the respective absorption and desorption processes differ. The main objective of this work was to use to gravimetric technique to determine how dissolution, evaporation and diffusivity contribute to the absorption and desorption kinetics of nanoscale bitumen films with various thicknesses.

5.3 Theoretical background

The most widely adopted approach of mass uptake evaluation is based on Fick's second law given by equation (60) [105]:

$$\frac{\partial c}{\partial t} = D \frac{\partial^2 c}{\partial x^2} \quad (60)$$

where c is the concentration of the penetrant in a film; D is its diffusion coefficient; x and t are the spatial coordinate and time, respectively.

If equation (60) is solved for a Fickian diffusion case with constant vapor concentration (c_∞) at the film free surface at any time and D is a function of c only, equation (61) is obtained:

$$\frac{M_t}{M_\infty} = 1 - \frac{8}{\pi^2} \sum_{n=0}^{\infty} \frac{1}{(2n+1)^2} \times \exp \left[\frac{-D(2n+1)^2 \pi^2 t}{l^2} \right] \quad (61)$$

Equation (61) can be further approximated for a constant D case to yield a commonly used equation for the estimation of diffusion coefficient (equation (62)):

$$\frac{M_t}{M_\infty} = \frac{4}{\sqrt{\pi}} \frac{D^{1/2}}{l} \sqrt{t} \quad (62)$$

There are no general models for describing a desorption process occurring in a heterogeneous nanoscale film. [105] However, the above equations can be used to describe the desorption if the penetrant is initially uniformly distributed through out the film. In this work, given the time we used for saturating the bitumen films in the absorption process, we felt justified to assume that there is a uniform cyclohexane concentration in the bitumen film prior to the desorption experiments.

5.4 Experimental section

Materials

In the current study, we used a rich-grade oil sands ore obtained from the Institute for Oil Sands Innovation (IOSI) at the University of Alberta. ACS certified cyclohexane (99%) was purchased from Fisher Chemical. Nitrogen (99.999% purity) was purchased from Praxair and used as a carrier gas. Kaolin clay was provided by ACROS Organics. All size fractions of borosilicate spherical glass beads were purchased from Sigma Aldrich. Standard testing sieve no. 325 was purchased from Advantech Manufacturing while other standard testing sieves (no. 35, 70, and 100) were purchased from ThermoFisher Scientific.

Samples preparation

In this study, we prepared a series of bitumen film samples with film thicknesses at the nanoscale. This was accomplished by coating bitumen on particles with different particle size distributions and bitumen contents. The detailed procedures of coating the particles with bitumen are described in our previous work [149,164]. The coating was done using the Heidolph

Hei-VAP rotary evaporator at 50 °C at 40-60 rpm. The resulted samples were subjected to the CHNS analyser to determine the actual bitumen content that was used for the subsequent bitumen film thickness calculation.

Table 5-1 summarizes the bitumen contents and the corresponding film thicknesses of all the samples prepared. The bitumen film thickness was calculated using the method described elsewhere [149]. As can be seen from Table 5-1, most of the samples had thicknesses below the value of 1,000 nm. Here, sample A (*SA*) was composed of monodisperse borosilicate spherical glass beads with average diameter 150 μm (the average size was selected based upon the average weight size of the original gangue sample as described in our first work [149]). Sample B (*SB*) was composed of polydisperse sample mimicking the real gangue sample by adding the polydisperse spherical glass beads and fine particles (glass beads and kaolin clay) in the same size weight percentage as in actual gangue material. Sample C (*SC*) was the gangue collected from a Dean – Stark extraction process. Samples *SA*, *SB*, and *SC* were coated at five different amounts of bitumen varying from 0.5 wt% to 2 wt%. The cyclohexane mass uptake experiments of samples *SA-SC* were carried out by exposing the samples to two level of cyclohexane relative saturations (RS) – 90% and 20% separately.

Table 5-1 Samples with estimated bitumen film thicknesses (n = 5).

Sample	Actual bitumen content, wt%	Thickness, nm
SA	0.50 ± 0.03	276 ± 13
	0.74 ± 0.04	413 ± 20
	1.09 ± 0.06	613 ± 30
	1.14 ± 0.06	635 ± 31
	2.20 ± 0.11	1249 ± 61
SB	0.10 ± 0.01	57 ± 3
	0.54 ± 0.03	298 ± 15
	0.88 ± 0.04	488 ± 24
	0.98 ± 0.05	548 ± 27
	2.55 ± 0.13	1434 ± 70
SC	0.60 ± 0.03	338 ± 17
	0.70 ± 0.04	432 ± 21
	1.00 ± 0.05	563 ± 27
	1.88 ± 0.09	1045 ± 51
	2.00 ± 0.10	1154 ± 56

Bitumen content

CHNS analysis was done using the Thermo-Scientific Flash 2000 CHNS/O Analyzer. Each measurement was repeated at least 5 times and the average value was reported. The CHNS measurement was based on the analysis of the effluent gas in TCD detector after the sample combustion. The standard soil reference was used with 7.5 wt% carbon content.

Gravimetric analysis

A Hiden Isochema Intelligent Gravimetric Analyzer (IGA-002) with built-in microbalance (accuracy ±1 µg) was used to collect the mass uptake/release curves. For each sample, 1.05-1.08 g of sample was used, and experiment was repeated at least three times. The pre-conditioning and the experimental procedures are described in-detail elsewhere [149,164]. All experiments were carried out at 25 °C and 1 atm pressure that were controlled during each experiment.

5.5 Results

Absorption and desorption curves

Figures 5-1 and 5-2 show the relative mass uptake and relative mass release curves for twelve samples. For convenience, we only show the SA, SB and SC samples with the lowest and highest amounts of bitumen per unit surface area (i.e., the thinnest and thickest film thicknesses) saturated at 20% and 90% RS of cyclohexane in the carrier gas. Each curve was the result of a single experiment and each color corresponds to certain bitumen content. The color code in Figure 5-1 will be consistently retained throughout the entire article including the Supplementary Information (SI) document that contains all relative mass uptake and release curves. It should be pointed out that the delay in the mass uptake curves in the first 10-20 seconds was attributed to the fact that the carrier gas flowrate had not been stabilized. Mass uptake curves depict the relative mass uptake $\frac{M_t}{M_\infty}$, where M_t is the mass of solvent absorbed into the sample at a given time and M_∞ is the equilibrium amount of solvent absorbed. Here, the equilibrium concentration of cyclohexane in a bitumen film is governed by the cyclohexane RS used [105]. Mass release curves show the value of relative mass release $\frac{M_\infty - M_t}{M_\infty}$, plotted versus time. For instance, in the mass uptake experiment, at $t = 0$, M_t is equal to zero; so, $\frac{M_t}{M_\infty} = 0$ at $t = 0$. However, in the case of the mass release experiment, at $t = 0$, M_t is equal to M_∞ ; so, $\frac{M_\infty - M_t}{M_\infty} = 0$ at $t = 0$. The above definitions are made for convenience so that relative mass uptake and release curves asymptotically approach unity in both cases and will have positive slopes which are needed for the diffusion coefficient calculations.

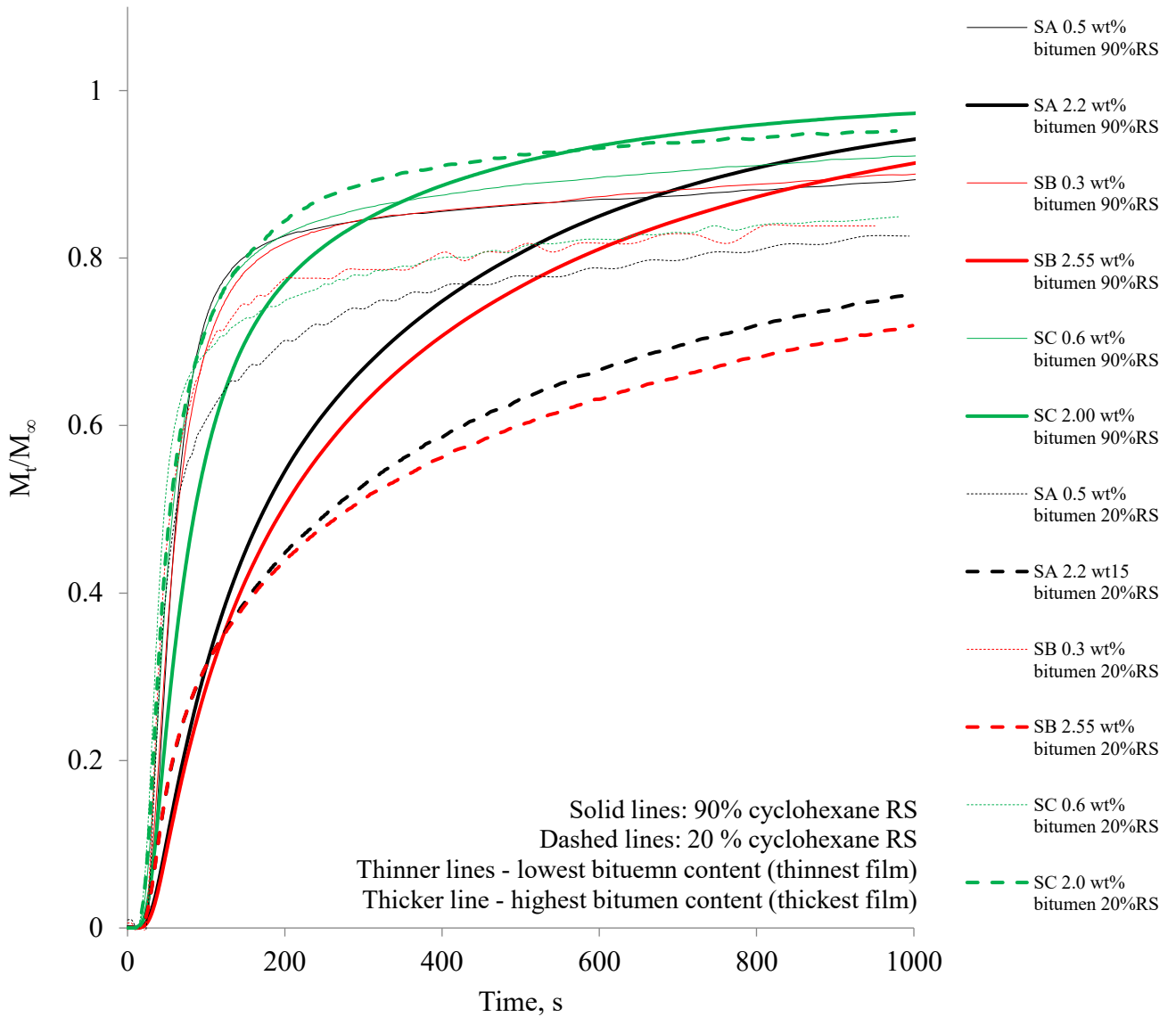


Figure 5-1: Selected absorption curves for samples exposed to cyclohexane vapor at 20% and 90% RS in the carrier gas

Figure 5-2 depicts the corresponding cyclohexane mass release curves of the same samples that were saturated in the corresponding absorption experiments shown in Figure 5-1. Again, all mass release curves are compiled in the SI document.

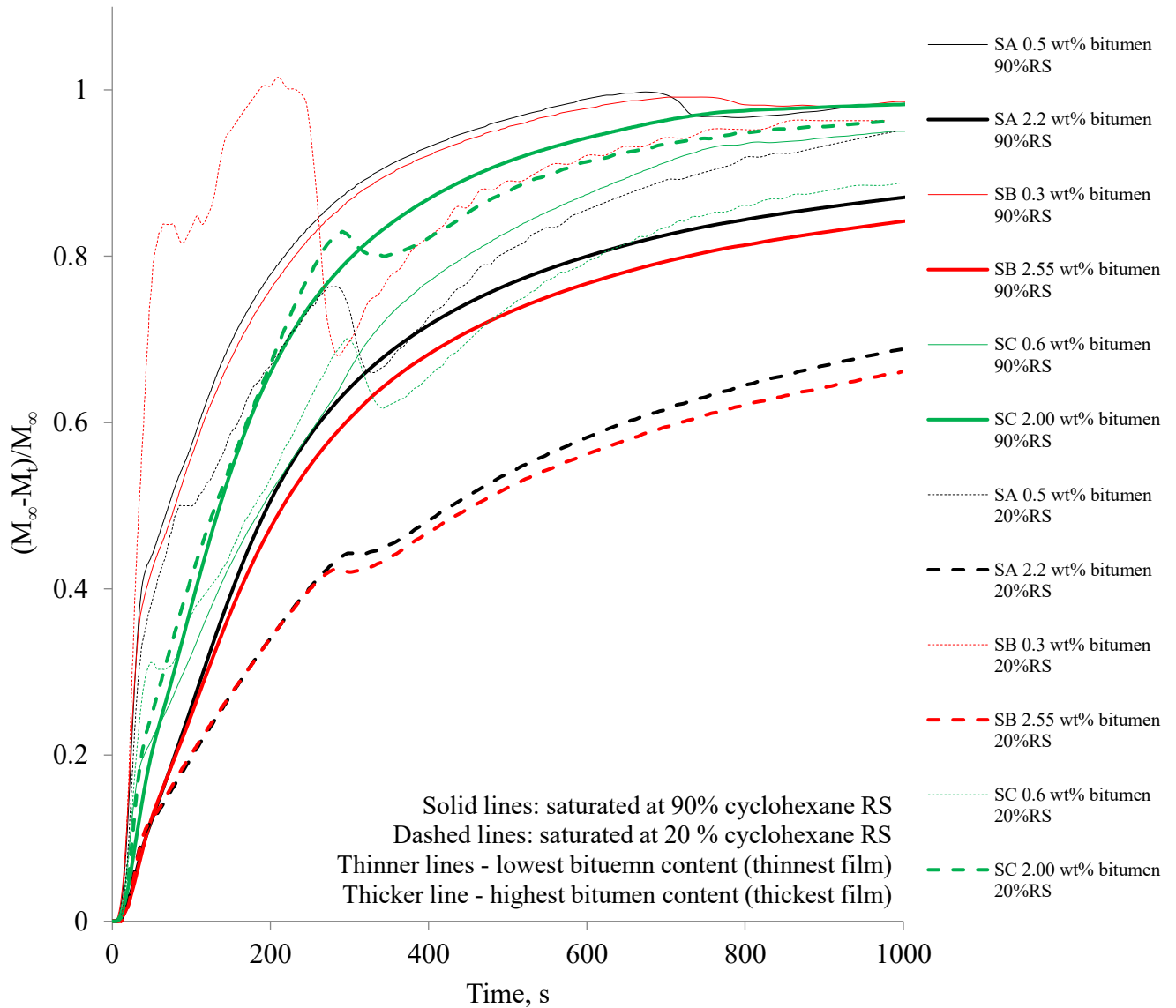


Figure 5-2: Desorption curves for the selected saturated samples obtained from the absorption experiments shown in Figure 5-1

Tables 5-2 and 5-3 summarize the initial relative mass uptake and release rates for both absorption and desorption processes. Here, samples shown in Table 5-2 were saturated with 90% RS of cyclohexane in the absorption experiments while those in Table 5-3 were saturated at 20% RS of cyclohexane.

Table 5-2. Initial relative mass uptake rates for all samples exposed to a 90% RS of cyclohexane in the carrier gas and the initial relative mass release rates of the corresponding saturated samples (n = 3).

Sample	Actual bitumen content, wt%	Thickness, nm	Absorption slopes, s ⁻¹	Desorption slopes, s ⁻¹
SA	0.5	108	0.204 ± 0.006	0.175 ± 0.005
	0.74	413	0.147 ± 0.004	0.095 ± 0.003
	1.09	613	0.135 ± 0.004	0.088 ± 0.003
	1.14	635	0.120 ± 0.004	0.065 ± 0.002
	2.20	1249	0.069 ± 0.002	0.040 ± 0.001
SB	0.1	57	0.189 ± 0.006	0.209 ± 0.006
	0.54	298	0.185 ± 0.006	0.108 ± 0.003
	0.88	488	0.157 ± 0.005	0.091 ± 0.003
	0.98	548	0.147 ± 0.004	0.087 ± 0.003
	2.55	1434	0.067 ± 0.002	0.043 ± 0.001
SC	0.60	338	0.179 ± 0.005	0.096 ± 0.003
	0.70	432	0.161 ± 0.005	0.084 ± 0.003
	1.00	563	0.152 ± 0.005	0.082 ± 0.002
	1.88	1045	0.134 ± 0.004	0.065 ± 0.002
	2.00	1154	0.129 ± 0.004	0.064 ± 0.002

Table 5-3. Initial relative mass uptake rates for all samples exposed to a 20% RS of cyclohexane in the carrier gas and the initial relative mass release rates of the corresponding saturated samples (n = 3).

Sample	Actual bitumen content, wt%	Thickness, nm	Absorption slopes, s ⁻¹	Desorption slopes, s ⁻¹
SA	0.5	108	0.221 ± 0.007	0.294 ± 0.009
	0.74	413	0.148 ± 0.004	0.136 ± 0.004
	1.09	613	0.143 ± 0.004	0.106 ± 0.003
	1.14	635	0.138 ± 0.004	0.092 ± 0.003
	2.20	1249	0.071 ± 0.002	0.047 ± 0.001
SB	0.1	57	0.242 ± 0.007	0.314 ± 0.009
	0.54	298	0.225 ± 0.007	0.190 ± 0.006
	0.88	488	0.171 ± 0.005	0.149 ± 0.004
	0.98	548	0.167 ± 0.005	0.134 ± 0.004
	2.55	1434	0.077 ± 0.002	0.054 ± 0.002
SC	0.60	338	0.259 ± 0.008	0.181 ± 0.005
	0.70	432	0.254 ± 0.008	0.143 ± 0.004
	1.00	563	0.223 ± 0.007	0.131 ± 0.004
	1.88	1045	0.208 ± 0.006	0.127 ± 0.004
	2.00	1154	0.187 ± 0.006	0.099 ± 0.003

Diffusion coefficients at the initial absorption stage at 90% and 20% RS of cyclohexane in the carrier gas and the corresponding initial desorption diffusion coefficients were estimated using equation (62) and the results are summarized in Tables 5-4 and 5-5, respectively.

Table 5-4. Initial absorption diffusion coefficients for samples exposed to a 90% RS of cyclohexane and the initial desorption diffusion coefficients of such saturated samples (n = 3).

Sample	Actual bitumen content, wt%	Thickness, nm	Absorption diffusion coefficient $\times 10^{16}$, m ² /s	Desorption diffusion coefficient $\times 10^{16}$, m ² /s
SA	0.5	108	0.96 \pm 0.05	0.71 \pm 0.04
	0.74	413	7.23 \pm 0.36	3.02 \pm 0.15
	1.09	613	13.44 \pm 0.67	5.71 \pm 0.29
	1.14	635	11.4 \pm 0.57	3.35 \pm 0.17
	2.20	1249	14.59 \pm 0.73	4.90 \pm 0.25
SB	0.1	57	0.19 \pm 0.01	0.24 \pm 0.01
	0.54	298	5.95 \pm 0.30	2.03 \pm 0.10
	0.88	488	11.53 \pm 0.58	3.87 \pm 0.19
	0.98	548	12.75 \pm 0.64	4.47 \pm 0.22
	2.55	1434	18.13 \pm 0.91	7.47 \pm 0.37
SC	0.60	338	7.19 \pm 0.36	2.07 \pm 0.10
	0.70	432	9.48 \pm 0.47	2.58 \pm 0.13
	1.00	563	14.39 \pm 0.72	4.19 \pm 0.21
	1.88	1045	38.51 \pm 1.93	9.06 \pm 0.45
	2.00	1154	43.49 \pm 2.17	10.70 \pm 0.54

Table 5-5. Initial absorption diffusion coefficients for samples exposed to a 20% RS of cyclohexane and the initial desorption diffusion coefficients of such saturated samples (n = 3).

Sample	Actual bitumen content, wt%	Thickness, nm	Absorption diffusion coefficient $\times 10^{16}$, m ² /s	Desorption diffusion coefficient $\times 10^{16}$, m ² /s
SA	0.5	108	1.13 \pm 0.06	1.99 \pm 0.10
	0.74	413	7.32 \pm 0.37	6.18 \pm 0.31
	1.09	613	15.08 \pm 0.75	8.29 \pm 0.41
	1.14	635	15.08 \pm 0.75	6.70 \pm 0.34
	2.20	1249	15.45 \pm 0.77	6.77 \pm 0.34
SB	0.1	57	0.32 \pm 0.02	0.93 \pm 0.05
	0.54	298	8.80 \pm 0.44	6.27 \pm 0.31
	0.88	488	13.68 \pm 0.68	10.39 \pm 0.52
	0.98	548	16.46 \pm 0.82	10.60 \pm 0.53
	2.55	1434	23.95 \pm 1.20	11.78 \pm 0.59
SC	0.60	338	15.04 \pm 0.75	7.35 \pm 0.37
	0.70	432	23.60 \pm 1.18	7.48 \pm 0.47
	1.00	563	30.97 \pm 1.55	10.69 \pm 0.53
	1.88	1045	59.67 \pm 4.64	14.78 \pm 0.74
	2.00	1154	65.76 \pm 4.57	15.91 \pm 0.80

It is obvious in Figures 5-1 and 5-2 that there exist fluctuations in both relative mass uptake and release curves in the 20% RS samples while this is not the case for the 90% RS samples. The fluctuations are even more pronounced at low bitumen contents. It is also important to point out that the reason that the relative mass uptake/release curves do not converge to unity in Figures 5-1 and 5-2 is because only the first 1,000 s of data are shown as most of the absorption and desorption took place in this period. In fact, either an absorption or a desorption experiment would take about 7-8 hours to complete.

5.6 Discussions

Since the desorption curves exhibit considerable fluctuations in mass release, especially those of low film thickness samples saturated at low RS of cyclohexane, this led us to speculate whether such observation was a unique feature of the nano-scale bitumen films. To determine whether this is the case, we prepared additional samples using SA as the substrate by coating its particles with different amounts of bitumen that yielded film thicknesses over two orders of magnitude – 51 nm, 707 nm, and 6,500 nm and carried out the absorption experiments at 90% RS prior to the desorption measurements. The 90% RS was used because such samples did not exhibit obvious transitions. The resultant mass release curves are plotted in Figure 5-3.

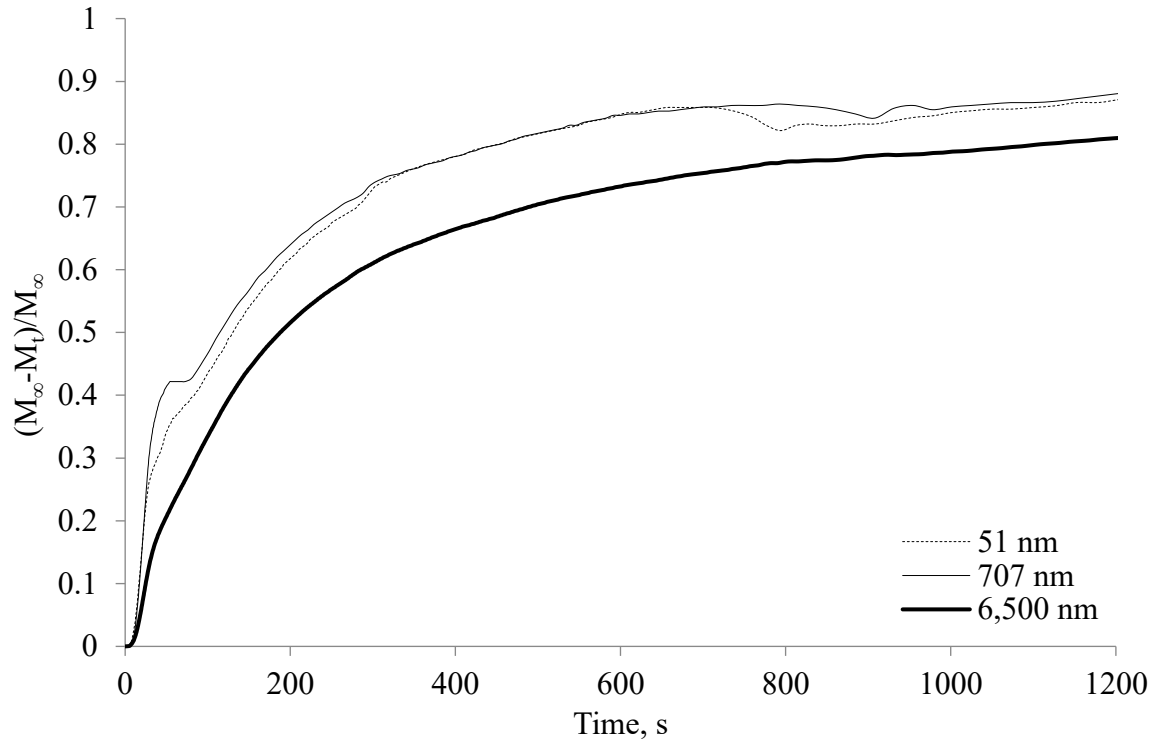


Figure 5-3: Relative mass release curves of the SA sample coated with bitumen films with thicknesses over two orders of magnitude from 51 nm – 6,500 nm. The samples were saturated at 90% RS of cyclohexane prior to the desorption measurements

Figure 5-3 shows that the shape of the relative mass release curve becomes less smooth as the film thickness decreases. In other words, fluctuations observed in the desorption of the nano-scale bitumen films are a unique feature of such films. In fact, fluctuations observed in the 20% RS samples suggest that there was mass gain during the early stage of the desorption process (see Figure 5-3) and this observation will be discussed in detail later.

Tables 5-2 and 5-3 show that the initial desorption rates are generally slower than the initial absorption rates for the majority of samples. The results indicate that saturating a bitumen film requires less time than de-saturating the same film. As mentioned earlier, given the inhomogeneous nature of bitumen, desorption is not just simple the reverse of absorption.

Previous work showed [149,164] that at the outset of the absorption process, the bitumen film

contains a concentration gradient of the polar molecules in the film thickness direction from high polar molecules (low non polar molecules) concentration at the substrate surface to low polar molecules (high non polar molecules) concentration at the free surface. Such concentration gradient would be very different at the outset of the desorption of a cyclohexane saturated bitumen film. Such difference would lead to differences in the cyclohexane concentrations at the free surfaces, rendering differences in the cyclohexane diffusivity in absorption and desorption. Nonetheless, the data shown in Tables 5-2 and 5-3 are also compiled in Figures 5-4 and 5-5 that will give us a clear visualization of them. In addition to the differences in the overall absorption and desorption rates, Figures 5-4 and 5-5 further show that the bitumen film thickness dependence of the initial relative mass uptake rate exhibits a linear inverse relationship while that of the relative mass release rate a nonlinear inverse relationship. Also, the 20% RS samples exhibit higher absorption and desorption rates than those of the 90% RS samples.

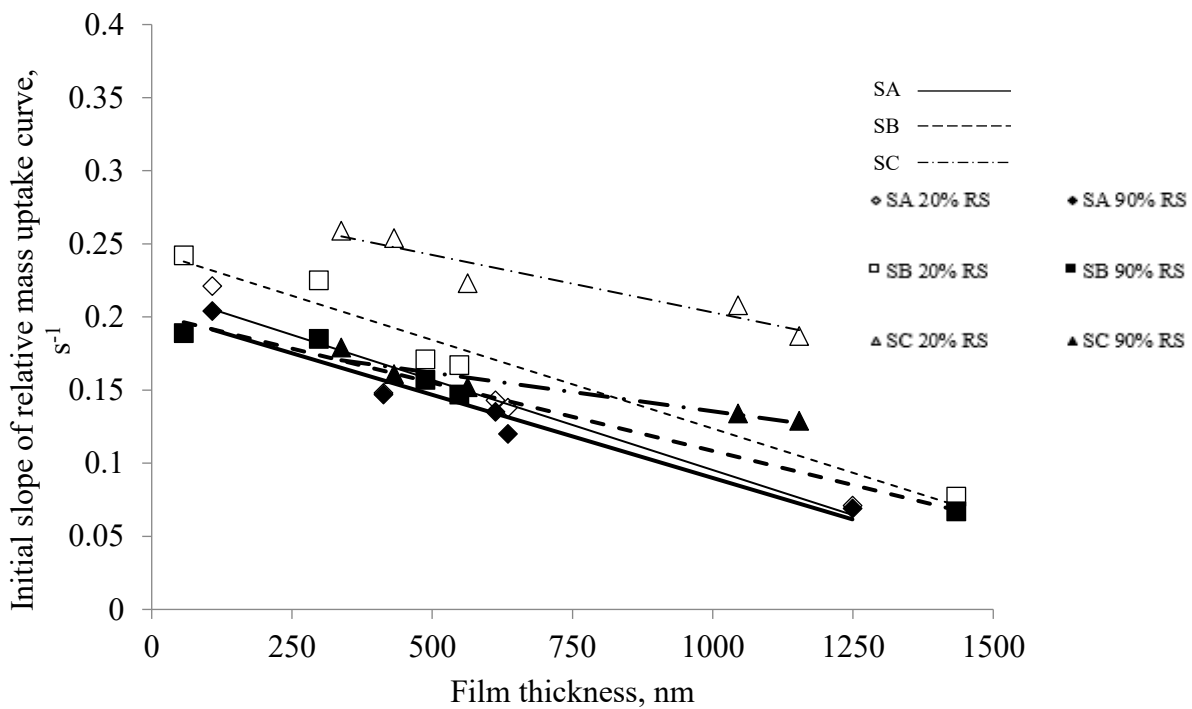


Figure 5-4: Initial rates of relative mass uptake for 90% (filled legends) and 20% RS (open legends) samples

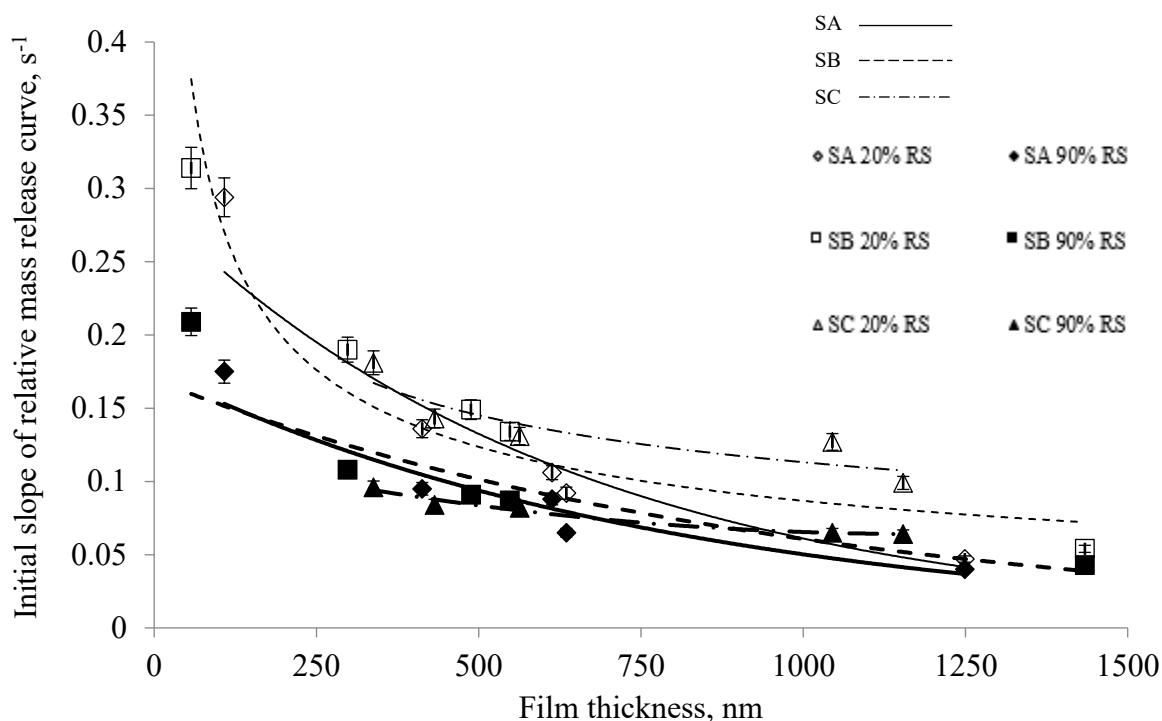


Figure 5-5: Initial rates of relative mass release for 90% (filled legends) and 20% RS (open legends) samples

Given that absorption involves the dissolution of cyclohexane at the free surface of a bitumen film followed by the diffusion of cyclohexane from the free surface to the of the film and that desorption involves the diffusion of cyclohexane from the bulk to the free surface followed by evaporation, we calculated the cyclohexane diffusivity using equation (62) to check if it contributes to the relative mass uptake and release behaviors observed in Figures 5-4 and 5-5. Figures 5-6 and 5-7 show the absorption and desorption diffusion coefficients as a function of bitumen film thickness and the data are summarized in Tables 5-4 and 5-5, respectively.

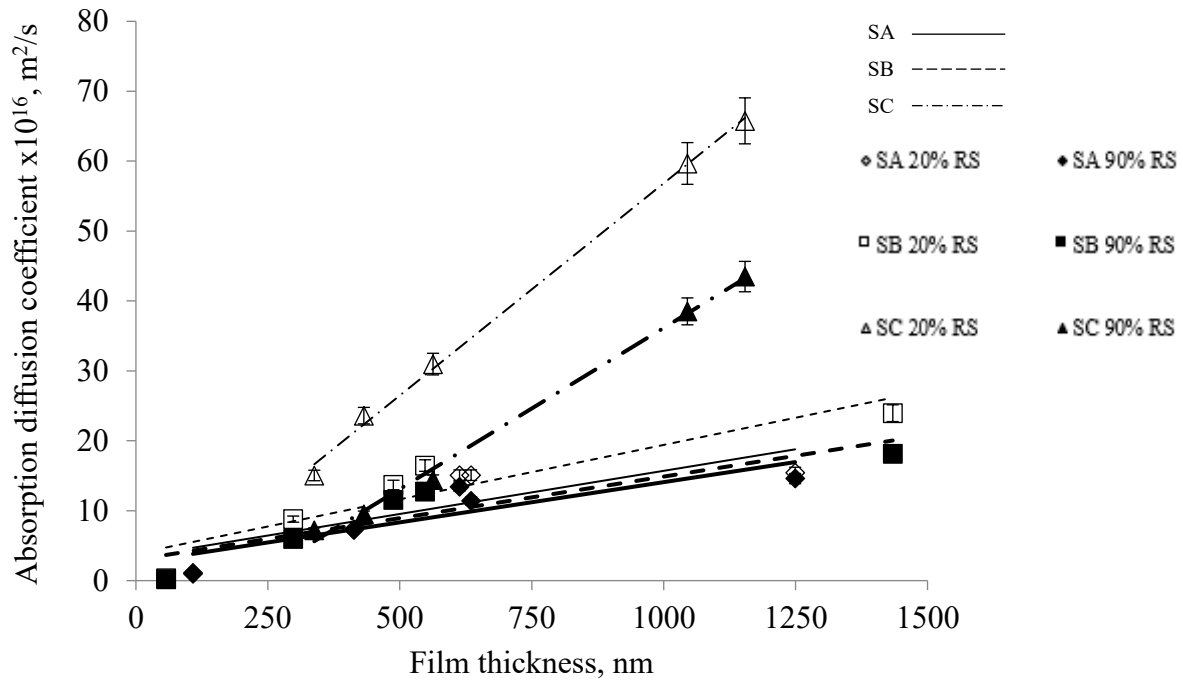


Figure 5-6: Absorption diffusion coefficients for 90% RS (filled legends) and 20% RS (open legends) samples

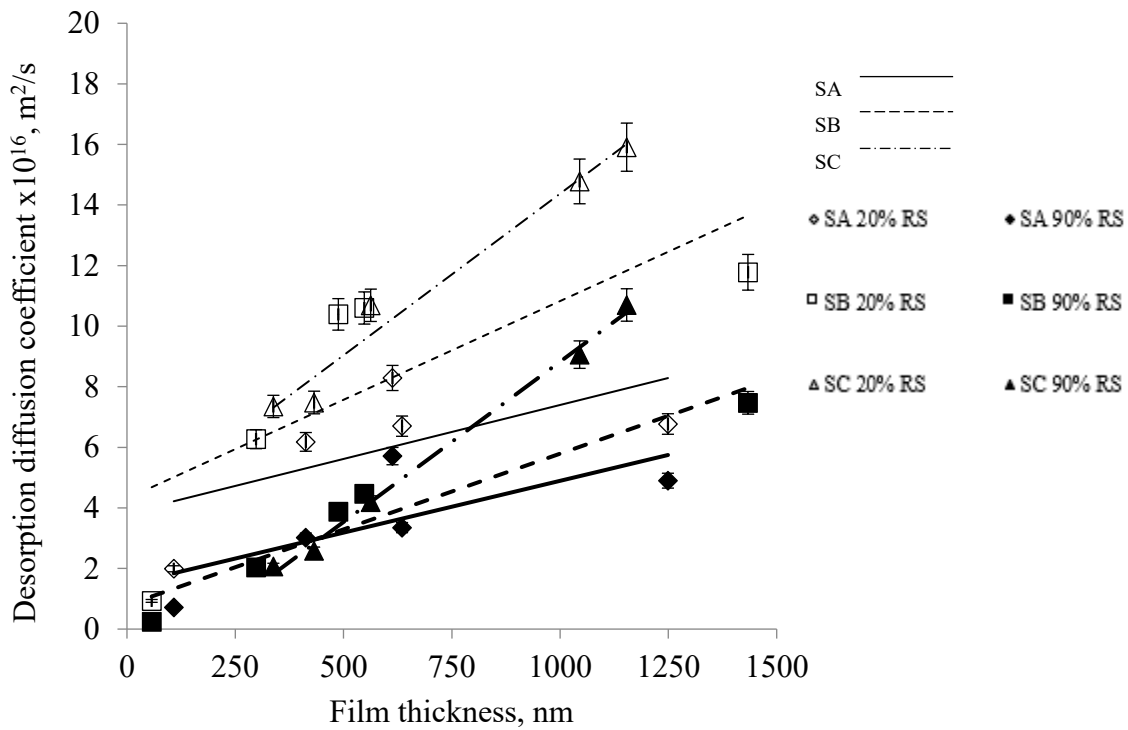


Figure 5-7: Desorption diffusion coefficients for 90% RS (filled legends) and 20% RS (open legends) samples

It is clear from the above data that the cyclohexane diffusivity in absorption are generally higher than that in desorption. This seems to explain the observation that the absorption rate is higher than the desorption rate. However, the same set of data also show that the cyclohexane diffusivity exhibits a linear positive film thickness dependence in both absorption and desorption experiments. Given the inverse dependence of initial relative mass uptake/release rates on film thickness, it means that the dissolution/evaporation steps dominate the absorption/desorption processes. In other words, the dissolution/evaporation steps are the rate determining steps, not the diffusivity of cyclohexane. Since the rate of the cyclohexane penetration in or out of the bitumen film is the product of its diffusivity and solubility (i.e., $P = D \times S$), the questions are: why is dissolution stronger than evaporation? Why is the film thickness dependence of the dissolution linear and that of evaporation non-linear?

As mentioned earlier, the chemical compositions of a given bitumen film at the outsets of absorption and desorption are very different. Since the free surface of a bitumen film contains high concentrations of non-polar compounds, cyclohexane in the carrier gas is expected to dissolve into the film surface readily (i.e., high dissolution rate). On the other hand, desorption involves the evaporation of cyclohexane from a bitumen solution into the carrier gas containing no cyclohexane. Since cyclohexane and non-polar bitumen molecules are miscible with each other, evaporation is not as favorable as dissolution (i.e., low evaporation rate). The inverse film thickness dependence is likely attributed to the influence of the polar substrate. In the case of absorption, when the film thickness is low, majority of relatively polar bitumen molecules are attracted to the polar substrate screening its charges, making the free surface less polar. This is not the case in the thick films. In other words, thinner films (less polar free surfaces) facilitate the dissolution of cyclohexane. However, in the case of desorption, the activity of cyclohexane

(i.e., the tendency to escape from the free surface) decreases with increasing film thickness because polarity of the free surface decreases with increasing thickness, meaning that thicker films (less polar free surfaces) impede evaporation. The non-linearity of the desorption rate as a function of film thickness is likely attributed to the non-linear effect of the substrate on the activity of cyclohexane.

Another observation in Figures 5-6 and 5-7 is that the relative mass uptake/release rates of the 20% RS samples are higher than those of the 90% RS, especially at low film thicknesses. This is simply due to the fact that we used the initial relative mass uptake/release rates rather than the absolute mass uptake/release rates in the figures. The rationale of using the relative rates is that it allowed us to use equation (62) to calculate the cyclohexane diffusivity. Also, using relative rates would not change the trends of film thickness dependence observed in Figures 5-6 and 5-7. Nevertheless, when the absolute mass uptake/release are plotted as a function of time, the resultant slopes of the 90% RS samples are higher than those of the 20% RS samples.

Finally, let us now discuss the relative mass release curves observed in Figure 5-4. The increase of relative mass change during the desorption process is of particular interest. This phenomenon was only observed for very thin 20% RS samples. As mentioned earlier, the activity of cyclohexane (nonpolar) in such bitumen samples (polar) is relatively high, thereby facilitating evaporation. Here, as Figure 5-4 shows, most of the cyclohexane (70-80%) is evaporated in the first 5 minutes of the experiment. It is believed that cyclohexane vapor rapidly built up in the carrier gas adjacent to the film surface, leading to a reverse in cyclohexane concentration across the free surface. As a result, some cyclohexane can dissolve back into the bitumen film. Indeed, at around 5 minutes into the desorption experiment, a massive mass uptake rather than mass

release is observed. Cyclohexane concentration reversal seems not to take place in thicker samples saturated at higher RS of cyclohexane prior to the desorption measurements.

We also ran desorption experiments using samples denoted as SA and SB in Chapter 4. Let us label them as samples SD and SE here since SA, SB, and SC already exist. The entire set of relative mass uptake and release curves with SD and SE included are depicted in the Appendix C in Figures C5 and C6. Figures C10-C15 show all the mass uptake and release curves of Samples SD and SE only. Initially we did not include these samples in the published article because we did not run SD and SE at 20% cyclohexane RS and only used 90%.

First observation from Figures C10-C13 is that for both samples SD and SE one can notice that the fine particles content does not affect the initial desorption rate. For a given bitumen content the initial desorption rate seems to stay constant for any fine particles content and only changes when the bitumen amount in the sample is changed. On one hand, the increase of fine particles content results in the increased total area available for residing the bitumen, which should result in a thinner film in high fine particle content samples given the bitumen weight fraction is the same in all samples. This, according to our previous studies should result in an increasing desorption rate as the film gets thinner. However, we see no effect on the initial desorption rate in samples SD and SE. It is possible that the variation in thickness is not sufficient, for instance in sample SD with 0.5 wt% bitumen film the thickness decreases from 339 to 240 nm. At the

same time in samples SE the thickness variation of a few hundred nm is observed while the initial desorption rate is still the same.

As with samples SA-SC the rate of initial relative mass release was lower than that of mass uptake. Table 5-6 shows the values of initial relative mass release values of samples SD and SE.

Table 4-3 in Chapter 4 shows the relative mass uptake data for the same samples.

Table 5-6. Initial rates of relative mass release in samples SD and SE (n = 3)

Sample	Initial Mass Release Slope (s ⁻¹)	
	0.5 wt% bitumen	2 wt% bitumen
SD (5 wt% fine)	0.151 ± 0.007	0.067 ± 0.003
SD (10 wt% fine)	0.146 ± 0.007	0.071 ± 0.003
SD (15 wt% fine)	0.156 ± 0.007	0.073 ± 0.003
SD (20 wt% fine)	0.148 ± 0.007	0.068 ± 0.003
SE (5 wt% fine)	0.118 ± 0.007	0.072 ± 0.003
SE (10 wt% fine)	0.119 ± 0.007	0.070 ± 0.003
SE (15 wt% fine)	0.110 ± 0.007	0.070 ± 0.003
SE (20 wt% fine)	0.116 ± 0.007	0.069 ± 0.003

As in the Chapter 4, where the properties of the substrate affected the rate of initial mass uptake, Figure 5-8 shows that the substrate surface also affects the relative mass release rate at the initial stage. The negative dependence is also observed for the desorption process and this dependence is stronger for more hydrophilic substrate (SD).

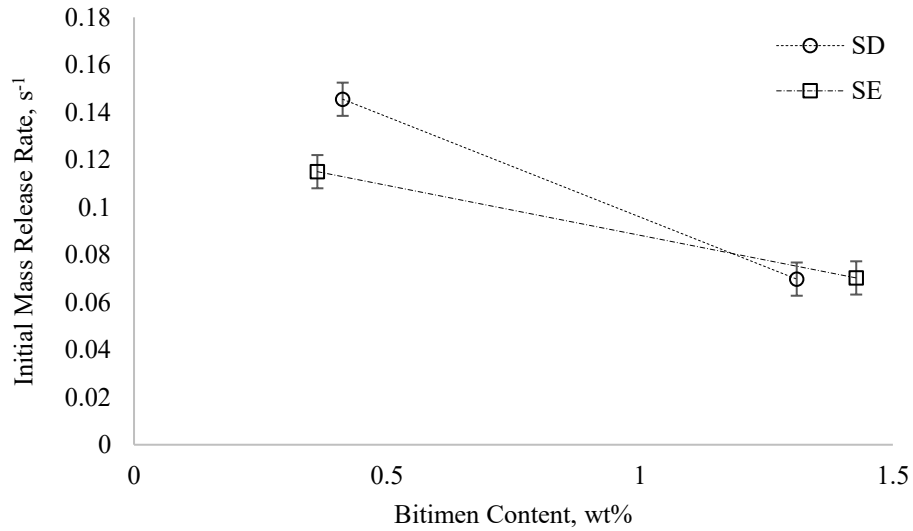


Figure 5-8: The initial mass release rates of SD and SE samples

Diffusion coefficient values are shown in Table 5-7 and Figure 5-9.

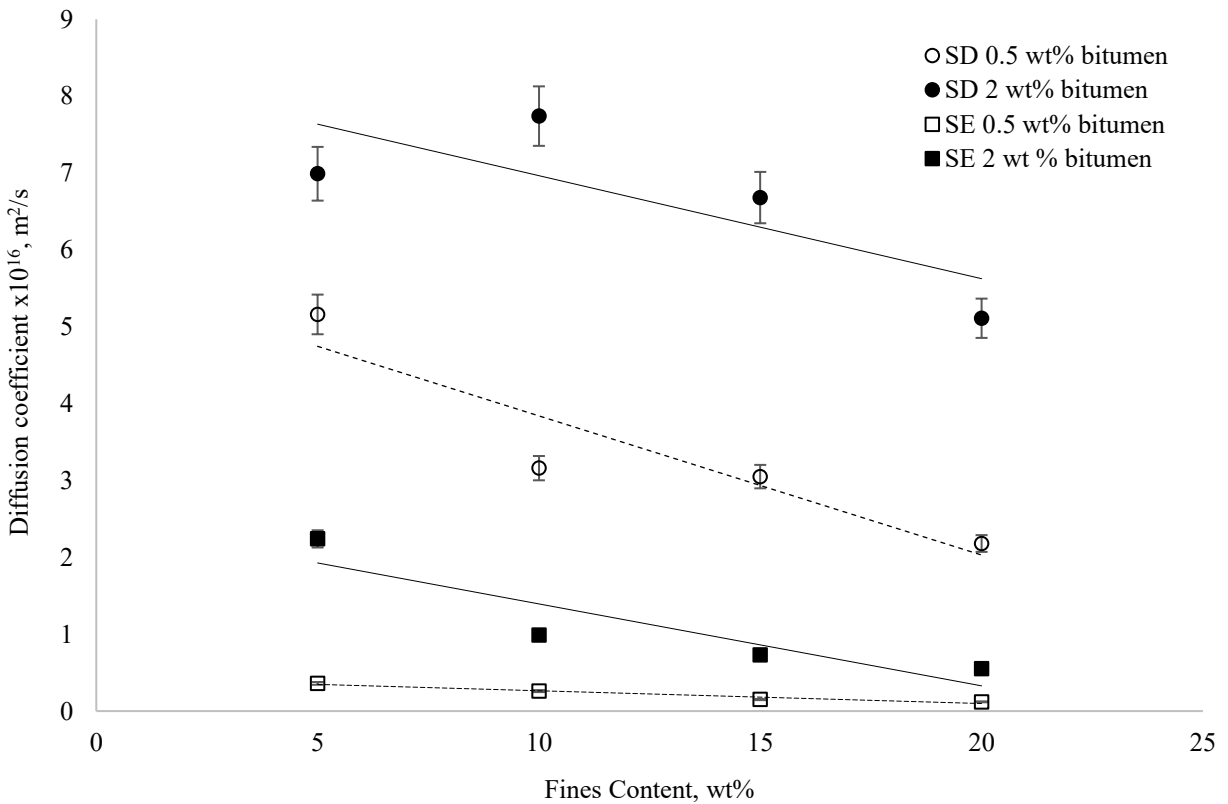


Figure 5-9: The fine content dependence of measured diffusion coefficient of cyclohexane in SD and SE

Table 5-7. Measured desorption diffusion coefficients at various bitumen film thicknesses of SD and SE samples (n = 5 for thickness, n = 3 for diffusion coefficients).

Sample	0.5 wt% bitumen		2 wt% bitumen	
	Thickness, nm	D, x10 ¹⁶ m ² /s	Thickness, nm	D, x10 ¹⁶ m ² /s
SA (5 wt% fine)	339	5.2 ± 0.3	892	7.2 ± 0.5
SA (10 wt% fine)	294	3.2 ± 0.3	882	7.6 ± 0.5
SA (15 wt% fine)	250	3.0 ± 0.3	801	6.7 ± 0.5
SA (20 wt% fine)	240	2.2 ± 0.3	750	5.1 ± 0.5
SB (5 wt% fine)	114	0.4 ± 0.03	469	2.2 ± 0.3
SB (10 wt% fine)	96	0.3 ± 0.03	319	1.1 ± 0.3
SB (15 wt% fine)	83	0.2 ± 0.03	277	0.7 ± 0.3
SB (20 wt% fine)	67	0.1 ± 0.03	242	0.6 ± 0.3

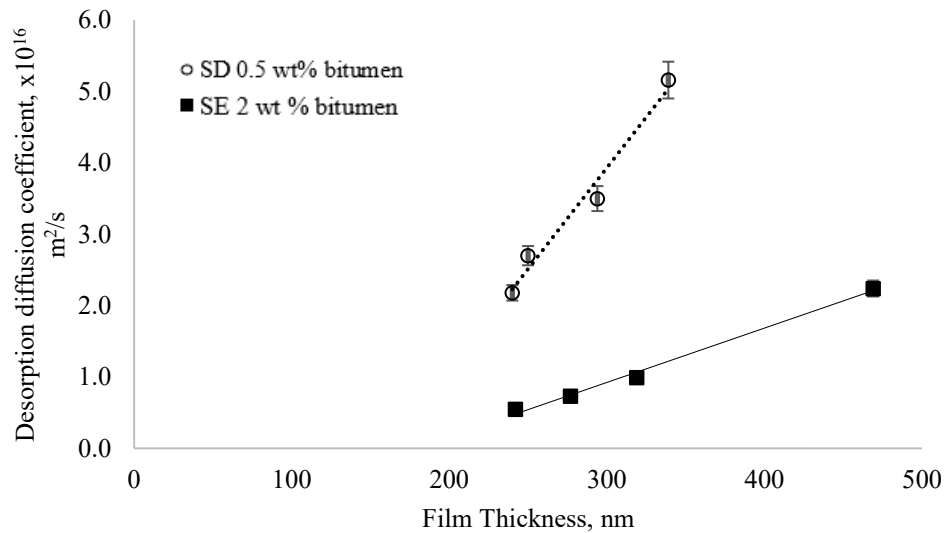


Figure 5-10: Desorption diffusion coefficients of cyclohexane in SD and SE samples with comparable bitumen film thicknesses

When desorption diffusion coefficients plotted for samples SD and SE for compatible range of thickness, it becomes clear that the positive thickness dependence is valid for both samples. However, the slope of the desorption diffusion coefficient increase is significantly higher for SD compared to the desorption diffusion coefficient of SE. This can be attributed to a higher activity of nonpolar cyclohexane in a more polar environment, which in this case is glass substrate in SD.

5.7 Conclusions

A gravimetric technique was used to study the cyclohexane absorption and desorption kinetics at 25 °C and 1 atm for bitumen films with thicknesses in the range of ~50 nm to ~1000 nm. It was found that the initial relative mass uptake rates were about two times faster than the initial relative mass release rates. However, in the absorption process, the initial relative mass uptake rate exhibited a linear inverse dependence on the film thickness but in the desorption process, the initial relative mass release rate exhibited a non-linear inverse dependence on the film thickness. The cyclohexane diffusivity in both absorption and desorption processes was calculated to determine its contribution to the observed relative mass uptake/release rates. Interestingly, it exhibited a positive dependence on the film thickness, suggesting that the absorption and desorption rates were controlled by the amounts of cyclohexane dissolved and evaporated in the absorption and desorption processes, respectively, not the cyclohexane diffusivity. Here, the amounts of cyclohexane dissolution and evaporation were controlled by its miscibility with the bitumen molecules in the free surfaces of the films. The observed inverse film thickness dependence observed in the absorption (linear) and desorption (non-linear) was attributed to the diminishing influence of the hydrophilic substrates as the film thickness was increased. The desorption curves for the 20% RS samples at low thicknesses exhibited significant fluctuations. Indeed, in the early stage of desorption, mass uptake was observed for such samples. This

observation was attributed to a cyclohexane concentration reversal across the film surface as a result of the cyclohexane vapor built up in the carrier gas adjacent to the film surface.

Chapter 6

Concluding notes and future work

The main observation of this experimental study was that the transport of cyclohexane vapor into nano-scale bitumen film is a process that depends on many factors such as bitumen film thickness, chemistry of the substrate, and relative saturation of cyclohexane in the vapor phase. An important qualitative finding is that the diffusion coefficient of cyclohexane in bitumen film is extremely small (on the order of 10^{-16} m²/s) regardless of the film thickness. Also, we demonstrated that the desorption process is about two times slower than the absorption, which means that cyclohexane is not likely to be removed once it is dissolved in the residual bitumen.

Mass transport of cyclohexane in the absorption process is governed by two major stages. In the first stage, cyclohexane from the vapor phase dissolves in the film at the interphase due to favorable intermolecular interactions. This is established due to a polarity concentration gradient within the bitumen film in such a way that the more polar fraction of bitumen molecules moves towards the substrate while the less polar components reside at the film interface. In the second stage, the dissolved cyclohexane molecules diffuse in the bulk (due to a cyclohexane concentration gradient) towards the substrate until the saturation equilibrium is reached. The equilibrium saturation concentration of cyclohexane in the film depends on the relative saturation of cyclohexane in the vapor phase—the higher the relative saturation, the higher the equilibrium concentration of cyclohexane.

In this work, we attempted to control the chemical structure of the substrate surface and we found that the substrate also affects the mass transport properties. The more hydrophilic substrate (gauge particles contain more sand than clay particles) appears to lead to higher cyclohexane

diffusion coefficients, in both absorption and desorption processes, and has a stronger negative thickness dependence than samples with less hydrophilic surfaces such as those containing more clays. In all experiments, diffusion coefficients appeared to be higher for the samples with thicker bitumen film and had a positive linear dependence.

We also found that the initial rates of desorption of cyclohexane from the film had a negative nonlinear dependence in comparison with the absorption process in which the dependence was negative linear. This was attributed to a polar molecules' gradient in the film before the absorption experiment, which was not the case in the desorption experiments due to the presence of cyclohexane in the film. In some desorption experiments when the initial cyclohexane concentration in the film was low, mass uptake rather than mass release was observed, indicating the presence of a reverse process.

6.1 Novelty and contribution

The novelty of this research is the implementation of a conventional analytical method for measuring diffusion coefficients in nanofilms made of a heterogeneous substance - bitumen. One of the major findings was that the measured diffusion coefficients were film thickness dependent and were comparable determined either from absorption or desorption. However, the mass uptake rate was about two times faster than the mass release rate, suggesting that the desorption is not just simply the reverse process of the absorption. The concept of polarity gradient in the bitumen films at nanoscale thickness due to the interactions with substrate surfaces is introduced for the first time to explain the above findings.

6.2 Practical implementation

The results of this study yield the following practical implications. One crucially important implication is to recover as much bitumen as possible from the NAE process. This is necessary because the more bitumen that is left in the gangue solids, the higher the bitumen film thickness, which means that the rate of initial mass release of the solvent from the film is much lower, thereby reducing the amount of solvent being recovered. It is evident from our study that in cases when the film is very thin (<100 nm), the fraction of solvent removed from the sample in the first few minutes might be up to 60%, while this number drops down to 15% as the film thickness increases. The mass release process following the initial rapid release can be impractically long.

Of course, factors such as the chemical composition of the solids are out of anyone's control; however, it is worthy to evaluate the chemistry of the inorganic solids to learn what to expect when using the NAE process for bitumen recovery.

Let us make a very rough estimation. Consider a case in which the extraction was done well (0.5 wt% bitumen and 0.5 wt% cyclohexane in the gangue), and the fine particle content is 5 wt% and the fines are made up of clay. This is more or less close to what is encountered in practice. The desorption diffusion coefficient is approximately $0.4 \times 10^{-16} \text{ m}^2/\text{s}$. If there is 90% solvent RS, it means that the equilibrium solvent concentration (C_1) is $\sim 0.4 \text{ g cyclohexane per g of bitumen}$. The film thickness is low and the rate of initial mass release is quite high. More than 50% (so that $C_2 = 0.2 \text{ g}_{\text{solvent}}/\text{g}_{\text{bitumen}}$) of the solvent is released in the initial phase (linear part of the curve). Given all of those factors, let us assume that the mass transport follows Fick's first law:

$$J = D \frac{(C_1 - C_2)}{l}$$

For this case, thickness was found to be ~114 nm. The flux can be estimated around 7×10^{-5} g cyclohexane/m²/s.

Let us say we have 1,000 kg of gangue solids after NAE. Given the characteristics from the previous paragraph we have:

- 1,000 kg gangue solids
- 20 kg bitumen (20,000 gram or 0.02 m³ roughly assuming density of bitumen as 1 g/cm³)
- 5 kg of cyclohexane

For simplicity, let us consider the average particle size (diameter) to be 150 μm. Then, given the particle geometry and aforementioned bitumen film thickness, we can find the volume of bitumen on one particle, on the surface area of this film, and the total amount of particles in 1,000 kg of gangue particles. See estimations below.

Diameter of a gangue particle: $150 \mu m = 150,000 \text{ nm}$

Diameter of a coated particle (film thickness is 114 nm): $150,228 \text{ nm}$

Surface area of a bitumen-coated particle: $A = \pi D^2 \cong 7.09 \times 10^{-8} m^2$

Volume of bitumen on a single particle: $Volume \text{ coated} - Volume \text{ uncoated} =$

$$\left(\frac{4}{3}\pi r_{coated}^3\right) - \left(\frac{4}{3}\pi r_{uncoated}^3\right) \cong 8 \times 10^{-15} m^3$$

Given the total volume of bitumen in 1,000 kg of gangue solids and assuming all particles are coated evenly, we can find the total number of particles:

$$\frac{0.02 m^3}{8 \times 10^{-15} m^3} \cong 2.5 \times 10^{12} \text{ particles}$$

Then, combining the number of particles and the area of one coated particle, we can find the total area:

$$A_{total} = 2.5 \times 10^{12} \text{ particles} \times 1.8 \times 10^{-8} m^2 \cong 43,926 m^2$$

Now that we know the total flux, which is the amount of diffusant per unit time per unit area, (per 1 m³ of bitumen, hence we need to scale it to our 0.02 m³), the amount of cyclohexane leaving the system, and total area, we can estimate the time required for the process keeping track of units (we divide total amount of solvent by 2 because we assumed the concentration decreases 50%):

$$5000 \text{ gram solvent} / (2 \times F \times 0.02 m_{bit}^3 \times A_{total}) \cong 7 \text{ days}$$

We got something around 7 days to evaporate half of the solvent from 1,000 kg of residual sand. Now, this number needs some comments. Again, this is the time it takes for only half the solvent to be removed. This number is based on the fastest rate of desorption. Further removal rate decreases exponentially based on the mass release curves. The number 7 days is based on rough estimation of the system (average particle size is known, even distribution, etc.). The number 7 days should not be used as a guideline time for the process estimation. What it means, is that the process is very long (talking about a scale of weeks). We assumed that the evaporation/diffusion process follows Fick's first law and of course this is not completely true and from our studies we know that the process slows down drastically as the sample approaches desaturation equilibrium. And lastly, although from definition, we know that there is no Knudsen diffusion taking place in the cyclohexane mass transport in the sand as we already showed in Chapter 3 (the mean free path of cyclohexane is at the order of magnitude of dozens nanometers while the pore size is at

the micron scale), we cannot totally eliminate effect of eddy diffusion when the solvent particles can migrate back and forth in the channels of the sand rather than moving all in one direction when outside the bitumen film, especially when the sand is reach on fine particles.

6.3 Future work

In light of the sub-chapter 6.2, it becomes an important practical problem to develop amore detailed model of solvent evaporation from the residual bitumen. Since all the numbers such as concentrations, diffusion coefficients, particle size distribution, etc., are known, it is important study the effect of different particles in the sample and the calculation needs to take in account a variation of particle sizes, thicknesses of bitumen films, and pore sizes in which the bitumen travels between the films.

As it was mentioned at the very beginning of this report, the research done and described here is only the initial part of addressing the big problem. But to solve the actual engineering problem, further research needs to be done. Specifically, the next step requires looking deeper into the effect of water on mass transfer of cyclohexane in the residual bitumen. It is known and was mentioned in Chapter 2 that there is connate water bound to the sand particle surface and separating bitumen form the actual sand particle. In our research experiments, we did not consider the effect of water, and moreover, we did everything to avoid any presence of water. Now, in the next stage of the research, it is important to hydrate the substrate particles before coating bitumen. The mixing procedure should be as follows: sand \rightarrow water \rightarrow bitumen. In this case, the surface of the sand particles will be hydrated properly and the water nanolayer will be established between the particle surface and bitumen film. This layer might affect the initial gradient of polar/nonpolar molecules distribution prior to absorption process by screening the

polar forces acting on the substrate surface. At the same time, water molecules might be able to establish new interactions with some bitumen fractions (i.e., those fractions capable of hydrogen bonding).

Another important consideration to be done is in the desorption step. In the experiments described in Chapter 5, the desorption experiment was done by shutting down the solvent stream while keeping the carrier gas stream. This resulted in the full recovery of cyclohexane from the sample returning its mass to the original value. Of course, it shows that the solvent on industrial scale can be recovered by passing air through the residual solids. This would require a large amount of energy input which may make commercialization of NAE process less attractive.

Lastly, from the scientific point of view, it might be beneficial and interesting to evaluate the sorption process of bitumen nanofilms coated on different substrates. They can be other polar surfaces, nonpolar surfaces, polar and nonpolar polymers, other heterogeneous substances, etc. As it was pointed out in Chapter 5, mass transfer in heterogeneous substances is of a great scientific interest.

References:

- [1] Clean Energy and Electricity Infrastructure 2020. <https://www.nrcan.gc.ca/climate-change/canadas-green-future/clean-energy-and-electricity-infrastructure/21294> (accessed April 13, 2020).
- [2] Investing in Canada: Canada's Long-Term Infrastructure Plan 2018. <https://www.infrastructure.gc.ca/plan/icp-publication-pic-eng.html> (accessed April 13, 2020).
- [3] Renewable energy facts 2020. <https://www.nrcan.gc.ca/science-and-data/data-and-analysis/energy-data-and-analysis/energy-facts/renewable-energy-facts/20069> (accessed April 13, 2020).
- [4] Hydrocarbon Production. Energy Prod 2020. <https://www.cer-rec.gc.ca/nrg/ntgrtd/mrkt/nrgsstmprfls/cda-eng.html> (accessed April 13, 2020).
- [5] Executive Summary 2020. <https://www.cer-rec.gc.ca/nrg/ntgrtd/fttr/2019/xctvsmmry/index-eng.html> (accessed April 13, 2020).
- [6] Provincial and Territorial Energy Profiles – Alberta 2020. <https://www.cer-rec.gc.ca/nrg/ntgrtd/mrkt/nrgsstmprfls/ab-eng.html> (accessed April 13, 2020).
- [7] Ekabutr P, Chuysinuan P, Suksamrarn S, Sukhumsirichart W, Hongmanee P, Supaphol P.

- Development of antituberculosis melt-blown polypropylene filters coated with mangosteen extracts for medical face mask applications. *Polym Bull* 2019;76:1985–2004. <https://doi.org/10.1007/s00289-018-2468-x>.
- [8] Lugao AB, Otaguro H, Parra D. Review on the production process and uses of controlled rheology polypropylene—Gamma radiation versus electron beam processing. *Radiat Phys Chem* 2007;76:1688–90.
- [9] No Title. InterPipeline 2020. <https://www.iplheartland.com/about-heartland/the-project.cfm> (accessed April 13, 2020).
- [10] Leahy S. This is the world’s most destructive oil operation—and it’s growing. *Natl Geogr Mag* 2019.
- [11] Oil Sands Facts and Stats. Alberta Gov 2017. <https://open.alberta.ca/dataset/b6f2d99e-30f8-4194-b7eb-76039e9be4d2/resource/063e27cc-b6d1-4dae-8356-44e27304ef78/download/fsoilsands.pdf> (accessed April 14, 2020).
- [12] Lin F, Stoyanov SR, Xu Y. Recent Advances in Nonaqueous Extraction of Bitumen from Mineable Oil Sands : A Review. *Org Process Res Dev* 2017;21:492–510.
- [13] Oil sands – Overview. Alberta Gov 2020. <https://www.alberta.ca/oil-sands-overview.aspx> (accessed April 14, 2020).
- [14] Kasperski KL. Review of research on aqueous extraction of bitumen from mined oil sands (p.17). Devon: Western Research Centre; 2001.
- [15] Masliyah JH, Czarnecki JA, Xu Z. Handbook on Theory and Practice of Bitumen

- Recovery from Athabasca Oil Sands-Vol. 1: Theoretical Basis. Calgary: Kingsley Publishing Services; 2011.
- [16] Masliyah JH, Zhou Z, Xu Z, Czarnecki J, Hamza H. Understanding Water-Based Bitumen Extraction from Athabasca Oil Sands. *Can J Chem Eng* 2008;82:628–54.
- [17] Vedoy D, Soares J. Water-soluble polymers for oil sands tailing treatment: A Review. *Can J Chem Eng* 2015;93:888–904.
- [18] Rao F, Liu Q. Froth Treatment in Athabasca Oil Sands Bitumen Recovery Process: A Review. *Energy and Fuels* 2013;27:7199–207.
- [19] Sjöblom J, Simon S, Xu Z. Model molecules mimicking asphaltenes. *Adv Colloid Interface Sci* 2015;218:1–16.
- [20] Long Y, Hamsa H, Dabros T. Selective Solvent Deasphalting for Heavy Oil Emulsion Treatment. *Asph. heavy oils, Pet.*, New York: Springer, New York; 2007, p. 511–47.
- [21] He L, Lin F, Li X, Sui H, Xu Z. Interfacial sciences in unconventional petroleum production: from fundamentals to applications. *Chem Soc Rev* 2015;44:5446–94.
- [22] Teare M, Miller S, Overland S, Marsh R. Alberta’s Energy Reserves 2014 and Supply/Demand Outlook 2015–2024. Calgary: 2015.
- [23] Doherty B. Kenney says Alberta has reduced oilsands emissions, but oil-related pollution is actually increasing. Here’s why. *Star Calgary* 2019.
<https://www.thestar.com/calgary/2019/11/15/kenney-says-alberta-has-reduced-oilsands-emissions-but-oil-related-pollution-is-actually-increasing-heres-why.html> (accessed April

- 14, 2020).
- [24] Tailings. Alberta Energy Regul 2015. <https://www.aer.ca/providing-information/by-topic/tailings.html> (accessed April 14, 2020).
- [25] Methods for managing Tailings. 2018.
- [26] Gosselin P, Hrudey S, Naeth A, Plourde A, Therrien R, Van Der Kraak G, et al. Environmental and Health Impacts of Canada's Oil Sands Industry. Ottawa: 2010.
- [27] Foght JM. Microbial metagenomics of oil sands tailings ponds: small bugs, big data. *Genome* 2015;58:507–10.
- [28] Raymond CG. Process for separating oil from bituminous sands, shales, etc. No. 2,825,677. 4, 1958.
- [29] Leary TS. Recovery of bitumen from bituminous sand. 3,117,922, 1964.
- [30] Benson AM. Filtration of solvent-water extracted tar sand. 3,459,653, 1969.
- [31] Blaine NF. Solvent extraction of oil from tar sands utilizing a trichloroethylene solvent. 4,046,669, 1977.
- [32] Leung H, Phillips CR. Solvent extraction of mined Athabasca oil sands. *Ind Eng Chem Fundam* 1985;24:373–9.
- [33] Sparks BD, Meadus FW. Solvent extraction spherical agglomeration of oil sands. 4,719,008, 1988.
- [34] Sparks BD, Meadus FW. A study of some factors affecting solvent losses in the solvent

- extraction — spherical agglomeration of oil sands. *Fuel Process Technol* 1981;4:251–64.
- [35] Pal K, da Paz Nogueira Branco L, Heintz A, Choi P, Gray M, Liu Q, et al. Performance of Solvent Mixtures for Non-aqueous Extraction of Alberta Oil Sands. *Energy and Fuels* 2015;29:2261–7.
- [36] Meadus FW, Chevrier P, Sparks BD. Solvent extraction of athabasca oil-sand in a rotating mill Part 1. Dissolution of bitumen. *Fuel Process Technol* 1982;6:277–87.
- [37] Painter P, Williams P, Mannebach E. Recovery of Bitumen from Oil or Tar Sands Using Ionic Liquids. *Energy and Fuels* 2010;24:1094–8.
- [38] Holland A, Wechsler D, Patel A, Molloy B, Boyd A, Jessopab P. Separation of bitumen from oil sands using a switchable hydrophilicity solvent. *Can J Chem* 2012;90:805–10.
- [39] Jessop PG. Switchable hydrophilicity solvents and methods of use thereof. 8,580,124, 2013.
- [40] Nikakhtari H, Vagi L, Choi P, Liu Q, Gray MR. Solvent screening for non-aqueous extraction of Alberta oil sands. *Can J Chem Eng* 2013;91:1153–60.
- [41] Fundamentals of Non-Aqueous Extraction of Oilsands. *Sci Data* 2018.
<https://www.nrcan.gc.ca/science-and-data/funding-partnerships/funding-opportunities/current-investments/fundamentals-non-aqueous-extraction-oilsands/16124>
(accessed March 31, 2020).
- [42] Noorjahan A, Tan X, Liu Q, Gray MR, Choi P. Study of cyclohexane diffusion in athabasca asphaltenes. *Energy and Fuels* 2014;28:1004–11.

- [43] Berger BD, Anderson KE. Modern petroleum : a basic primer of the industry. 3rd ed. Tulsa, Okla: PennWell Books; 1992.
- [44] Strausz OP. The chemistry of Alberta oil sands, bitumens and heavy oils. 7th ed. Calgary: Alberta Energy Research Institute; 2003.
- [45] Summons RE. Biogeochemical Cycles. *Org. Geochem.*, Boston, MA: Springer; 1993, p. 3–21. https://doi.org/https://doi.org/10.1007/978-1-4615-2890-6_1.
- [46] Tissot B, Pelet R. Nouvelles donnees sur les mecanismes de genese et de migration du petrole simulation mathematique et application a la prospection. In 8th World Petroleum Congress. 8th World Pet. Congr., Moscow: 1971, p. 12.
- [47] Peters K, Moldowan M. Biomarkers and isotopes in petroleum systems and Earth history. *Biomark. Guid. 2, Biomarkers Isot. Pet. Syst. Earth Hist. Second Ed.* 2nd ed., Cambridge: Cambridge University Press; 2005, p. 475–1155.
- [48] Evans CR, Rogers MA. Evolution and alteration of petroleum in western Canada. *Chem Geol* 1971;8:147–70. [https://doi.org/https://doi.org/10.1016/0009-2541\(71\)90002-7](https://doi.org/https://doi.org/10.1016/0009-2541(71)90002-7).
- [49] Rubinstein I, Strausz OP. The biodegradation of crude oils: the origin of the Alberta oil sands. *Oil Sand Oil Shale Chem.*, New York: Verlag Chemie; 1978, p. 177–89.
- [50] Rubinstein I, Strausz OP, Spyckerelle C, Crawford R, Westlake D. The origin of the oil sand bitumens of Alberta- A chemical and a microbiological simulation study. *Geochim Cosmochim Acta* 1977;41:1341–53.
- [51] Palmer S. Effect of Biodegradation and Water Washing on Crude Oil Composition. *Org.*

Geochem., Boston, MA: Springer; 1993, p. 511–33.

https://doi.org/https://doi.org/10.1007/978-1-4615-2890-6_23.

- [52] Connan J. Biodegradation of crude oils in reservoirs. *Adv Pet Geochemistry* 1984;1:229–335.
- [53] Allan J, Creaney S. Oil Families of the Western Canada Basin. *Bull Can Pet Geol* 1991;39:107–22.
- [54] Vigrass L. Geology of Canadian Heavy Oil Sands. *Am Assoc Pet Geol Bull* 1968;52:1984–99.
- [55] Bichard J. Oil Sands Composition and Behaviour Research: The Research Papers of John A. Bichard. 1987.
- [56] Hepler LG. Alberta oil sands: Industrial procedures for extraction and some recent fundamental research. AOSTRA technical publication No. 14. Edmonton: Alberta Oil Sands Technology and Research Authority; 1994.
- [57] Wightman D, Rottenfusser B. Geology of the Alberta oil sands deposits. AOSTRA, Tech. Handb. oil sands, bitumens, heavy oils Alberta Oil Sands Technol. Res. Auth. Tech. Publ. Ser., 1989, p. 3–6.
- [58] Kotlyar L, Sparks BD. Organic rich solids from oil sands: properties and role in processing. *Rev Process Chem Eng* 1998;1:81–110.
- [59] Kotlyar L, Kodama H, Sparks BD. Non-crystalline inorganic matter-humic complexes in Athabasca oil sand and their relationship to bitumen recovery. *Appl Clay Sci* 1987;2:253–

- 71.
- [60] Takamura K. Microscopic structure of athabasca oil sand. *Can J Chem Eng* 1982;60:538–45. <https://doi.org/10.1002/cjce.5450600416>.
- [61] Israelachvili J. *Intermolecular and surface forces*. 3rd ed. Waltham, MA: Academic Press; 2011.
- [62] Takamura K, Isaacs E. Interfacial properties. *AOSTRA Tech. Handb. oil sands, Bitum. heavy oils*, Edmonton: 1989, p. 99.
- [63] Darcovich K, Kotlyar L. Wettability study of organic-rich solids separated from Athabasca oil sands. *Energy and Fuels* 1989;3:386–91.
- [64] Berg J. *An introduction to interfaces & colloids : the bridge to nanoscience*. Singapore: World Scientific; 2010.
- [65] Speight J. *The Chemistry and Technology of Petroleum*. New York: Marcel Dekker; 1999.
- [66] Bulmer J, Starr J. *Syncrude Analytical Methods for Oil Sand Bitumen Processing*. Edmonton: 1979.
- [67] Haschke E, Gimber G, Groves K. Process for recovery of solvent from tar sand bitumen. 4,532,024, 1985.
- [68] Vorndran L, Serres A. Bitumen separation for experimental use. *Can J Chem Eng* 1980;58:580–7. <https://doi.org/10.1002/cjce.5450580506>.

- [69] Wallace D, Kratochvil B. Sampling Uncertainty in the Determination of Major Components in Athabasca Oil Sand. *AOSTRA J Res* 1981;1:31.
- [70] Liu J. Analytical Methods. *AOSTRA Tech Handb Oil Sands, Bitumens Heavy Oils* 1989;1:11–32.
- [71] Selucky M, Kim S. Structure-Related Properties of Athabasca Asphaltenes and Resins as Indicated by Chromatographic Separation. *Chem Asph* 1982;6:83–118.
- [72] Milan L, Yingli C. Chemical composition of Cold Lake bitumen. *Fuel* 1978;57:9–16.
[https://doi.org/https://doi.org/10.1016/0016-2361\(78\)90083-2](https://doi.org/https://doi.org/10.1016/0016-2361(78)90083-2).
- [73] Milan L, Yingli C. Chemical composition of Athabasca bitumen. *Fuel* 1977;56:369–81.
[https://doi.org/https://doi.org/10.1016/0016-2361\(77\)90061-8](https://doi.org/https://doi.org/10.1016/0016-2361(77)90061-8).
- [74] Payzant J, Hogg B, Montgomery D, Strausz OP. A Field Ionization Mass Spectrometric Study of the Maltene Fraction of Athabasca Bitumen. *AOSTRA J Res* 1985;1:183.
- [75] Strausz OP, Rubinstein MA. *Advances in the Chemistry of Alberta Tar Sands: Field Ionization Gas Chromatographic/Mass Spectrometric Studies*. *At. Nucl. Methods Foss. Energy Res.*, Boston, MA: Springer; 1982, p. 409–41.
- [76] Strausz OP, Mojelsky T, Lown E. The molecular structure of asphaltene: an unfolding story. *Fuel* 1992;71:1355–63. [https://doi.org/https://doi.org/10.1016/0016-2361\(92\)90206-4](https://doi.org/https://doi.org/10.1016/0016-2361(92)90206-4).
- [77] Payzant J, Mojelsky T, Strausz OP. Improved methods for the selective isolation of the sulfide and thiophenic classes of compounds from petroleum. *Energy and Fuels*

- 1989;3:449–54. <https://doi.org/https://doi.org/10.1021/ef00016a004>.
- [78] Mitchell D, Speight J. The solubility of asphaltenes in hydrocarbon solvents. *Fuel* 1973;52:149–52. [https://doi.org/https://doi.org/10.1016/0016-2361\(73\)90040-9](https://doi.org/https://doi.org/10.1016/0016-2361(73)90040-9).
- [79] Pfeiffer J. The properties of asphaltic bitumen. 1950.
- [80] Cottrell JH. Development of an anhydrous process for oil sand extraction. *Athabasca Oil Sands* 1963:193–206.
- [81] Kenchington JM, Cormack DE, Phillips CR, LeBlanc PJ. Parameters and Mechanisms in the Solvent Extraction of Mined Athabasca Oil Sand. *Can J Chem Eng* 1976;55:572–80.
- [82] Leung H, Phillips CR. Solvent Extraction of Mined Athabasca Oil Sands. *Ind Eng Chem Fundam* 1985;24:373–9. <https://doi.org/10.1021/i100019a015>.
- [83] Raymond CG. Process for separating oil from bituminous sands, shales, etc. 2,825,677, 1958.
- [84] Hanson D. Solvent extraction of tar sand. 4,139,450, 1979.
- [85] Wu J, Dabros T. Process for solvent extraction of bitumen from oil sand. *Energy and Fuels* 2012;26:1002–8.
- [86] Hooshiar A, Uhlik P, Liu Q, Etsell TH, Ivey DG. Clay minerals in nonaqueous extraction of bitumen from Alberta oil sands: Part 1. Nonaqueous extraction procedure. *Fuel Process Technol* 2012;94:80–5.
- [87] Wong GK, Yen TF. An electron spin resonance probe method for the understanding of

- petroleum asphaltene macrostructure. *J Pet Sci Eng* 2000;28:55–64.
[https://doi.org/10.1016/S0920-4105\(00\)00067-X](https://doi.org/10.1016/S0920-4105(00)00067-X).
- [88] Lin F, Xu Y, Nelson R. Determination and Understanding of Solvent Losses to Tailings from a Laboratory Hybrid Bitumen Extraction Process. *Energy and Fuels* 2018;32:9202–10. <https://doi.org/10.1021/acs.energyfuels.8b01978>.
- [89] Satterfield MB, Benziger JB. Non-Fickian water vapor sorption dynamics by nafion membranes. *J Phys Chem B* 2008;112:3693–704.
- [90] Satterfield MB, Benziger JB. Non-Fickian Water Vapor Sorption Dynamics by Nafion Membranes. *J Phys Chem B* 2008;112:3693–704. <https://doi.org/10.1021/jp7103243>.
- [91] De Rosa IM, Kenny JM, Puglia D, Santulli C, Sarasini F. Morphological, thermal and mechanical characterization of okra (*Abelmoschus esculentus*) fibres as potential reinforcement in polymer composites. *Compos Sci Technol* 2010;70:116–22.
<https://doi.org/10.1016/j.compscitech.2009.09.013>.
- [92] Tassios DP. *Applied chemical engineering thermodynamics*. Berlin: Springer-Verlag; 1993. <https://doi.org/10.1007/978-3-662-01645-9>.
- [93] Gray C, Gubbins K. *Theory of Molecular Fluids: Vol. 1: Fundamentals*. Oxford: Oxford: Oxford University Press; 1984.
- [94] Silberberg M. *Chemistry : the molecular nature of matter and change*. 6th ed. New York: McGraw-Hill; 2012.
- [95] Prausnitz JM. *Molecular thermodynamics of fluid-phase equilibria*. 3rd ed. Upper Saddle

- River, N.J.: Prentice Hall PTR; 1999.
- [96] Hamaker HC. The London-van der Waals attraction between spherical particles. *Physica* 1937;4:1058–72. [https://doi.org/10.1016/S0031-8914\(37\)80203-7](https://doi.org/10.1016/S0031-8914(37)80203-7).
- [97] Prausnitz JM, Lichtenthaler R, Gomes de Azevedo E. *Molecular Thermodynamics of Fluid-Phase Equilibria*. Upper Saddle River, New Jersey: Prentice Hall PTR; 1999.
- [98] Hildebrand J. Solubility. *J Am Chem Soc* 1916;38:1452–73. <https://doi.org/https://doi-org.login.ezproxy.library.ualberta.ca/10.1021/ja02265a002>.
- [99] Hildebrand J. Solubility. xii. Regular solutions 1. *J Am Chem Soc* 1929;51:66–80.
- [100] Rudin A, Choi P. *The elements of polymer science and engineering*. Waltham, Mass: Academic; 2013.
- [101] Hildebrand J. *Regular solutions*. Englewood Cliffs, N.J: Prentice Hall; 1962.
- [102] Scatchard G. Equilibria in Non-electrolyte Solutions in Relation to the Vapor Pressures and Densities of the Components. *Chem Rev* 1931;8:321–33.
- [103] McCabe WL. *Unit operations of chemical engineering*. 7th ed. Boston: McGraw-Hill; 2005.
- [104] Geankoplis C. *Transport processes and unit operations*. 3rd ed. Englewood Cliffs, N.J.: Prentice Hall PTR; 1993.
- [105] John C. *The mathematics of diffusion*. 2nd ed. Oxford: Oxford University Press; 1975.
- [106] Rubinstein M, Colby RH. *Polymer physics*. 1st ed. Oxford: Oxford University Press;

2003.

- [107] Bird RB. Theory of diffusion. Adv. Chem. Eng. vol.1, New York: Academic Press; 1956, p. 155–239.
- [108] Fick A. V. On liquid diffusion. London, Edinburgh, Dublin Philos Mag J Sci 1855;10:30–9. <https://doi.org/10.1080/14786445508641925>.
- [109] Wilke CR, Chang P. Correlation of diffusion coefficients in dilute solutions. AIChE J 1955;1:264–70. <https://doi.org/10.1002/aic.690010222>.
- [110] J. Crank GSP. Diffusion in Polymers. 1st ed. London: Academic Press; 1968.
- [111] Barrer RM. Measurement of diffusion and thermal conductivity "constants" in non-homogeneous media, and in media where these "constants" depend respectively on concentration or temperature. Proc Phys Soc 1946;58:321.
- [112] Barrer RM. Diffusion in and through Solids. Cambridge: Cambridge Univ. Press; 1951.
- [113] Carlslaw H, Jaeger J. Conduction of Heat in Solids. 2nd ed. Oxford: Clarendon Press; 1959.
- [114] Jacobs M. Diffusion Process. Springer-Verlag; 1967.
- [115] Wagner C, Jost W. Diffusion in solids, liquids, gases. Diffusion, New York: Academic Press; 1952, p. 71.
- [116] Jason AC, Peters GR. Analysis of bimodal diffusion of water in fish muscle. J Phys D Appl Phys 1973;6:512–21. <https://doi.org/10.1088/0022-3727/6/4/316>.

- [117] Barnes C. Diffusion Through a Membrane. *Physics* (College Park Md) 1934;5:4–8.
<https://doi.org/https://doi.org/10.1063/1.1745209>.
- [118] Daynes HA. The Process of Diffusion through a Rubber Membrane. *Proc R Soc London Ser A, Contain Pap a Math Phys Character* 1920;97:286–307.
- [119] Neale SM. Fundamentals of dye absorption. *J Colloid Sci* 1933;1:371–9.
[https://doi.org/https://doi.org/10.1016/0095-8522\(46\)90023-2](https://doi.org/https://doi.org/10.1016/0095-8522(46)90023-2).
- [120] Hill A V. Anaerobic and Aerobic Activity in Isolated Muscle. *Proc R Soc London Ser B, Contain Pap a Biol Character* 1928;105:313–22.
- [121] Kokes RJ, Long FA, Hoard JL. Diffusion of Acetone into Polyvinyl Acetate above and below the Second- Order Transition. *J Chem Phys* 1952;20:1711–6.
- [122] Funk EW. Behavior of tar sand bitumen with paraffinic solvents and its application to separations for athabasca tar sands. *Can J Chem Eng* 1979;57:333–41.
- [123] Meadus FW, Bassaw BP, Sparks BD. Solvent extraction of athabasca oil-sand in a rotating mill Part 2. Solids—liquid separation and bitumen quality. *Fuel Process Technol* 1982;6:289–300.
- [124] Buss F, Göcke J, Scharfer P, Schabel W. From Micro to Nano Thin Polymer Layers: Thickness and Concentration Dependence of Sorption and the Solvent Diffusion Coefficient. *Macromolecules* 2015;48:8285–93.
- [125] Vogt BD, Soles CL, Lee HJ, Lin EK, Wu WL. Moisture Absorption and Absorption Kinetics in Polyelectrolyte Films: Influence of Film Thickness. *Langmuir* 2004;20:1453–

8.

- [126] Majsztrik PW, Satterfield MB, Bocarsly AB, Benziger JB. Water sorption, desorption and transport in Nafion membranes. *J Memb Sci* 2007;301:93–106.
- [127] Vogt BD, Soles CL, Wang CY, Prabhu VM, Mcguiggan PM, Douglas JF, et al. Water immersion of model photoresists: Interfacial influences on water concentration and surface morphology. *J Microlithogr Microfabr Microsystems* 2005;4:1–6.
- [128] Eastman SA, Kim S, Page KA, Rowe BW, Kang S, Soles CL, et al. Effect of confinement on structure, water solubility, and water transport in Nafion thin films. *Macromolecules* 2012;45:7920–30.
- [129] Lin EK, Kolb R, Satija SK, Wu W. Reduced Polymer Mobility near the Polymer / Solid Interface as Measured by Neutron Reflectivity. *Macromolecules* 1999;32:3753–7.
- [130] Frank B, Gast AP. Polymer Mobility in Thin Films. *Macromolecules* 1996;29:6531–4.
- [131] Zheng X, Rafailovich MH, Sokolov J. Long-Range Effects on Polymer Diffusion Induced by a Bounding Interface. *Phys Rev Lett* 1997;79:241–4.
- [132] Fukao K, Miyamoto Y. Glass transitions and dynamics in thin polymer films : Dielectric relaxation of thin films of polystyrene. *Phys Rev E* 2000;61:1743–54.
- [133] Demaggio GB, Frieze WE, Gidley DW. Interface and Surface Effects on the Glass Transition in Thin Polystyrene Films. *Phys Rev Lett* 1997;78:1524–7.
- [134] Vogt BD, Soles CL, Lee HJ, Lin EK, Wu WL. Moisture absorption into ultrathin hydrophilic polymer films on different substrate surfaces. *Polymer (Guildf)*

2005;46:1635–42.

- [135] Li Y, Yang Q, Mei RA, Cai M, Heng JYY, Yang Z. Controlling the Accumulation of Water at Oil – Solid Interfaces with Gradient Coating. *J Phys Chem B* 2017;121:6766–72.
- [136] Zhang R, Liao W, Sun Y, Heng JYY, Yang Z. Investigating the Role of Glass and Quartz Substrates on the Formation of Interfacial Droplets. *J Phys Chem C* 2018;123:1151–9.
- [137] Yang Z, Abbott NL. Spontaneous Formation of Water Droplets at Oil - Solid Interfaces. *Langmuir* 2010;26:13797–804.
- [138] Tang JS. On the determination of diffusivities of volatile hydrocarbons in semi-solid bitumen. *Can J Chem Eng* 2001;79:164–8.
- [139] Fu BCH, Phillips CR. New technique for determination of diffusivities of volatile hydrocarbons in semi-solid bitumen. *Fuel* 1979;58:557–60.
- [140] Bird RB, Stewart WE, Lightfoot EN. *Transport Phenomena*. 2nd ed. New York: J. Wiley & Sons, Inc; 2007.
- [141] Neale SM, Stringfellow WA, Walker WP. the Absorption of Direct Dyestuffs By Cellulose. *J Text Inst Proc* 2009;24:P145–9.
- [142] Nikakhtari H, Wolf S, Choi P, Liu Q, Gray MR. Migration of fine solids into product bitumen from solvent extraction of Alberta oilsands. *Energy and Fuels* 2014;28:2925–32.
- [143] Dobreva A, Gutzow I, Schmelzer J. Stress and time dependence of relaxation and the Kohlrausch stretched exponent formula. *J Non Cryst Solids* 1997;209:257–63.

- [144] Fancey KS. A Latch-Based Weibull Model for Polymerie Creep and Recovery. *J Polym Eng* 2011;21:489–510.
- [145] Kokes RJ, Long FA. Diffusion of Organic Vapors into Polyvinyl Acetate. *J Am Chem Soc* 1953;75:6142–6.
- [146] Felder RM, Rousseau RW. *Elementary Principles of Chemical Processes*. 3rd ed. New York: John Wiley; 2005.
- [147] Bayati F, Boluk Y, Choi P. Inverse Gas Chromatography Study of the Permeability of Aroma through Hydroxypropyl Xylan Films. *ACS Sustain Chem Eng* 2015;3:3114–22.
- [148] Wang T, Zhang C, Zhao R, Zhu C, Yang C, Liu C. Solvent extraction of bitumen from oil sands. *Energy and Fuels* 2014;28:2297–304.
- [149] Kislitsin V, Choi P. Thickness Dependence of the Diffusivity and Solubility of Cyclohexane in Nanoscale Bitumen Films. *ACS Omega* 2019;4:21578–86.
- [150] Mamaliga I, Schabel W, Kind M. Measurements of sorption isotherms and diffusion coefficients by means of a magnetic suspension balance. *Chem Eng Process Process Intensif* 2004;43:753–63.
- [151] Burnett DJ, Garcia AR, Thielmann F. Measuring moisture sorption and diffusion kinetics on proton exchange membranes using a gravimetric vapor sorption apparatus. *J Power Sources* 2006;160:426–30.
- [152] Morris DR, Sun X. Water sorption and transport properties of Nafion 117 H. *J Appl Polym Sci* 1993;50:1445–52.

- [153] Rivin D, Kendrick CE, Gibson PW, Schneider NS. Solubility and transport behavior of water and alcohols in Nafion. *Polymer (Guildf)* 2001;42:623–35.
- [154] Takamatsu T, Hashiyama M, Eisenberg A. Sorption Phenomena in Nafion Membranes. *J Appl Polym Sci* 1979;24:2199–220.
- [155] Nourozieh H, Kariznovi M, Abedi J. Density and Viscosity of Athabasca Bitumen Samples at Temperatures Up to 200C and Pressures Up to 10 MPa. *SPE Reserv Eval Eng* 2015;18:375–86.
- [156] Carbonell RG, Sarti GC. Coupled Deformation and Mass-Transport Processes in Solid Polymers. *Ind Eng Chem Res* 1990;29:1194–204.
- [157] Asmatulu R. Removal of the discoloring contaminants of an East Georgia kaolin clay and its dewatering. *Turkish J Eng Environ Sci* 2002;26:447–53.
- [158] Sumner AL, Menke EJ, Dubowski Y, Newberg JT, Penner RM, Hemminger JC, et al. The nature of water on surfaces of laboratory systems and implications for heterogeneous chemistry in the troposphere. *Phys Chem Chem Phys* 2004;6:604–13.
- [159] Borysenko A, Clennell B, Sedev R. Experimental investigations of the wettability of clays and shales. *J Geophysical Res* 2009;114.
- [160] Leelamanie DAL, Karube J, Yoshida A. Clay effects on the contact angle and water drop penetration time of model soils. *Soil Sci Plant Nutr* 2010;56:371–5.
- [161] Minagawa H, Nishikawa Y, Ikeda I, Miyazaki K, Takahara N, Sakamoto Y, et al. Characterization of sand sediment by pore size distribution and permeability using proton

- nuclear magnetic resonance measurement. *J Geophys Res Solid Earth* 2008;113:1–9.
- [162] Jennings SG. The mean free path in air. *J Aerosol Sci* 1988;19:159–66.
- [163] Vedoy RL, Soares BP. Water-soluble Polymers for Oil Sands Tailing Treatment: A Review. *Can J Chem Eng* 2015;93:888–904.
- [164] Kislitsin V, Choi P. Initial mass uptake dynamics and diffusivity of cyclohexane vapor in nano-scale bitumen films coated on substrates with different degrees of hydrophilicity. *Fuel* 2020;271.
- [165] Gravimetric Gas & Vapor Sorption Analyzers. Hiden Isochema Ltd 2020:6.
<https://hidenisochema.com/content/uploads/2016/05/Hiden-Isochema-IGA-Series-Brochure.pdf> (accessed May 4, 2020).

APPENDIX

Appendix A

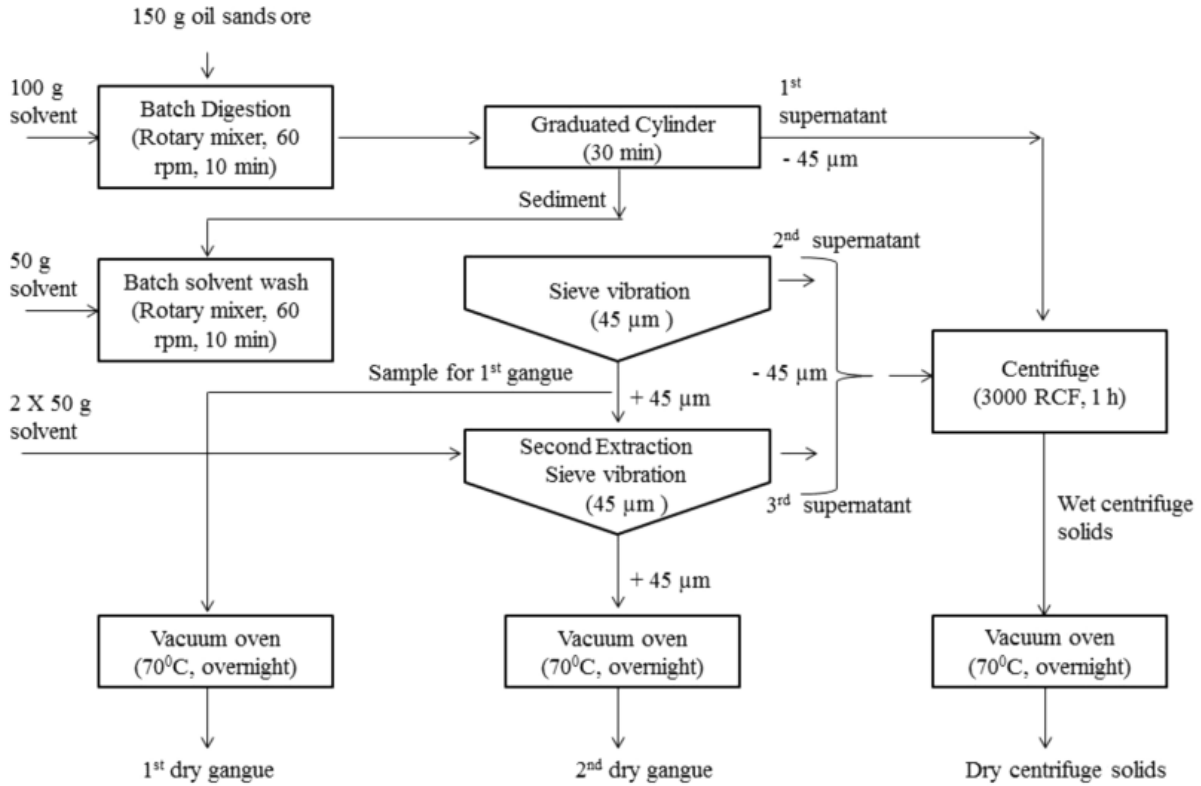


Figure A 1: Schematic NAE procedure developed by IOSI (reused from Pal et al [35] with ACS permission)

Experimental Setup

In our gravimetric experiments we used Hidden Isochema Intelligent Gravimetric Sorption analyzer (IGA) – 001 [165]. The schematic device setup is depicted in Figure A2.

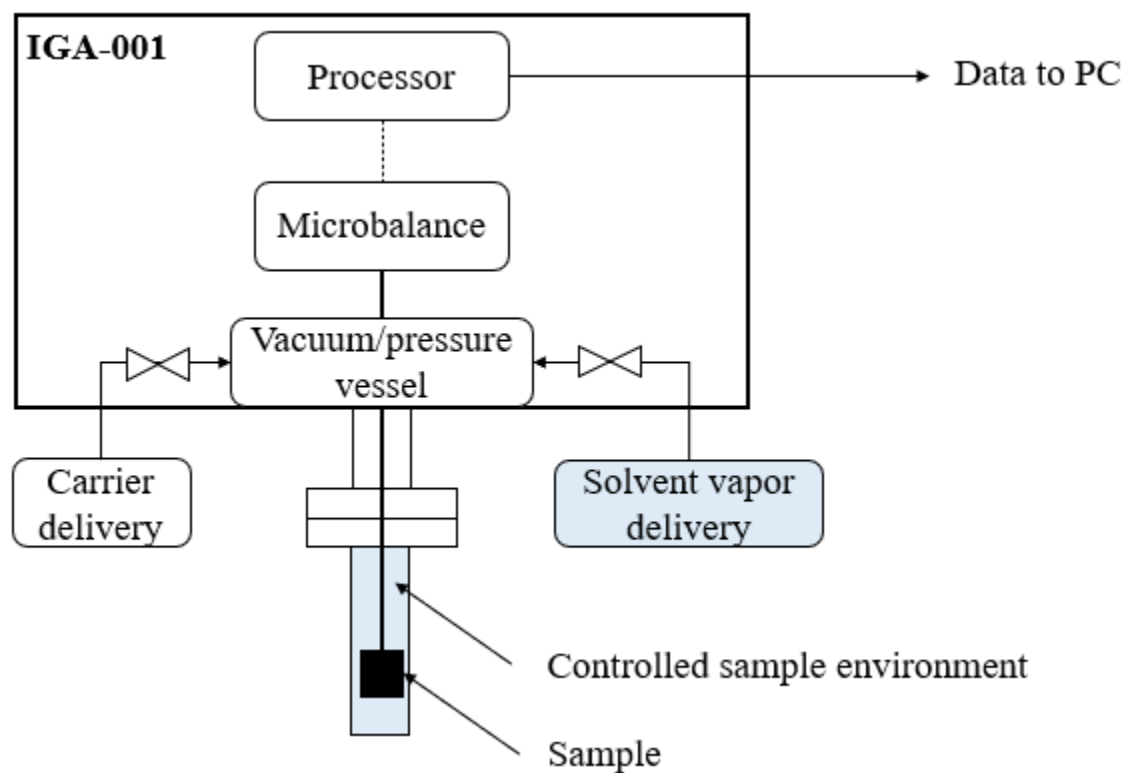


Figure A 2: Schematic representation of IGA-001 apparatus (from Hidden Isochema [1])

In the gravimetric experiment, the sample is placed in a metal sample holder and attached to the microbalance. The carrier gas and solvent vapor is delivered into the controlled environment sample compartment at the desired flowrates and ratios. The mass change of sample is measured by the microbalance with accuracy of $0.1 \mu\text{m}$. The measurements are made 3-4 times per second the data is collected and sent to the PC for further processing.

Appendix B

Thickness Dependence of the Diffusivity and Solubility of Cyclohexane in Nanoscale Bitumen Films

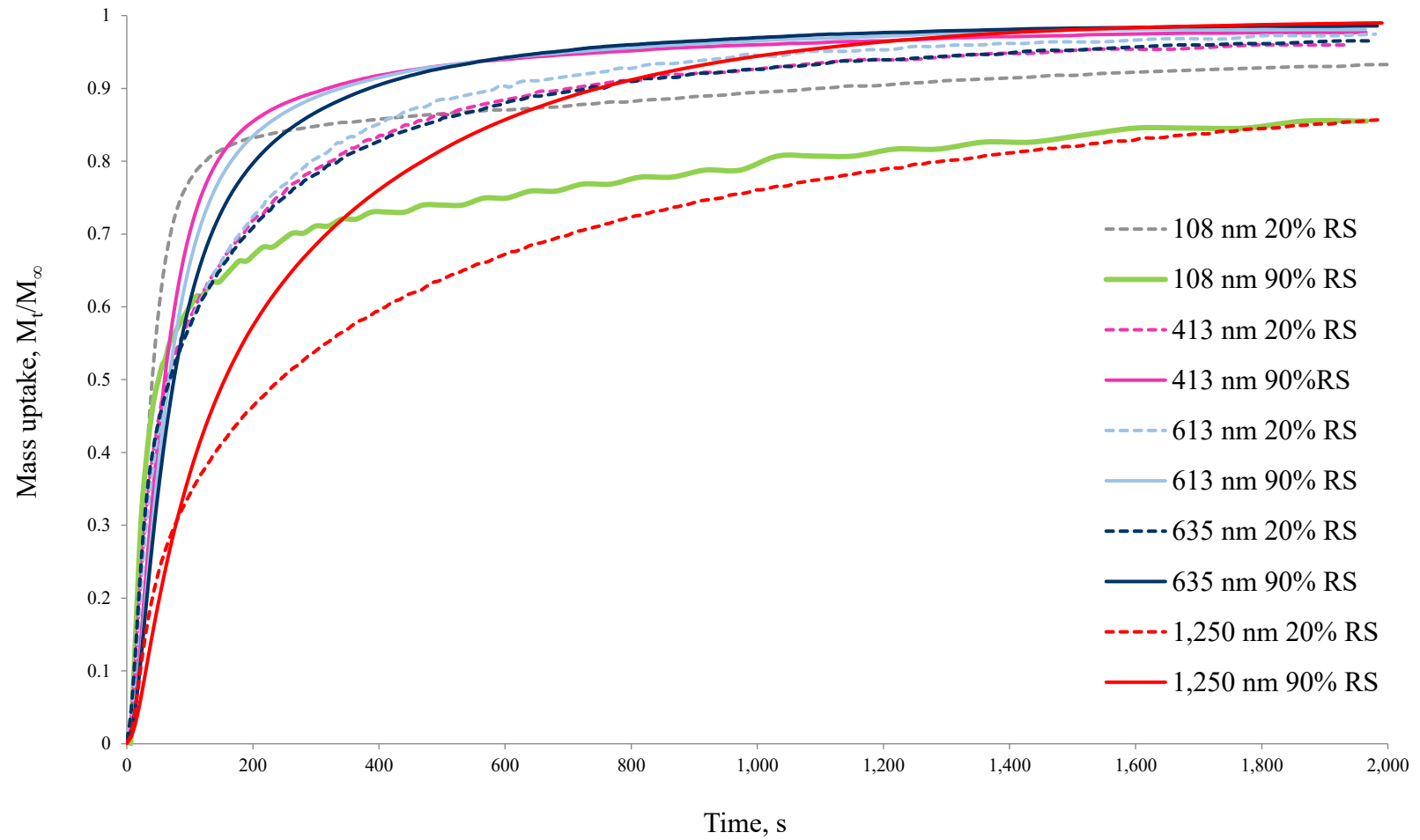


Figure B 1: Sample A absorption curves

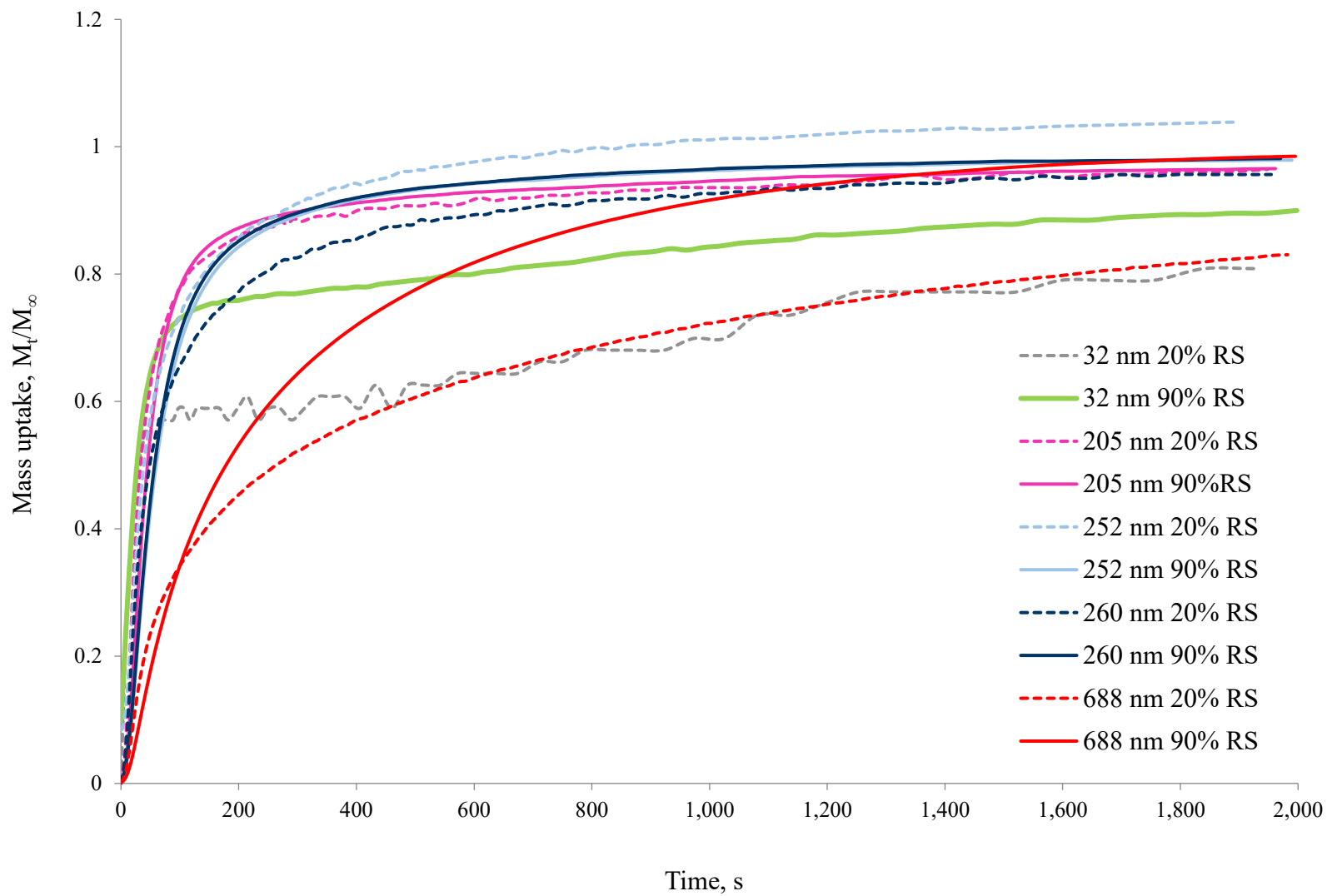


Figure B 2: Sample B absorption curves

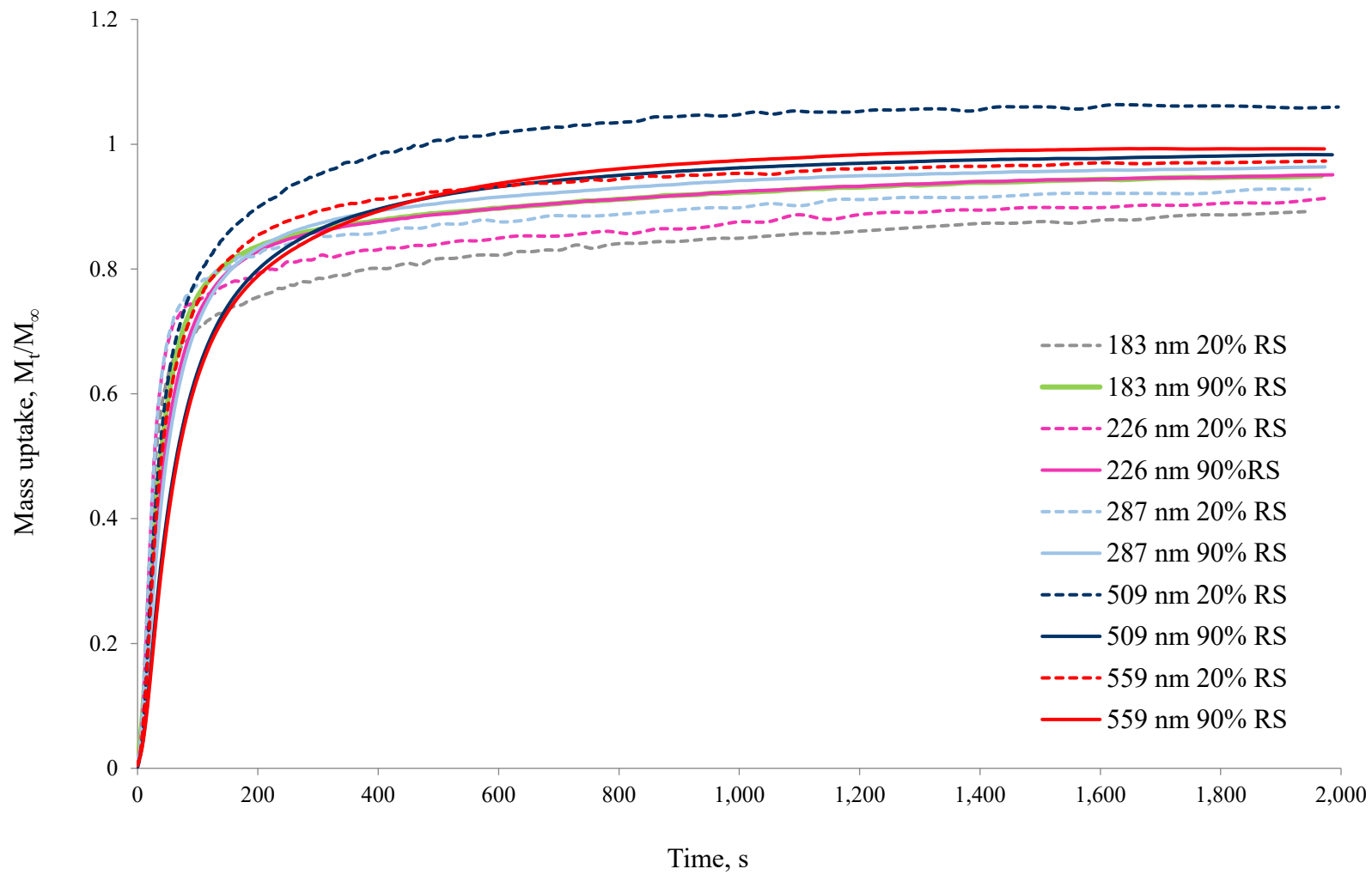
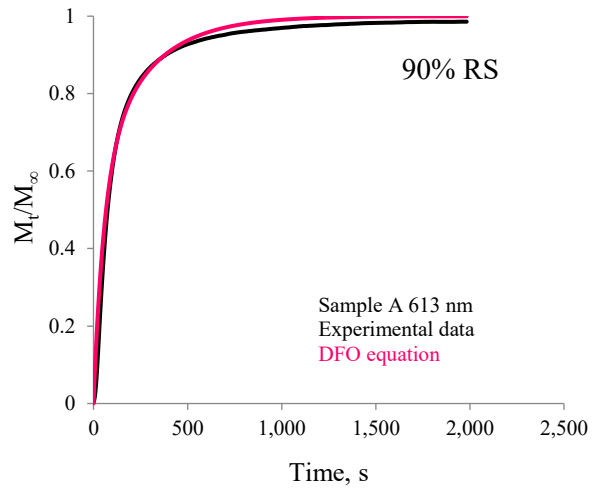
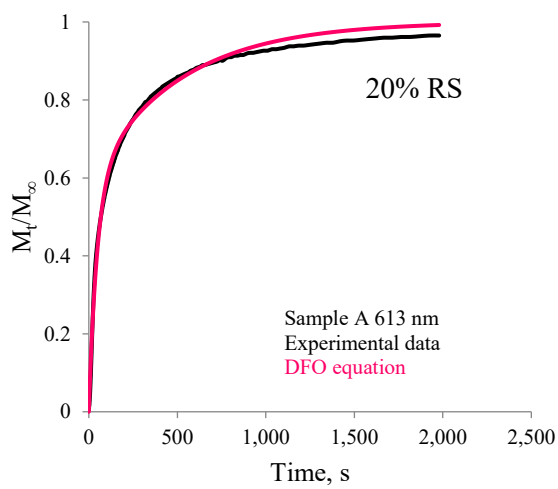
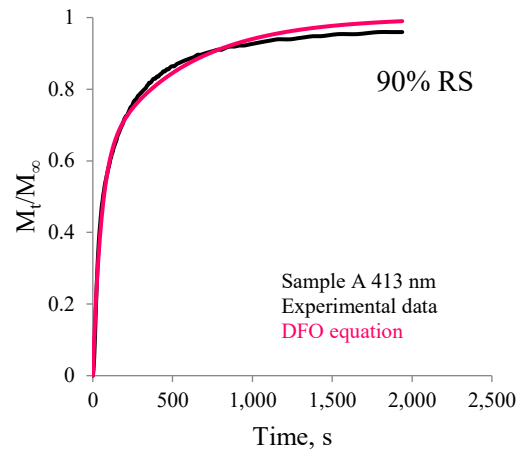
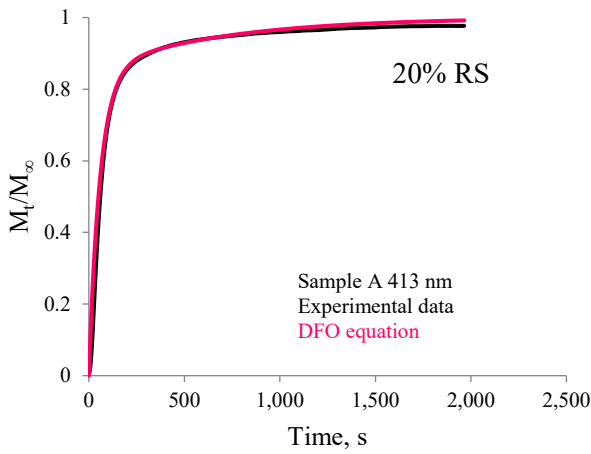
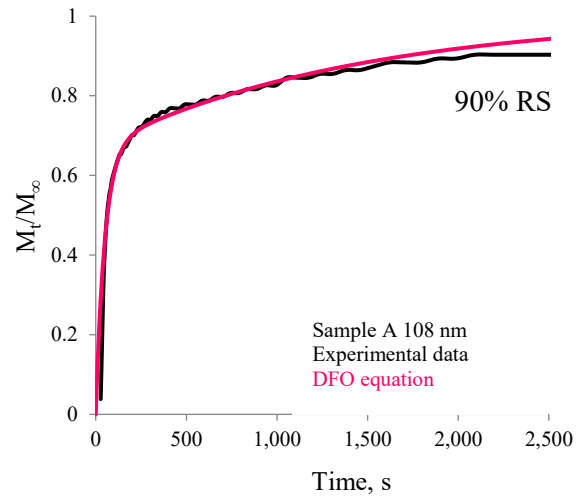
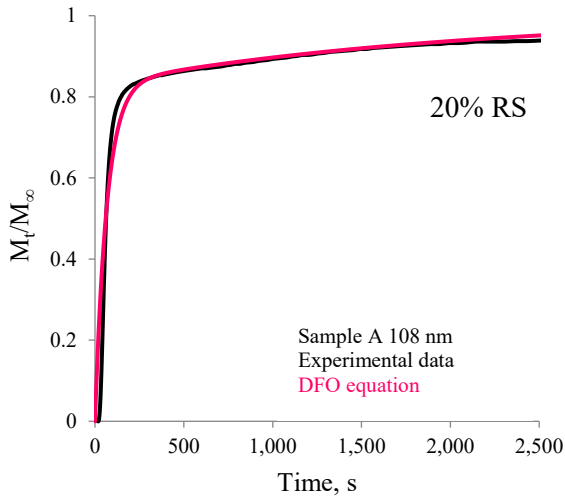
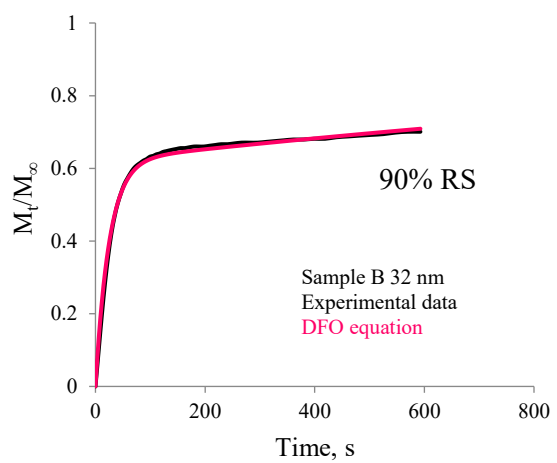
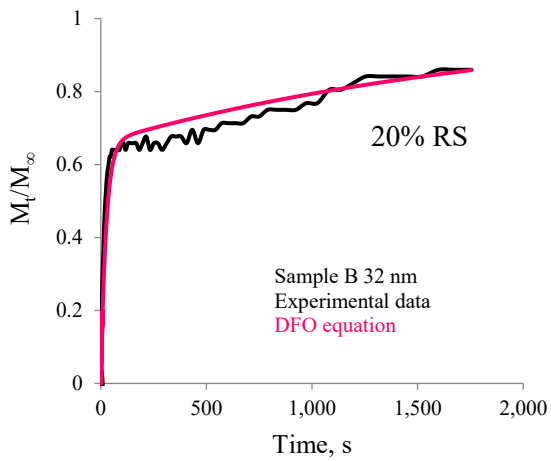
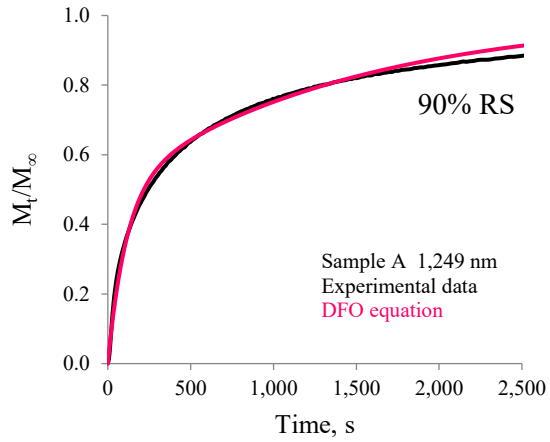
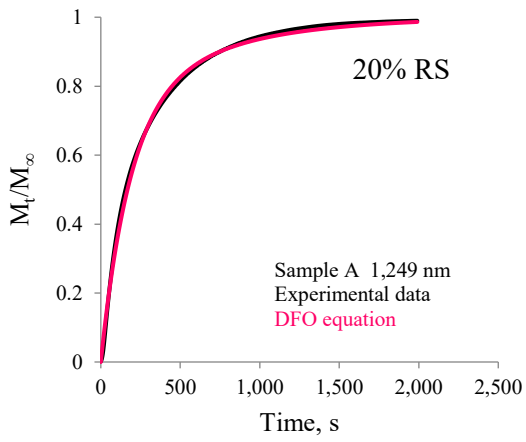
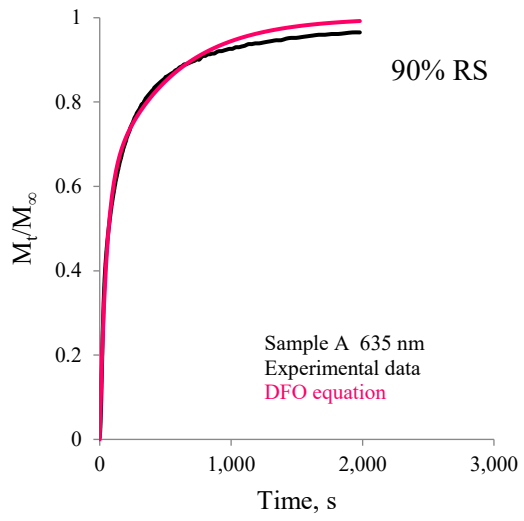
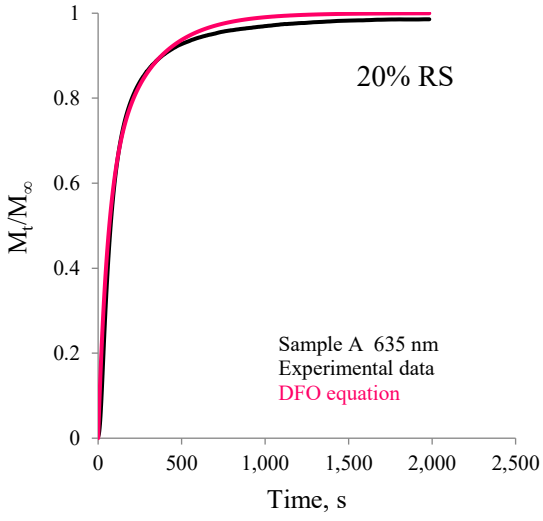
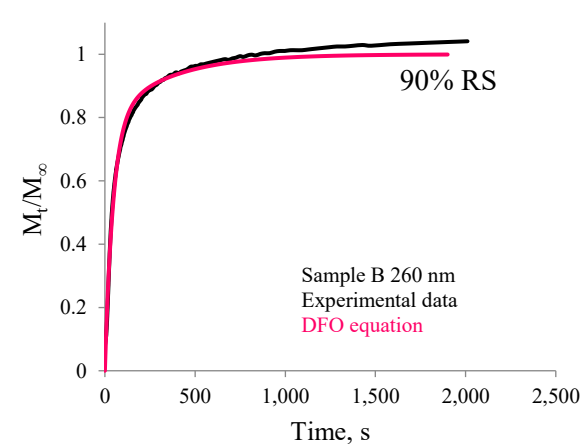
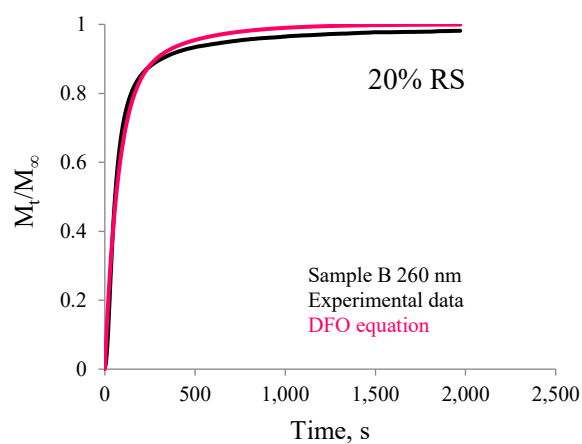
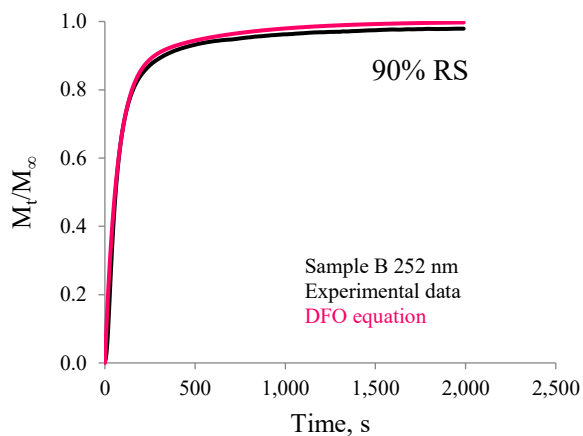
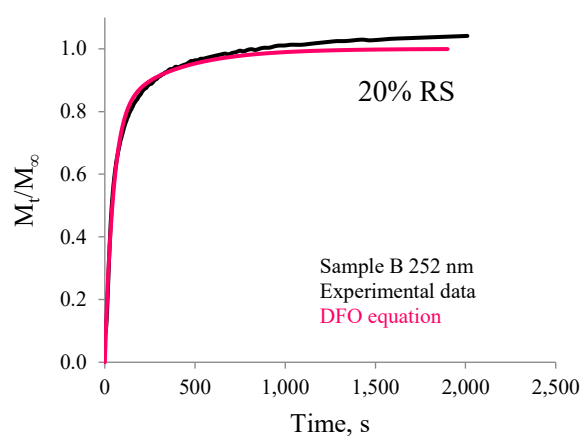
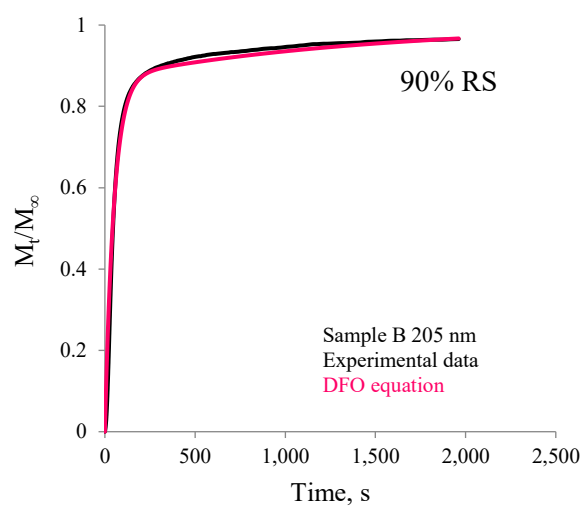
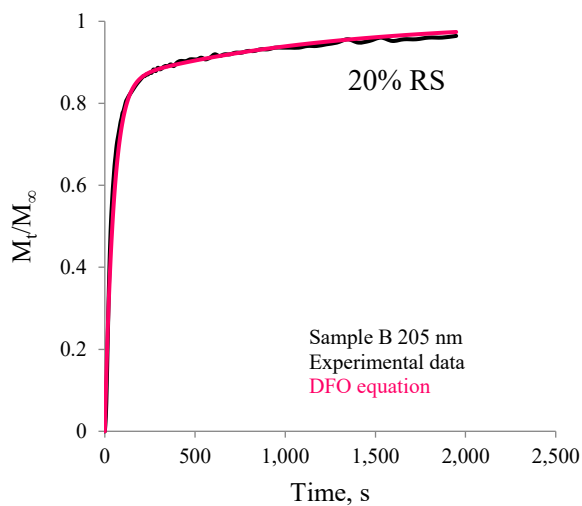
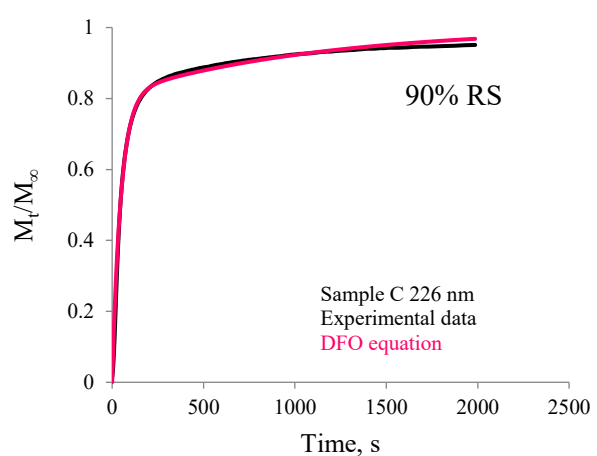
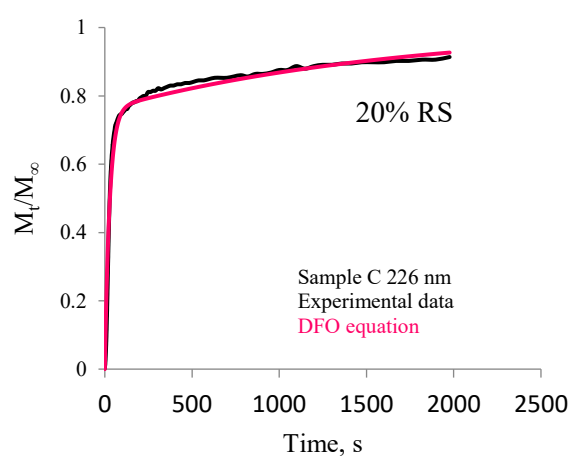
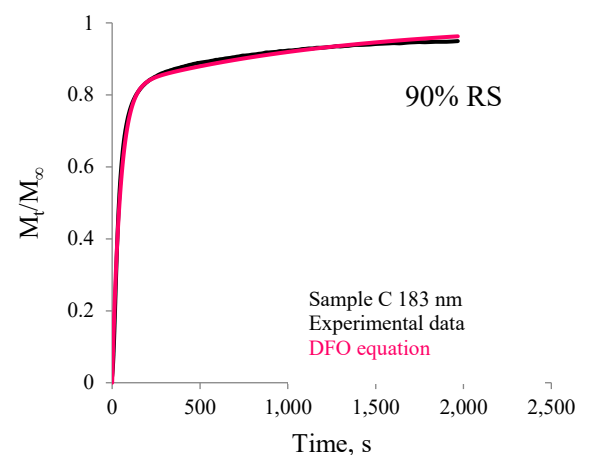
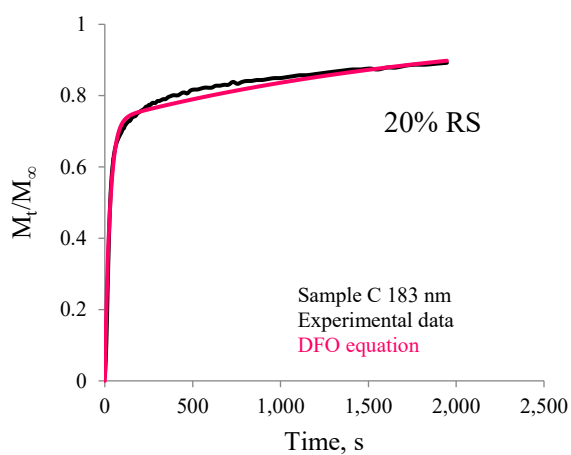
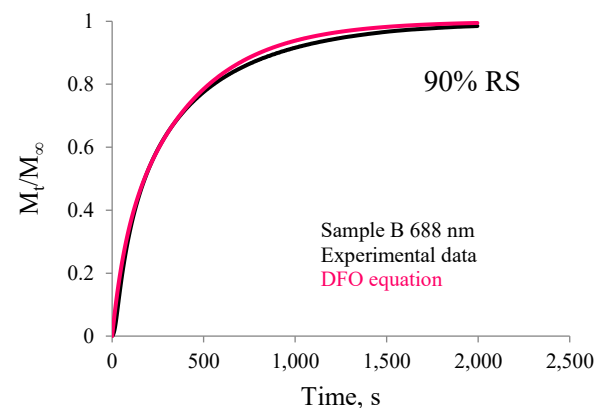
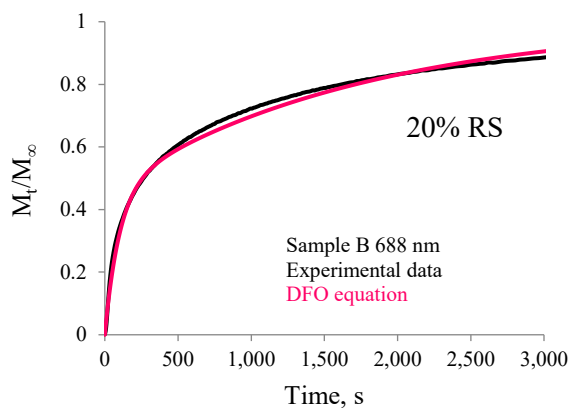


Figure B 3: Sample C absorption curves









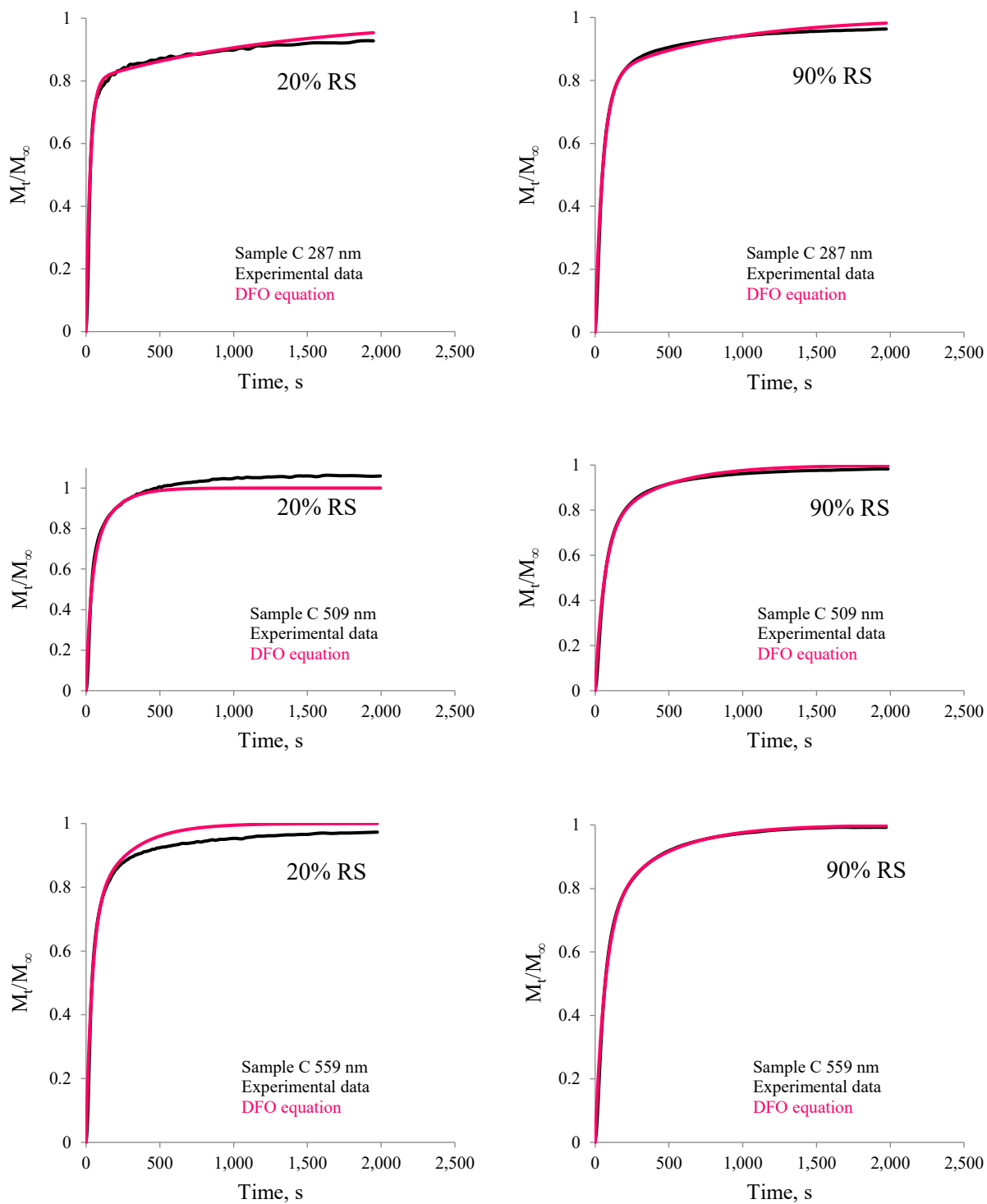


Figure B 4: Fitting of DFO equation into experimental data

Table B1. Values of fitted parameters k_1 and k_2 from Double-First-Order kinetics equation
Sample A

Bitumen film thickness (nm)	Cyclohexane relative saturation (%)	k_1	k_2
108	20	0.025	0.0006
	90	0.032	0.0007
413	20	0.02	0.0018
	90	0.017	0.0015
613	20	0.016	0.002
	90	0.014	0.0016
635	20	0.018	0.0038
	90	0.021	0.002
1249	20	0.015	0.0055
	90	0.012	0.005

Table B2. Values of fitted parameters k_1 and k_2 from Double-First-Order kinetics equation
Sample B

Bitumen film thickness (nm)	Cyclohexane relative saturation (%)	k_1	k_2
32	20	0.04	0.0005
	90	0.04	0.00045
205	20	0.026	0.0009
	90	0.02	0.0007
252	20	0.022	0.003
	90	0.015	0.002
260	20	0.02	0.003
	90	0.014	0.005
688	20	0.01	0.007
	90	0.015	0.0025

Table B3. Values of fitted parameters k_1 and k_2 from Double-First-Order kinetics equation Sample C

Bitumen film thickness (nm)	Cyclohexane relative saturation (%)	k_1	k_2
183	20	0.036	0.0005
	90	0.022	0.0008
26	20	0.036	0.0006
	90	0.021	0.0009
287	20	0.034	0.00075
	90	0.019	0.0012
509	20	0.03	0.004
	90	0.016	0.0025
559	20	0.025	0.005
	90	0.015	0.0025

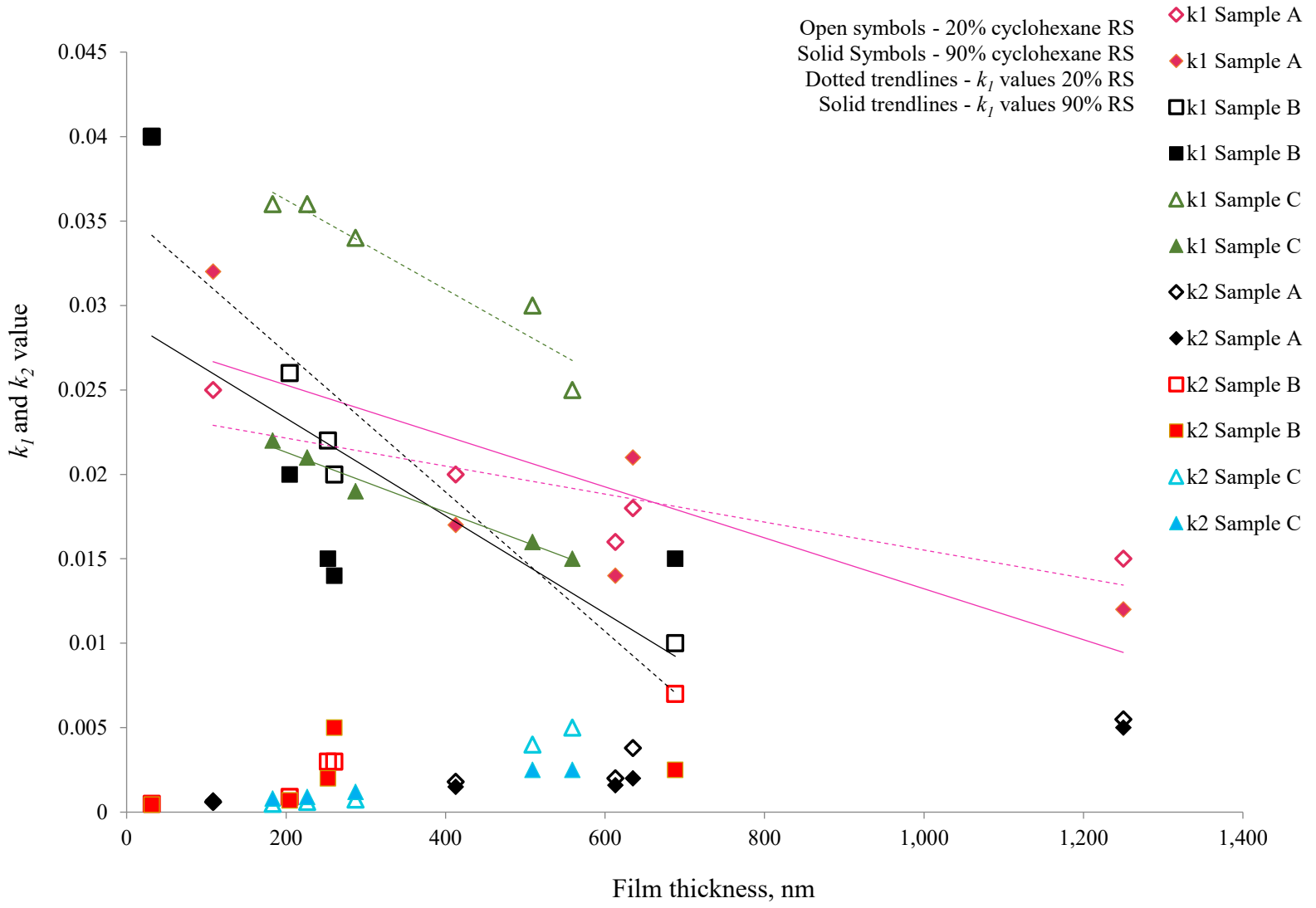


Figure B 5: Values of rate constants k_1 and k_2 of all samples

Table B4. Estimated diffusion coefficients and equilibrium concentrations of cyclohexane in Sample A at 25 °C (n = 3)

Bitumen coated (wt%)	Film Thickness (nm)	Cyclohexane relative saturation (%RS)	Diffusion coefficient at the initial absorption stage ($\times 10^{16} \text{ m}^2/\text{s}$)	Cyclohexane Concentration at saturation (g cyclohexane/g bitumen)
0.20	108	20	0.09	0.05 ± 0.004
		90	0.09	0.38 ± 0.045
0.74	413	20	1.01	0.04 ± 0.004
		90	1.05	0.39 ± 0.045
1.10	613	20	2.12	0.04 ± 0.004
		90	2.09	0.32 ± 0.045
1.14	635	20	2.28	0.04 ± 0.004
		90	2.15	0.40 ± 0.045
2.23	1,249	20	2.93	0.05 ± 0.004
		90	4.38	0.45 ± 0.045

Table B5. Estimated diffusion coefficients and equilibrium concentrations of cyclohexane in Sample B at 25 °C (n = 3)

Bitumen coated (wt%)	Film Thickness (nm)	Cyclohexane relative saturation (%RS)	Diffusion coefficient at the initial absorption stage ($\times 10^{16} \text{ m}^2/\text{s}$)	Cyclohexane Concentration at saturation (g cyclohexane/g bitumen)
0.10	32	20	0.02	0.05 ± 0.004
		90	0.02	0.42 ± 0.046
0.54	205	20	0.26	0.04 ± 0.004
		90	0.26	0.35 ± 0.046
0.88	252	20	0.57	0.05 ± 0.004
		90	0.40	0.38 ± 0.046
0.98	260	20	0.57	0.04 ± 0.004
		90	0.51	0.32 ± 0.046
2.55	688	20	0.83	0.04 ± 0.004
		90	1.18	0.42 ± 0.046

Table B6. Estimated diffusion coefficient and equilibrium concentration of cyclohexane in Sample C at 25 °C (n = 3)

Bitumen coated (wt%)	Film Thickness (nm)	Cyclohexane relative saturation (%RS)	Diffusion coefficient at the initial absorption stage ($\times 10^{16} \text{ m}^2/\text{s}$)	Cyclohexane Concentration at saturation (g cyclohexane/g bitumen)
0.61	183	20	0.15	0.04 ± 0.003
		90	0.12	0.25 ± 0.018
0.78	226	20	0.25	0.03 ± 0.003
		90	0.17	0.23 ± 0.018
1.01	287	20	0.39	0.03 ± 0.003
		90	0.25	0.22 ± 0.018
1.86	509	20	1.06	0.03 ± 0.003
		90	0.64	0.25 ± 0.018
2.06	559	20	1.19	0.03 ± 0.003
		90	0.75	0.26 ± 0.018

Appendix C

**Comparison between the kinetics of cyclohexane absorption and desorption
for heterogeneous bitumen nanofilms**

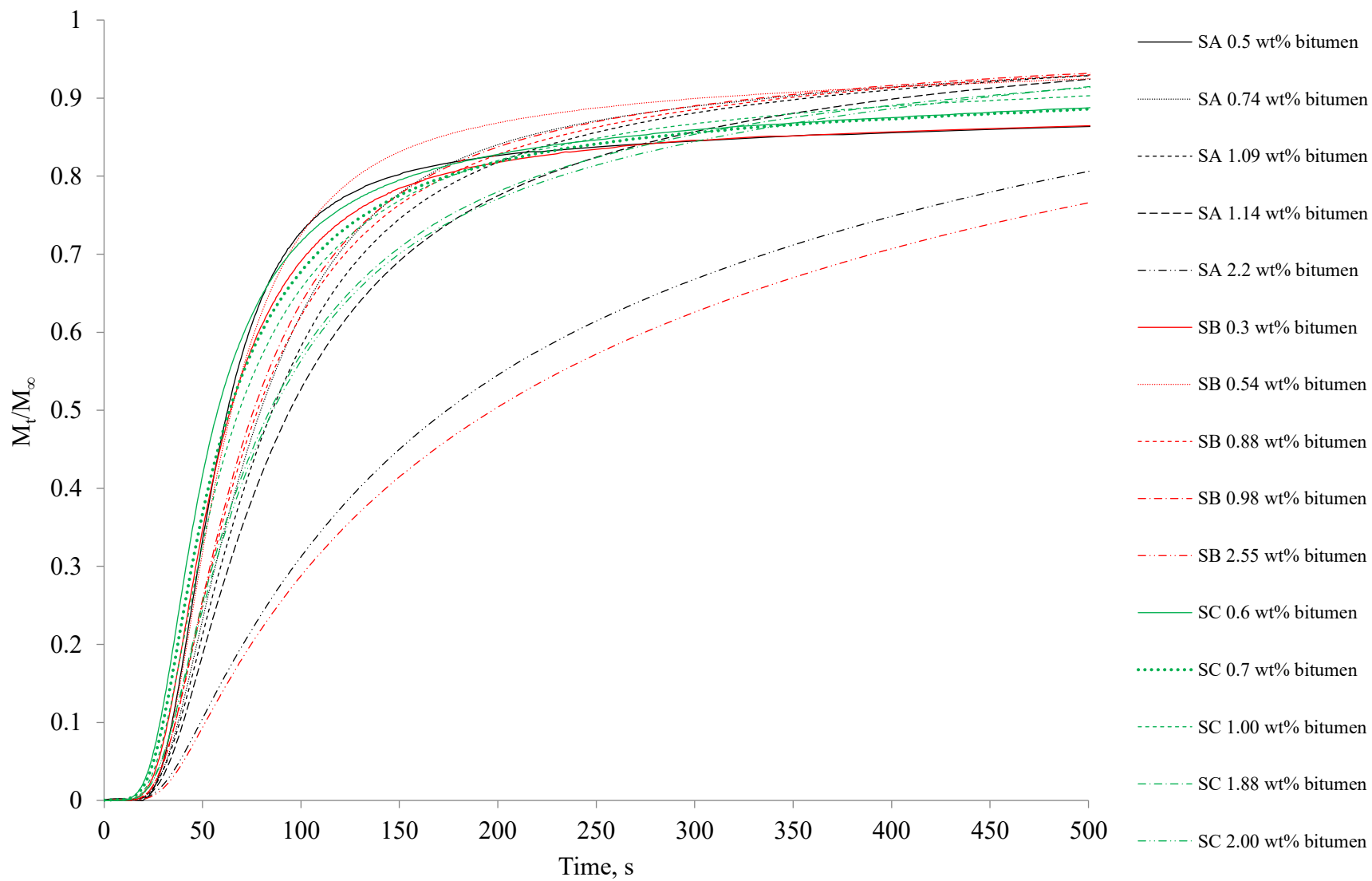


Figure C 1: All samples absorption curves at 90% cyclohexane RS

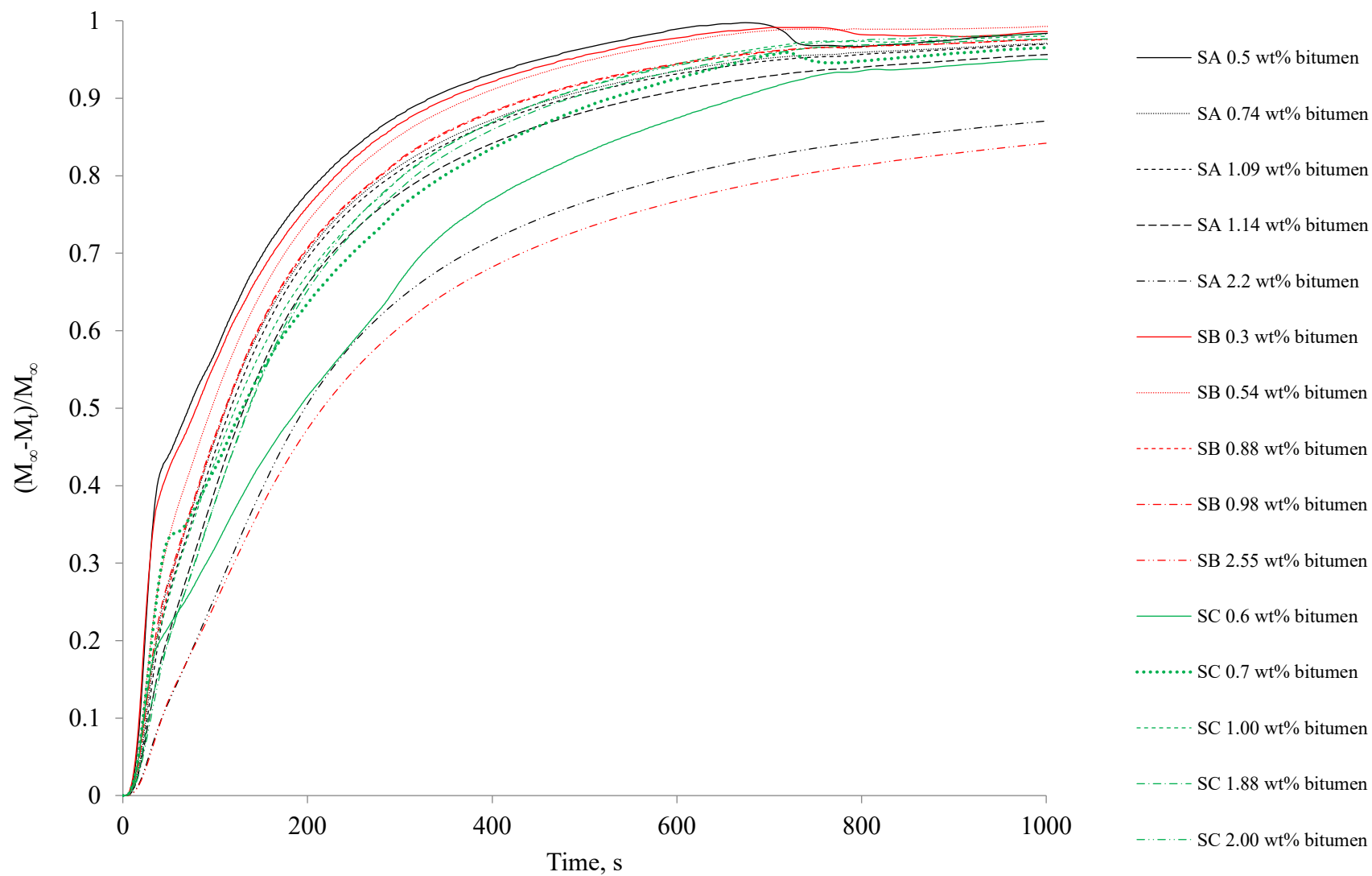


Figure C 2: All samples desorption curves at 90% cyclohexane RS

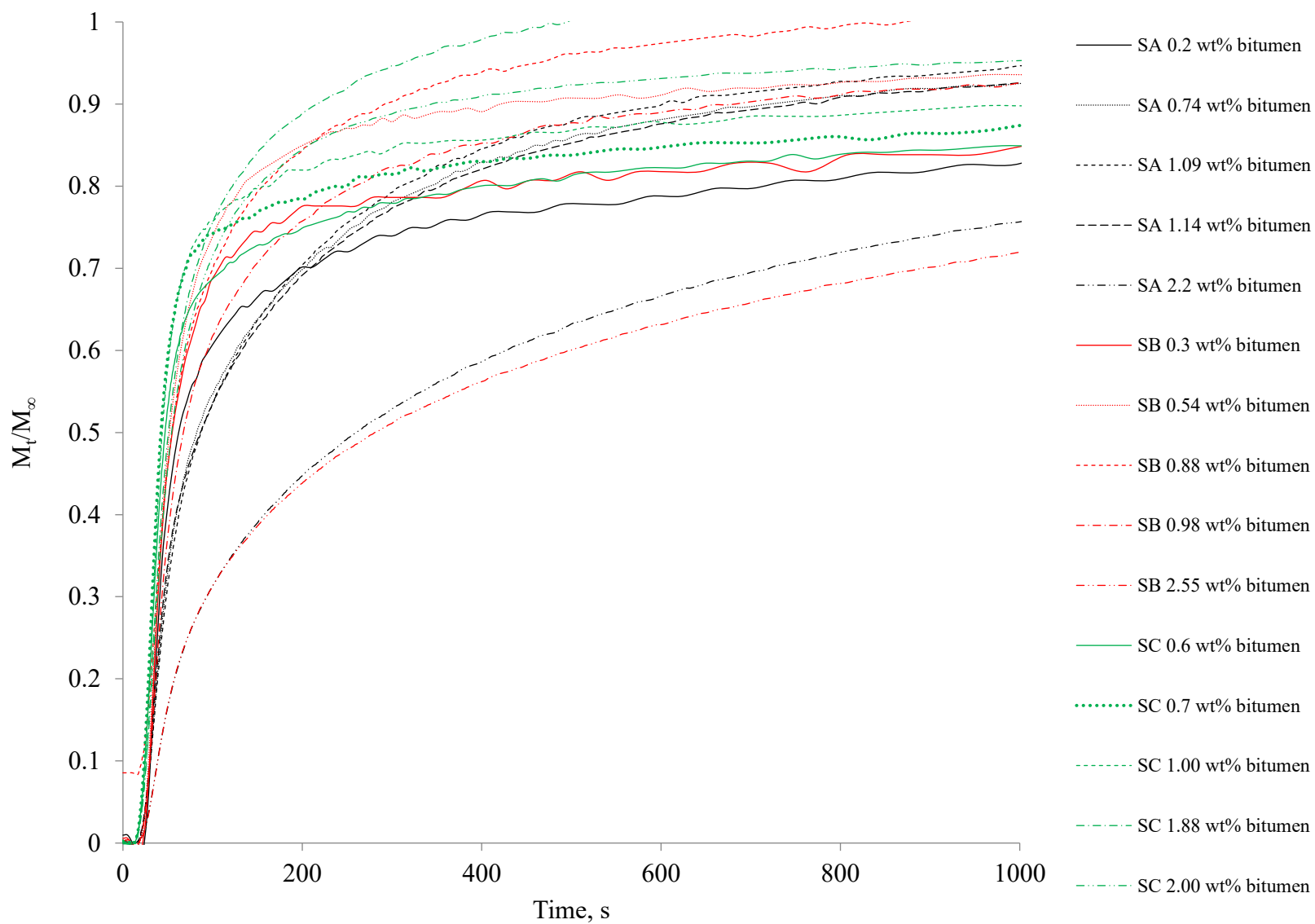


Figure C 3: Mass uptake curves of samples SA, SB, and SC at 20% cyclohexane RS

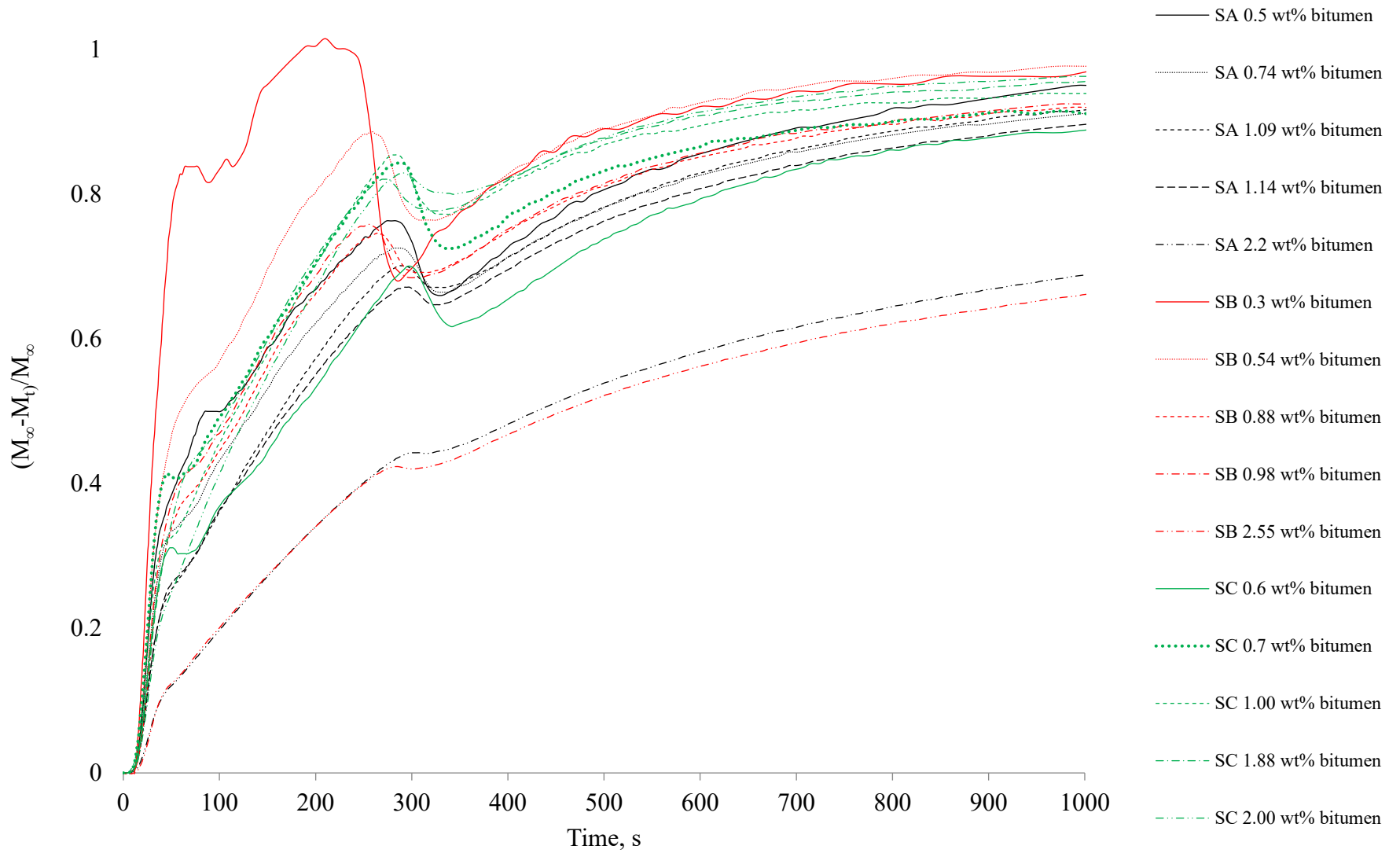


Figure C 4: Mass release curves of samples SA, SB, and SC at 20% cyclohexane RS

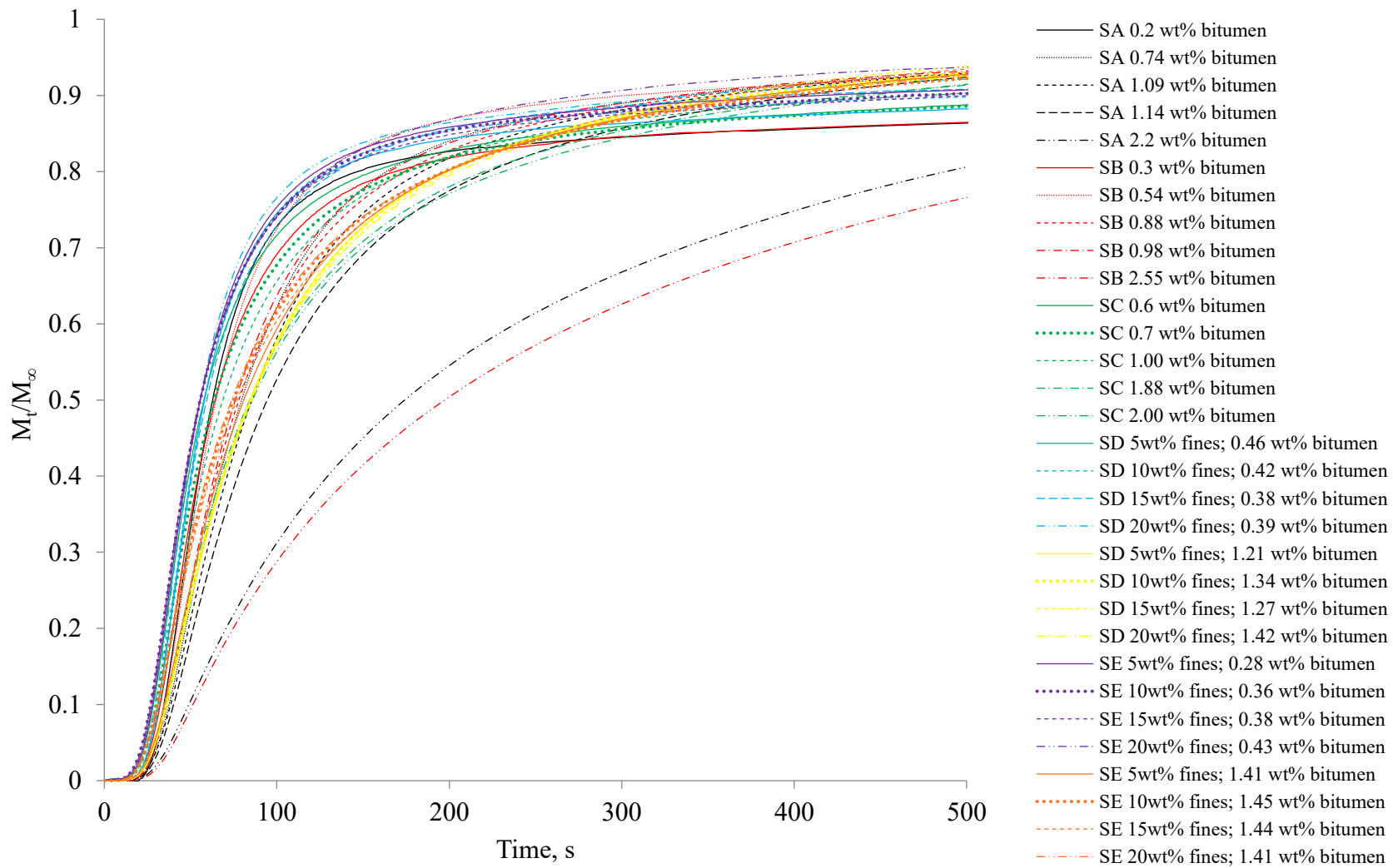


Figure C 5: All samples absorption curves at 90% cyclohexane RS

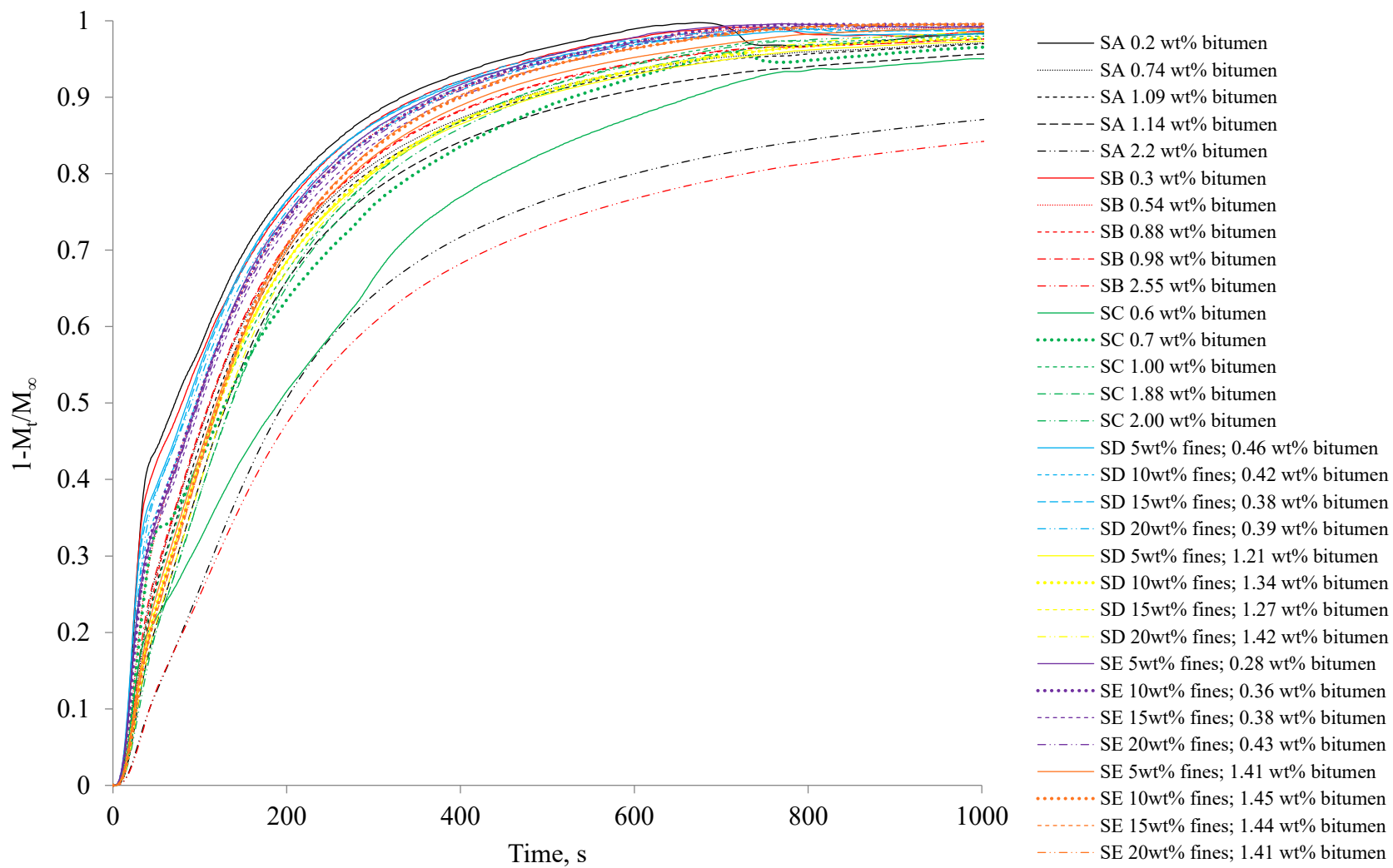


Figure C 6: All samples desorption curves at 90% cyclohexane RS

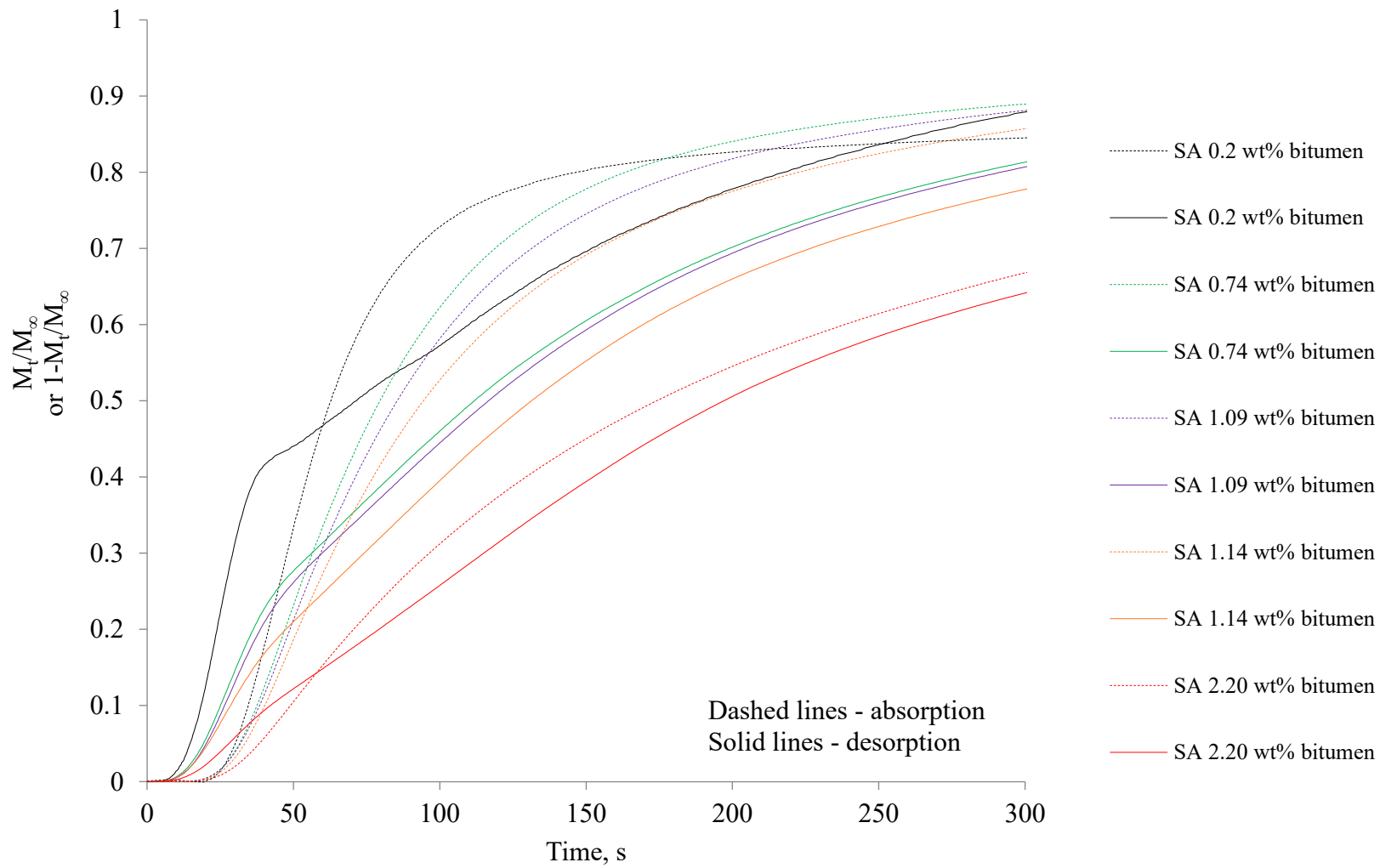


Figure C 7: Mass uptake/release curves of SA at 90% cyclohexane RS

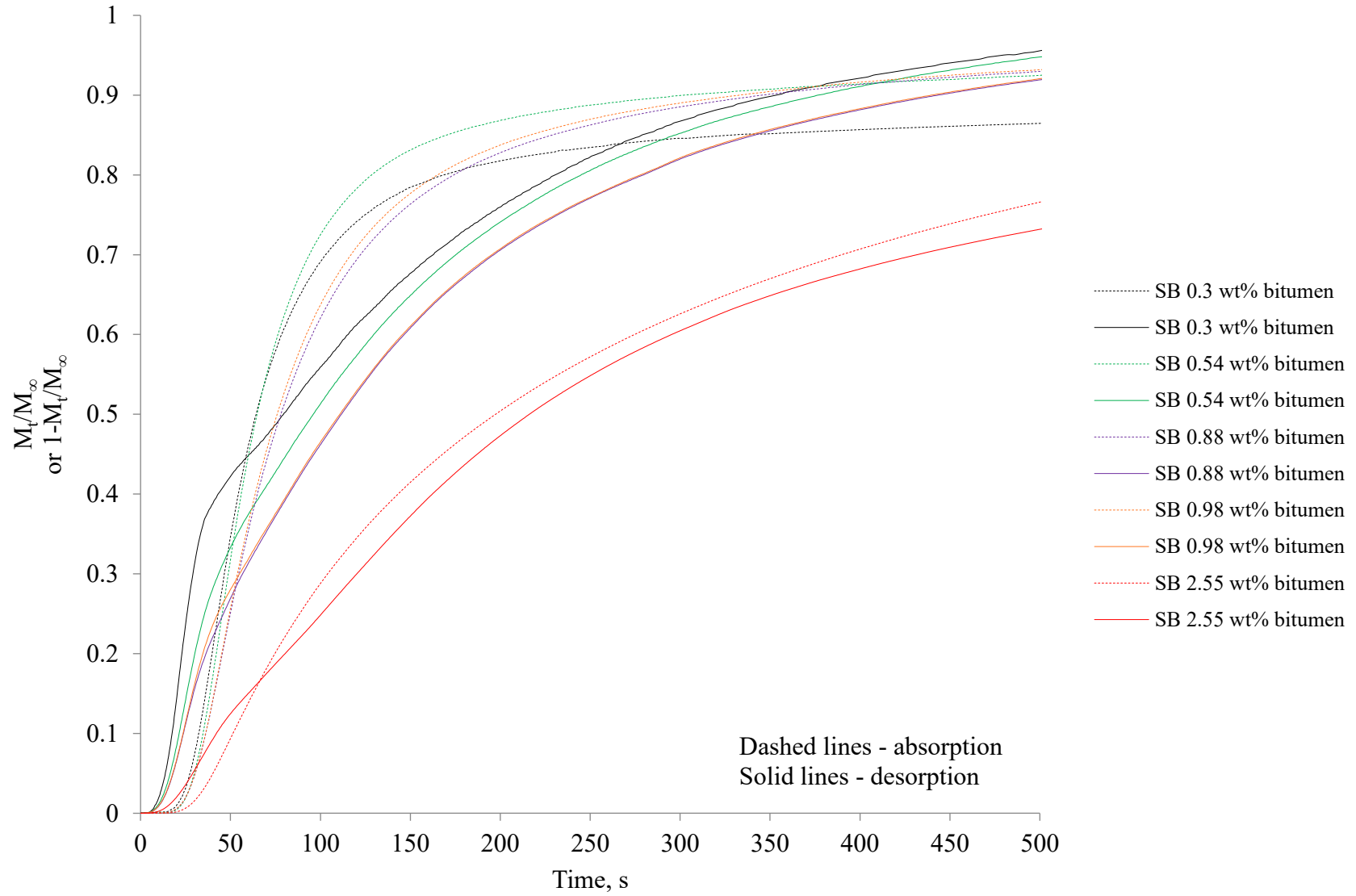


Figure C 8: Mass uptake/release curves of SA at 90% cyclohexane RS

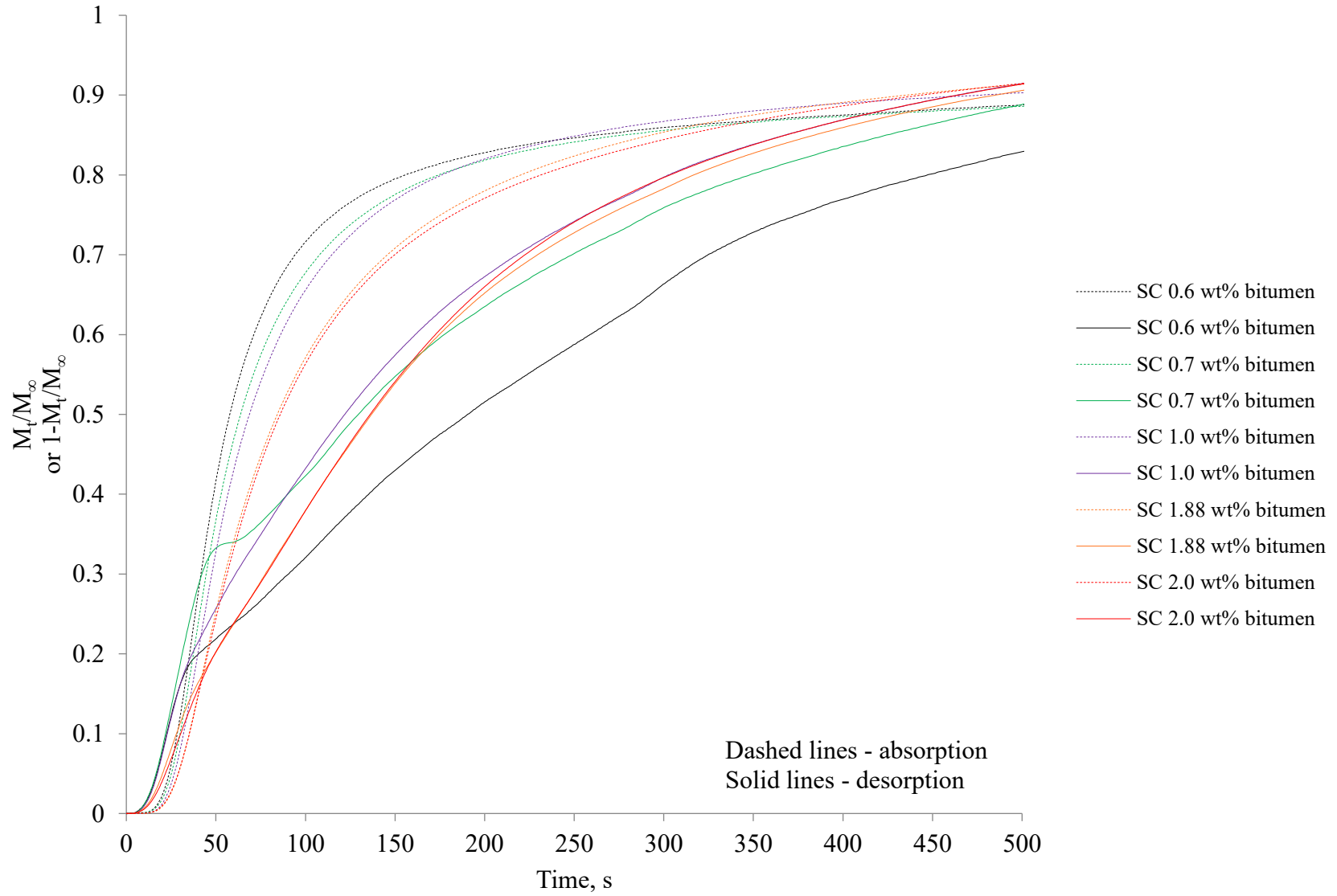


Figure C 9: Mass uptake/release curves of SC at 90% cyclohexane RS

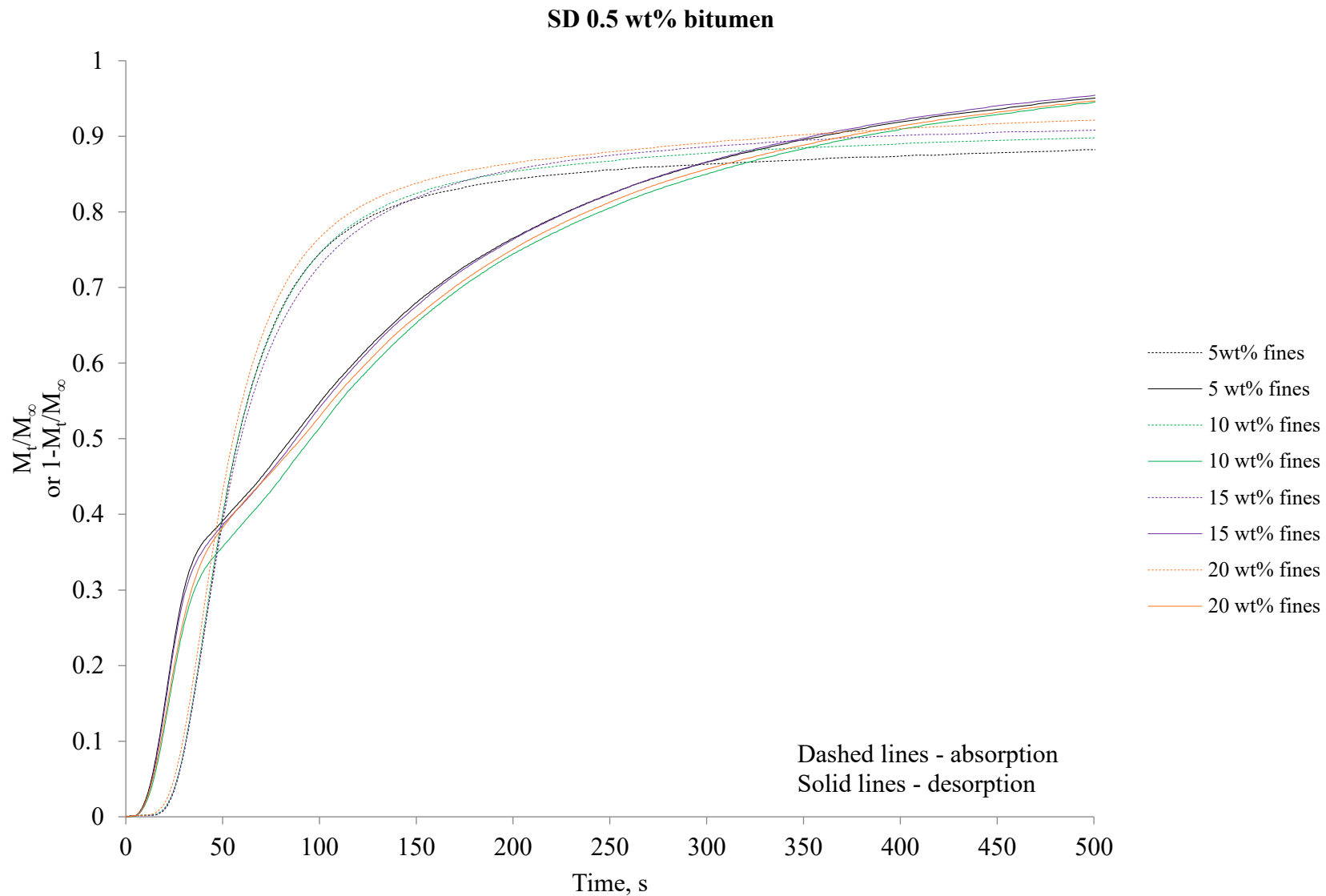


Figure C 10: Mass uptake/release curves of SD with 0.5 wt% bitumen content at 90% cyclohexane RS

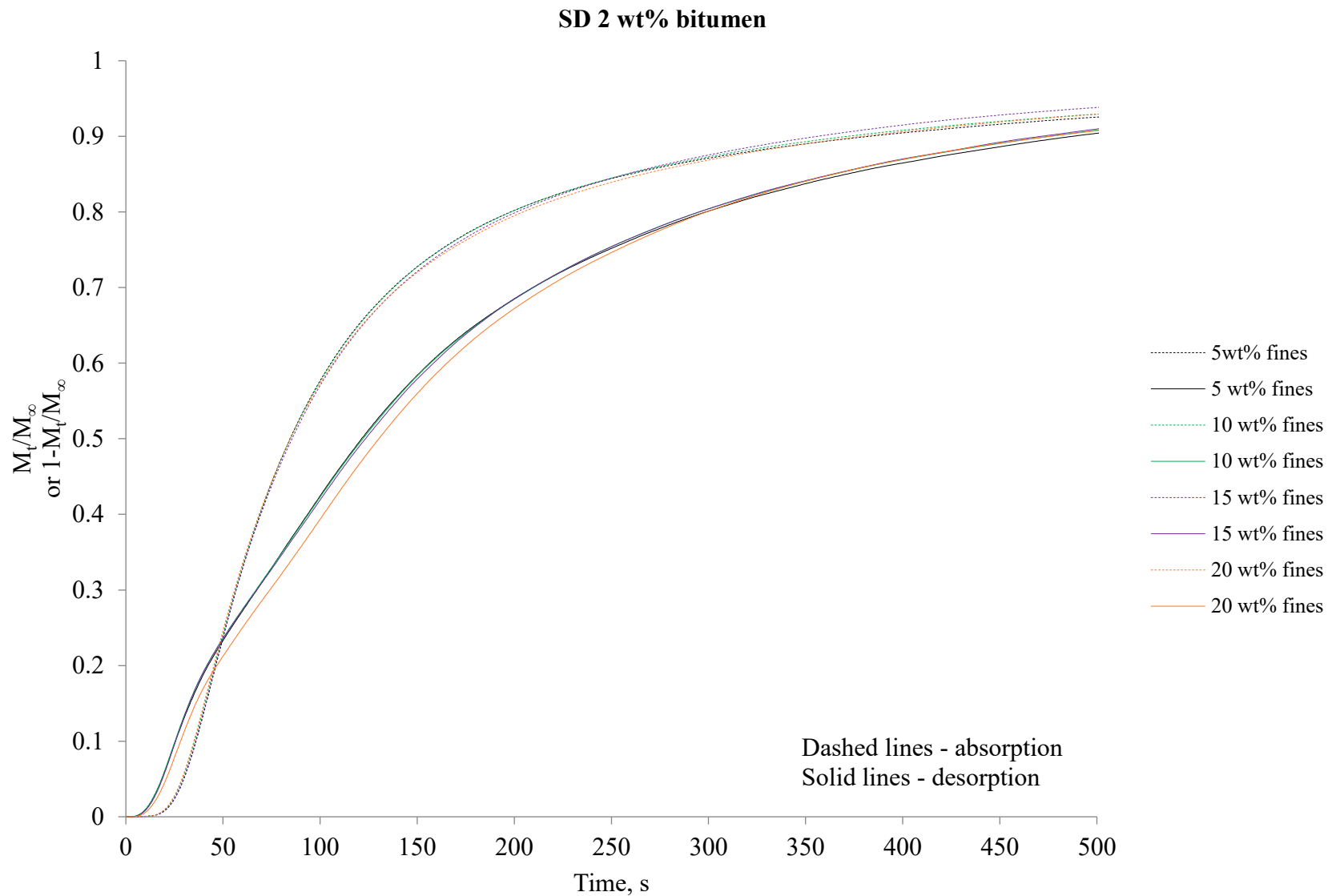


Figure C 11: Mass uptake/release curves of SD with 2 wt% bitumen content at 90% cyclohexane RS

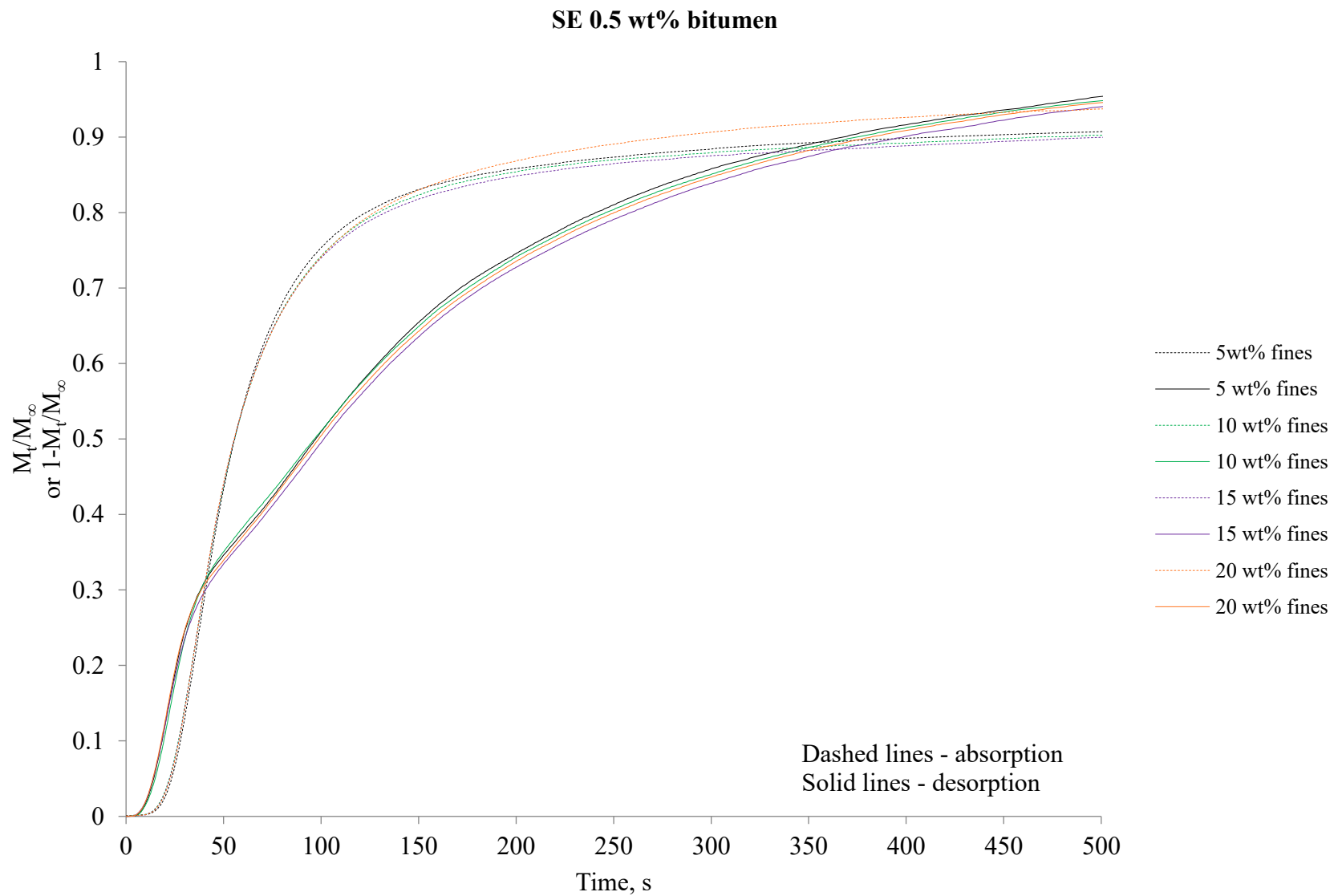


Figure C 12: Mass uptake/release curves of SE with 0.5 wt% bitumen content at 90% cyclohexane RS

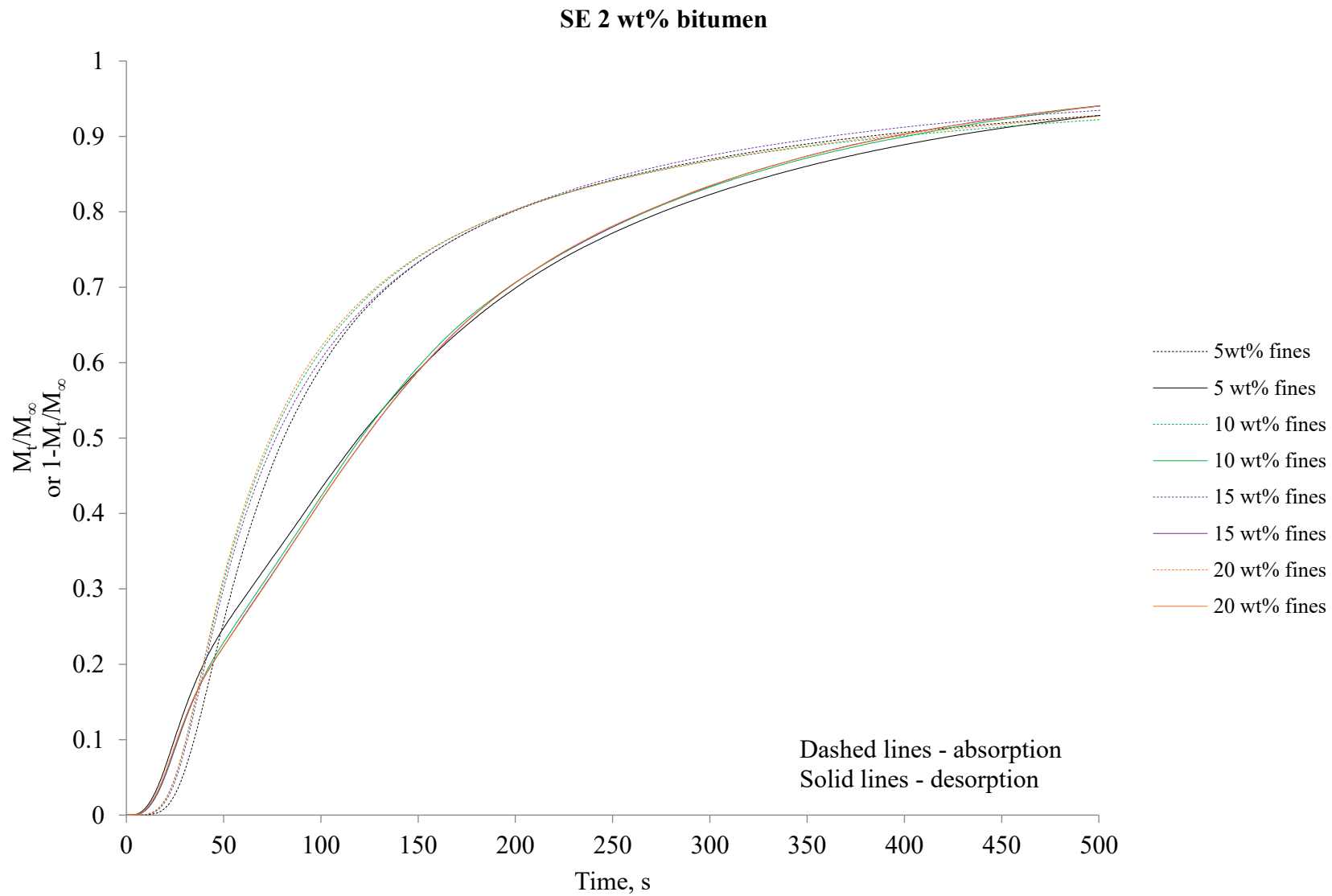


Figure C 13: Mass uptake/release curves of SE with 0.5 wt% bitumen content at 90% cyclohexane RS

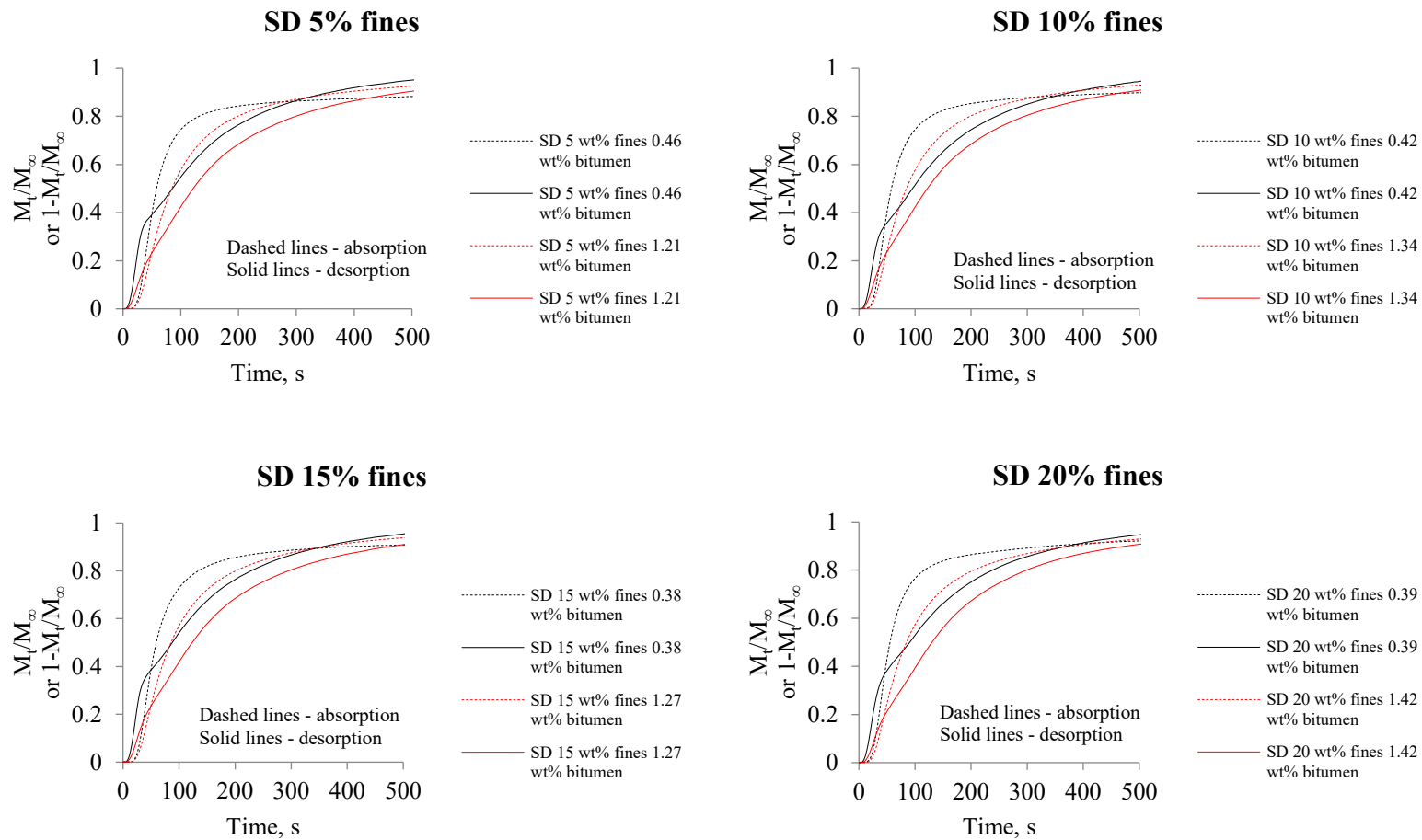


Figure C 14: Mass uptake/release curves of SD at 90% cyclohexane RS

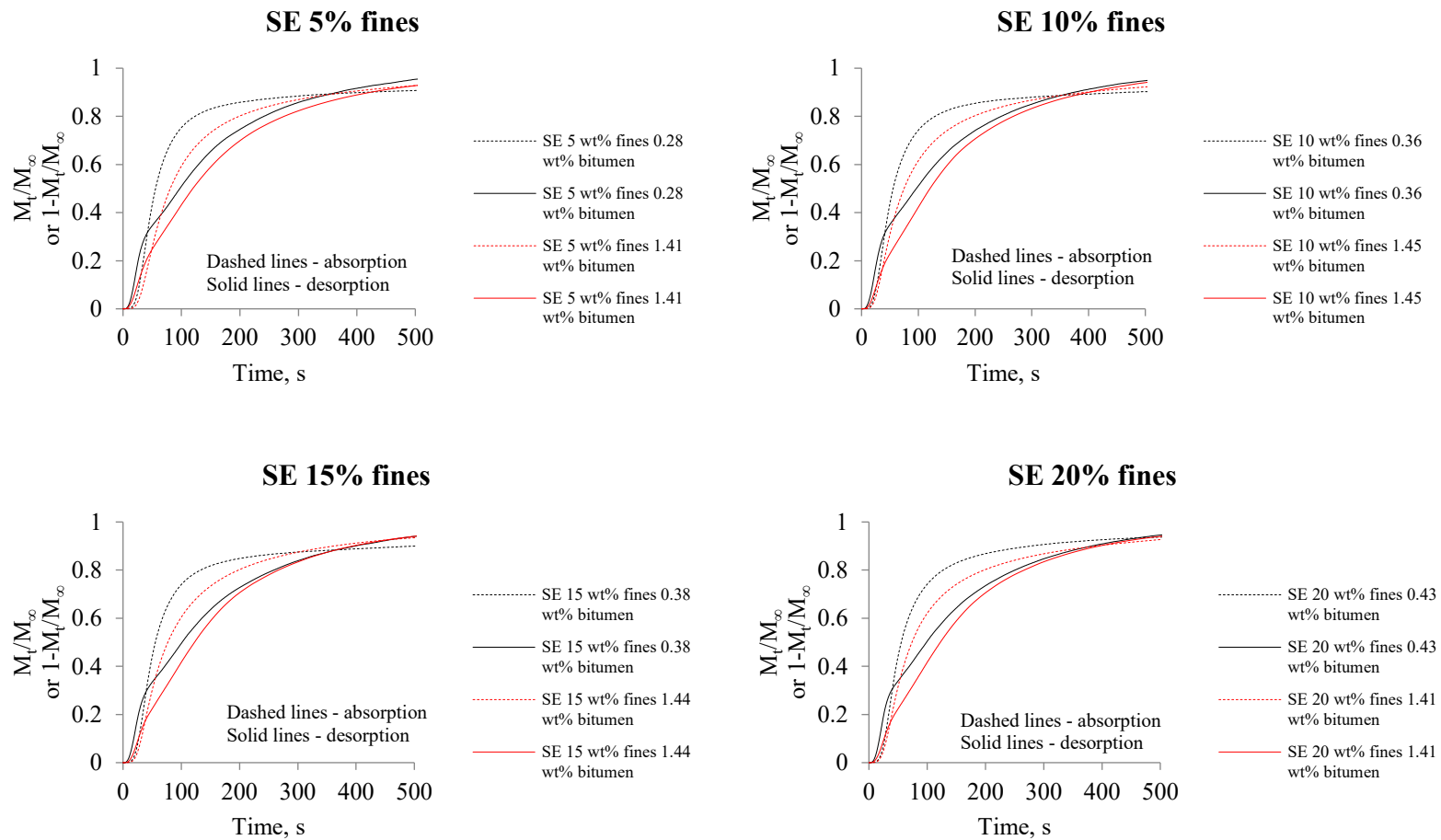


Figure C 15: Mass uptake/release curves of SE at 90% cyclohexane RS